3 1176 00028 9075

CONFIDENTIAL

Copy
RM L50C17a

NACA RM L50C17a

#104
Bell X-5/2
C.1

NACA

RESEARCH MEMORANDUM

STABILITY AND CONTROL CHARACTERISTICS AT LOW SPEED OF A $\frac{1}{4}$-SCALE BELL X-5 AIRPLANE MODEL

LATERAL AND DIRECTIONAL STABILITY AND CONTROL

By William B. Kemp, Jr. and Robert E. Becht

Langley Aeronautical Laboratory
Langley Air Force Base, Va.

CLASSIFICATION CANCELLED

Authority Docket 2809 Date 12/29/54

By [illegible] 11/18/54 See

CLASSIFIED DOCUMENT

This document contains classified information affecting the National Defense of the United States within the meaning of the Espionage Act, USC 50:31 and 32. Its transmission or the revelation of its contents in any manner to an unauthorized person is prohibited by law. Information so classified may be imparted only to persons in the military and naval services of the United States, appropriate civilian officers and employees of the Federal Government who have a legitimate interest therein, and to United States citizens of known loyalty and discretion who of necessity must be informed thereof.

NACA LIBRARY
LANGLEY AERONAUTICAL LABORATORY
Langley Field, Va.

NATIONAL ADVISORY COMMITTEE
FOR AERONAUTICS

WASHINGTON

June 20, 1950

UNCLASSIFIED

CONFIDENTIAL

UNCLASSIFIED

NATIONAL ADVISORY COMMITTEE FOR AERONAUTICS

RESEARCH MEMORANDUM

STABILITY AND CONTROL CHARACTERISTICS AT LOW SPEED OF A $\frac{1}{4}$-SCALE BELL X-5 AIRPLANE MODEL

LATERAL AND DIRECTIONAL STABILITY AND CONTROL

By William B. Kemp, Jr. and Robert E. Becht

SUMMARY

An investigation was made of the low-speed lateral and directional stability and control characteristics of a $\frac{1}{4}$-scale model of a preliminary Bell X-5 airplane design with various leading-edge-slat and trailing-edge-flap arrangements. The model was directionally unstable at high lift coefficients, but for the lower sweep angles instability occurred only beyond the stall. For all sweep angles, the values of effective dihedral were moderate at most lift coefficients but became small or negative at high lift coefficients. The slats caused positive effective dihedral to be maintained at high lift coefficients for all sweep angles and a full-span slat used on a 60° swept wing was beneficial in reducing the directional instability at high angles of attack. The directional control was adequate to trim the model to at least 15° yaw for all configurations. The aileron effectiveness was positive up through stall for all conditions of sweep and the accompanying yawing moments were favorable in the low angle-of-attack range.

INTRODUCTION

An investigation of the stability and control characteristics at low speed of a $\frac{1}{4}$-scale model of a preliminary Bell X-5 airplane design has been conducted in the Langley 300 MPH 7- by 10-foot tunnel. The Bell X-5 airplane is a proposed research airplane incorporating wings having a sweepback angle that can be varied continuously between 20° and 60°. Provision for longitudinal translation of the wing with respect to the fuselage is also made.

UNCLASSIFIED

The present paper contains the results of the lateral and directional stability and control tests of the model at four sweep angles and with various leading-edge-slat and trailing-edge-flap arrangements. The results of the longitudinal stability and control investigation are presented in reference 1.

SYMBOLS

The system of axes employed, together with an indication of the positive forces, moments, and angles, is presented in figure 1. The symbols used in this paper are defined as follows:

C_L	lift coefficient (Lift/qS)
C_X	longitudinal-force coefficient (X/qS)
C_Y	lateral-force coefficient (Y/qS)
C_l	rolling-moment coefficient (L/qSb)
C_m	pitching-moment coefficient ($M/qS\bar{c}_{50}$)
C_n	yawing-moment coefficient (N/qSb)
X	longitudinal force along X-axis, pounds
Y	lateral force along Y-axis, pounds
Z	force along Z-axis (Lift equals -Z), pounds
L	rolling moment about X-axis, foot-pounds
M	pitching moment about Y-axis, foot-pounds
N	yawing moment about Z-axis, foot-pounds
q	free-stream dynamic pressure, pounds per square foot ($\rho V^2/2$)
S	wing area, square feet
$\bar{c}$	wing mean aerodynamic chord, feet (based on plan forms shown in fig. 2)
$\bar{c}_{50}$	wing mean aerodynamic chord at 50° sweep, feet
c'	streamwise wing chord, feet

[redacted]

c	wing chord perpendicular to quarter-chord line of unswept wing, feet
b	wing span, feet
V	free-stream velocity, feet per second
A	aspect ratio (b^2/S)
ρ	mass density of air, slugs per cubic foot
α	angle of attack of thrust line, degrees
ψ	angle of yaw, degrees
i_t	angle of incidence of stabilizer with respect to thrust line, degrees
δ	control-surface deflection measured in a plane perpendicular to hinge line, degrees
Λ	angle of sweepback of quarter-chord line of unswept wing, degrees

Subscripts:

e	elevator
a	aileron
r	rudder
f	flap
ψ	denotes partial derivative of a coefficient with respect to yaw $\left(\text{example: } C_{l_\psi} = \frac{\partial C_l}{\partial \psi}\right)$

APPARATUS AND METHODS

Description of Model

The model used in the present investigation was a $\frac{1}{4}$-scale model of a preliminary Bell X-5 design and must, therefore, be considered only qualitatively representative of the Bell X-5 airplane.

[redacted]

Physical characteristics of the model are presented in figure 2, and photographs of the model on the support strut are given as figure 3. Figure 4 includes details of the various slats, flaps, and spoilers investigated. A plain, sealed aileron was installed in the left wing (fig. 2). The model was constructed of wood bonded to steel reinforcing members.

The wings were pivoted about axes normal to the wing-chord planes. Thus, the wing incidence measured in a streamwise direction was zero for all sweep angles. At all sweep angles, the wing was located so that the quarter chord of the mean aerodynamic chord fell at a fixed fuselage station. The moment reference center was located at this same fuselage station. (See fig. 2.)

The jet-engine ducting was simulated on the model by the use of an open, straight tube having an inside diameter equal to that of the jet exit and extending from the nose to the jet exit.

Tests

The tests were conducted in the Langley 300 MPH 7- by 10-foot tunnel at a dynamic pressure of 34.15 pounds per square foot which corresponds to a Mach number of 0.152 and a Reynolds number of 2,000,000 based on the mean aerodynamic chord of the wing at 50° sweep for average test conditions.

During the tests, no control was imposed on the flow quantity through the jet duct. Measurements made in subsequent tests indicated that the inlet-velocity ratio varied between 0.78 and 0.86, the higher values being observed at low angles of attack.

Two types of tests were employed for determining the lateral characteristics of the model. The parameters C_{n_ψ}, C_{Y_ψ}, and C_{l_ψ} were determined from tests through the angle-of-attack range at yaw angles of 0° and 5°. The lateral characteristics were also determined from tests through a range of yaw angles at constant angle of attack.

Corrections

The angle-of-attack, drag, and pitching-moment results have been corrected for jet-boundary effects computed on the basis of unswept wings by the methods of reference 2. Independent calculations have shown that the effects of sweep on these corrections are negligible. All coefficients have been corrected for blocking by the model and its wake by the method of reference 3.

[redacted]

Corrections for the tare forces and moments produced by the support strut have not been applied. It is probable, however, that the significant tare corrections would be limited to small increments in pitching moment and drag.

Vertical buoyancy on the support strut, tunnel air-flow misalinement, and longitudinal pressure gradient have been accounted for in computation of the test data.

RESULTS AND DISCUSSION

Presentation of Results

The lateral-stability parameters and aerodynamic characteristics in yaw for the basic model and its component parts are presented in figures 5 to 18 with the wing at varying degrees of sweep. The effects of high-lift and control devices on these parameters and aerodynamic characteristics are presented as follows:

	Figure
Effect of slats	19 to 25
Effect of flaps	26 to 29
Effect of slats and flaps	30 to 32
Directional control	33 to 36
Lateral control	37 to 42

The aerodynamic coefficients presented herein are based on the wing area and span of the sweep configuration in question and on the mean aerodynamic chord of the wing at 50° sweep. Thus, the pitching-moment coefficients are based on a reference length which is fixed in the fuselage and is independent of the sweep angle, whereas all other coefficients are of the usual form.

Basic Lateral Stability Characteristics

The static-lateral-stability parameters determined from tests at yaw angles of 0° and 5° are plotted against lift coefficient in figure 5 for the complete basic model with the wing positioned at varying degrees of sweep. Lift curves for these configurations are presented in figure 6. The results of yaw tests at various angles of attack for the four sweep configurations are given in figure 7.

The wing dimensions given in figure 2 indicate that a significant reduction in wing span accompanies an increase in sweep angle. Inasmuch

as the yawing- and rolling-moment-coefficient values are dependent on span as well as the actual moments, the reduction in span with increasing sweep must be kept in mind in interpreting the data presented. Thus, the increase with sweep of the directional stability at low and moderate lift coefficients, as shown in figure 5, may be largely attributed to the wing-span reduction with sweep rather than to any change in the actual moments.

At high lift coefficients, figure 5 indicates that directional instability was encountered at all sweep angles. For the low sweep angles, instability occurred only beyond the stall, but at 60° sweep an extensive range of lift coefficient in which directional instability was experienced existed below the stall. In this discussion, the stall is considered as the first major break in the lift curve. Inspection of figure 7(d) indicates that this instability existed over a wide range of yaw angles. It may be observed from figures 5 and 7 that the loss in directional stability was accompanied by a reduction in effective dihedral. The values of C_{l_ψ} decreased and even became negative at high sweep angles.

At low lift coefficients, the rate of increase of effective dihedral with lift coefficient increased with sweep as would be predicted by simple sweep theory. As the lift coefficient was increased, the effective dihedral reached a peak and then dropped off. The lift coefficient for maximum effective dihedral was progressively reduced as sweep increased and corresponded roughly to the lift coefficient at which initial separation on the wing occurred (see pitching-moment and drag data of reference 1). It is probable that at higher Reynolds numbers, the initial separation would be delayed to higher lift coefficients with a corresponding increase in the maximum value of effective dihedral.

The contribution of the tail to the lateral characteristics of the model at each sweep angle investigated is presented in figures 8 to 15.

For the tail-off tests, the vertical and horizontal tails were removed as a unit. Thus, at equal angles of attack, comparison of the tail-on and tail-off results indicates an increment of lift coefficient representing the lift of the horizontal tail.

A comparison of figures 10 and 14 shows a greater directional instability of the wing-fuselage combination and a greater contribution of the tail to directional stability for 60° sweep than for 35° sweep. Here again, this phenomenon may be attributed largely to the reduction of wing span with sweep. It may be observed that the increased directional instability at high angles of attack previously mentioned was experienced to some extent with the tail removed, especially at 60° sweep (fig. 14).

[redacted]

The characteristics through the yaw-angle range are presented in figures 16 and 17 for the fuselage-tail combination and the fuselage alone. The coefficients presented are based on the area and span of the wing at 60° sweep. In figure 18 the lateral characteristics of various combinations of model components are presented as a function of angle of attack. The data presented indicate that the wing alone and the fuselage alone do not contribute significantly to the directional instability of the model utilizing 60° wing sweep. The wing-fuselage and the fuselage-tail combinations, however, do have large unstable trends at high angles of attack. Thus, the directional instability of the complete model must be a result of the mutual interference between the wing, fuselage, and tail. Although the mechanism of this phenomenon is not fully understood at present, it is probable that the unsymmetrical stalling of the yawed swept wing, the sidewash on the vertical tail caused by the strong vortex field shed from the swept wing, and the interference of the fuselage on the tail at the high angles of attack required to stall the swept wing are all important factors in producing the directional instability observed.

Effect of Slats

The lift curves for the model with various slat locations are given in figure 19 for sweep angles of 20°, 35°, and 60°. The lateral characteristics are presented for 20° sweep in figure 20, for 35° sweep in figures 21 and 22, and for 60° sweep in figures 23 to 25. At 20° sweep extension of the slats at low lift coefficients produced a small increase in directional stability and a decrease in effective dihedral. For the higher sweep angles, all slat configurations tested had very little effect on the lateral characteristics at low lift coefficients. At high lift coefficients all slat configurations were effective in reducing or eliminating the loss in dihedral effect which occurred with slats retracted. The slats at 20° sweep actually caused the effective dihedral to increase at the stall. For 20° and 35° sweep, the slats tested increased the lift coefficient at which directional instability occurred. This increase may be attributed to the increased maximum lift attainable with the slats since directional instability occurred only after flow separation was fairly complete. At 60° sweep, extending the entire slat to position A again increased the lift coefficient for directional instability although, in this case, the maximum lift coefficient was not increased. The effect of extending only the outboard halves of the slat, however, was detrimental to directional stability at high lift coefficients.

[redacted]

Effect of Flaps

The lift curves for the model with flaps A, B, and C deflected 50° on the wing at 20° sweep and flap B deflected 50° on the wing at 60° sweep are presented in figure 26. The effects of a 50° deflection of flaps A, B, and C on the lateral-stability parameters of the model with 20° sweep are given in figure 27. Very little change in the directional stability occurred when flap A or B was deflected other than to delay the decreased stability associated with wing stall to higher lift coefficients. An appreciable increase in directional stability below the stall resulted from deflection of flap C. Only moderate changes in effective dihedral resulted from deflection of any of the flaps on the 20° swept wing. The effect of flap B deflected 50° on the model when the wings were at 60° sweep (fig. 29) was such as to produce varying increases in directional stability through the lift-coefficient range. Instability was thus delayed to higher lift coefficients. The effective dihedral was increased at low lift coefficients by the use of flap B, but at high lift coefficients large negative values of effective dihedral were obtained.

Effect of Slats and Flaps

Lift curves for the model with the wing swept to 20°, slats extended, and flaps deflected are presented in figure 30. The lateral-stability parameters for these configurations are given in figure 31. A comparison of figures 31 and 27 shows that deflecting the flaps did not appreciably alter the effects of the slats previously noted for 20° sweep; that is, extending the slats caused an increase in effective dihedral at the stall, and only minor changes in directional stability and effective dihedral below the stall.

Directional Control

The effects of rudder deflection on the aerodynamic characteristics of the model in yaw are given for a sweep angle of 20° in figures 33 and 34 and for 60° sweep in figures 35 and 36. The rudder effectiveness, that is, the yawing-moment coefficient produced by a given rudder deflection, was essentially unaffected by the changes in model configuration and angle of attack made at each sweep angle. The change in rudder effectiveness with sweep may be approximately accounted for by the change in wing span with sweep. In each configuration, the model could be trimmed at about 15° yaw by full rudder deflection except for the 60° sweep, high-angle-of-attack case (fig. 36) in which the decreased directional stability allowed higher trimmed yaw angles. At low angles of attack, for which the center of pressure of the vertical tail was above the center of gravity, a negative rolling-moment increment accompanied negative rudder deflections. This trend was eliminated or reversed at higher angles of attack.

[redacted]

Lateral Control

The effect of aileron deflection on the aerodynamic characteristics of the model is presented for various model configurations in figures 37 to 40. These data were obtained with only the left aileron deflected. Although the existence of rolling moments for zero aileron deflection indicates unsymmetric flow separation from the wings combined with some asymmetry in model construction and mounting, the incremental effects of aileron deflection should be essentially independent of the unsymmetrical conditions. In all cases, the ailerons were effective up to and beyond the stall.

The yawing moments accompanying aileron deflection were favorable at low angles of attack. Since the favorable yawing moments observed would not be anticipated for the isolated wing-aileron combination, it is believed that sidewash induced at the tail by aileron deflection contributed significantly to the yawing moments of the complete model.

In view of the possibility that aileron control would become inadequate at transonic speeds, some exploratory tests were made to determine the low-speed characteristics of spoiler ailerons located as shown in figure 4. Generally speaking, the results of these tests (figs. 41 and 42) show that the rolling moments produced by the inboard spoiler were comparable to those produced by about 20° deflection of one aileron. The outboard spoiler was slightly more effective at 20° sweep, but considerably less effective at 60° sweep, than the inboard spoiler. At 20° sweep the spoilers lost effectiveness rapidly near the stall with reversal indicated slightly above stall. The associated yawing moments were favorable and reasonably constant up to about 8° angle of attack. When the wings were swept to 60°, the inboard spoiler produced small and varying unfavorable yawing moments. The yawing moments for the outboard spoiler were again favorable at low angles of attack. An increase in drag at low angles of attack was exhibited with a nose-up trim change for both sweeps and spoiler locations. Although the spoiler configurations investigated do not necessarily represent an optimum spoiler design, further development was not undertaken in view of the satisfactory aileron characteristics obtained.

[redacted]

CONCLUSIONS

An investigation at low speed of the lateral and directional stability and control of a $\frac{1}{4}$-scale model of a preliminary Bell X-5 airplane design indicates the following conclusions:

1. Directional instability at high lift coefficients was observed for all sweep angles but occurred only beyond the stall for the lower sweep angles. This instability is the result of the mutual interference between the wing, fuselage, and tail.

2. For all sweep angles, the values of effective dihedral were moderate at most lift coefficients but became small or negative at high lift coefficients.

3. The slats were effective at all sweep angles in maintaining positive effective dihedral at high lift coefficients, and the use of full-span slats at 60° sweep was helpful in alleviating directional instability at high lift coefficients.

4. Rudder control was adequate to trim the model to at least 15° yaw for all configurations.

5. The ailerons were effective up to and beyond the stall, and the aileron yawing moments were favorable at low angles of attack.

Langley Aeronautical Laboratory
National Advisory Committee for Aeronautics
Langley Air Force Base, Va.

[redacted]

REFERENCES

1. Kemp, William B., Jr., Becht, Robert E., and Few, Albert G., Jr.: Stability and Control Characteristics at Low Speed of a $\frac{1}{4}$-Scale Bell X-5 Airplane Model. Longitudinal Stability and Control. NACA RM L9K08, 1950.

2. Gillis, Clarence L., Polhamus, Edward C., and Gray, Joseph L., Jr.: Charts for Determining Jet-Boundary Corrections for Complete Models in 7- by 10-Foot Closed Rectangular Wind Tunnels. NACA ARR L5G31, 1945.

3. Herriot, John G.: Blockage Corrections for Three-Dimensional-Flow Closed-Throat Wind Tunnels, with Consideration of the Effect of Compressibility. NACA RM A7B28, 1947.

[redacted]

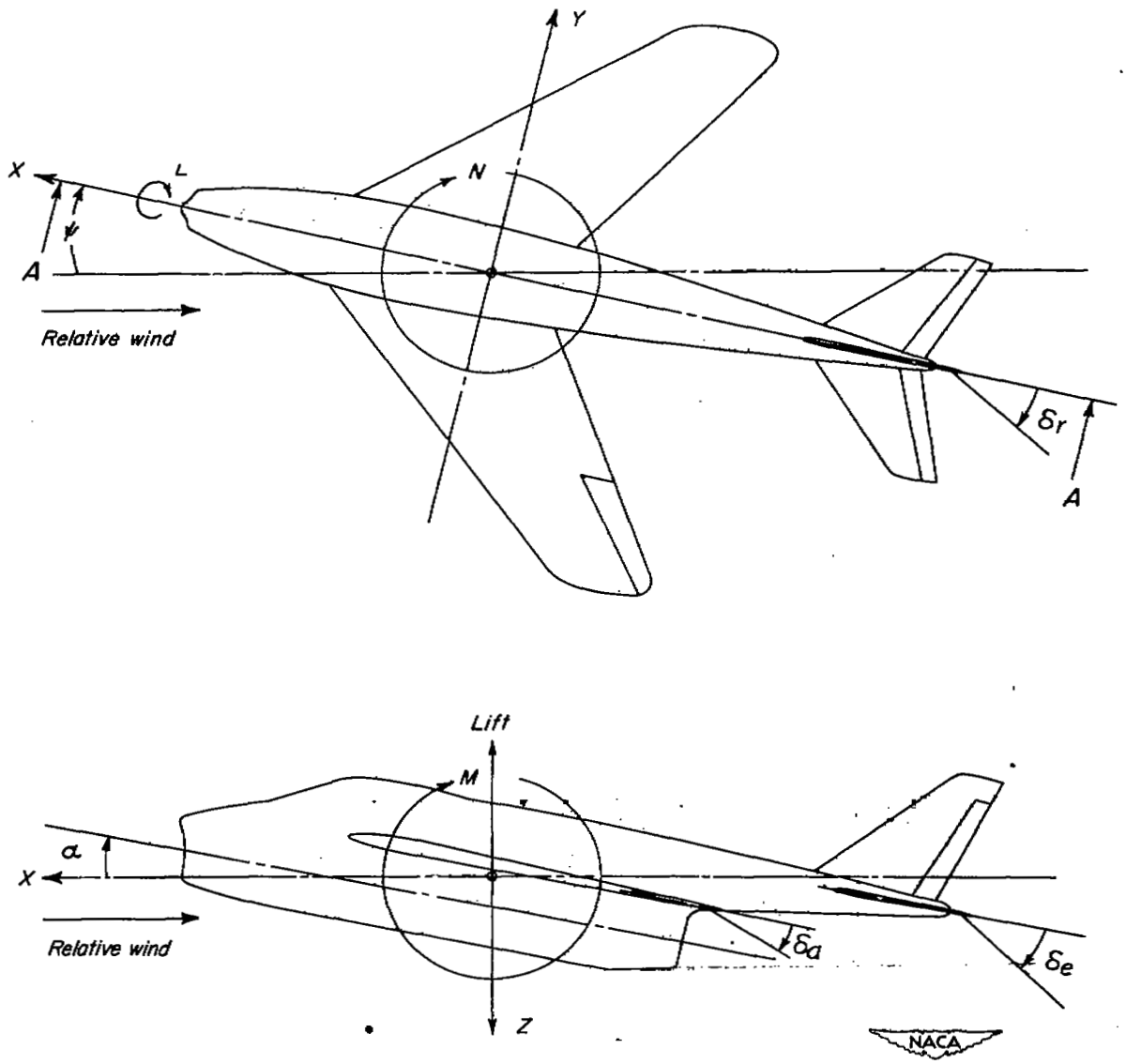

View A-A

Figure 1.- System of axes and control-surface deflections. Positive values of forces, moments, and angles are indicated by arrows.

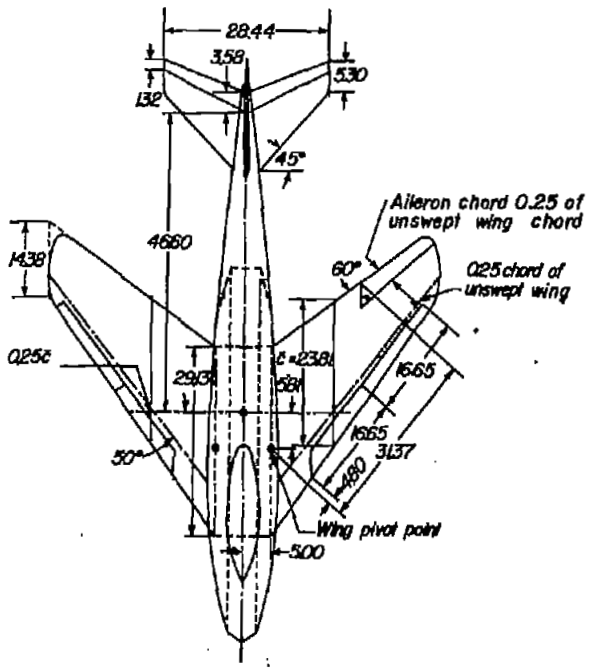

Physical characteristics

Wing

Sweep, deg	20	35	50	60
Area, sq ft	10.33	10.45	10.80	11.33
Aspect ratio	5.76	4.56	2.98	1.92
Span, ft	7.72	6.90	5.67	4.66
Mean aerodynamic chord, ft	1.396	1.579	1.965	2.535

Incidence, deg 0
Dihedral, deg -2
Airfoil section perpendicular to 0.25c
Root NACA $64_{(10)}$-010.3
Tip NACA 64-008

Horizontal tail
Area, sq ft 1.94
Aspect ratio 2.89

Vertical tail
Area, sq ft 1.33
Aspect ratio 1.46

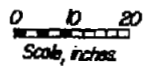

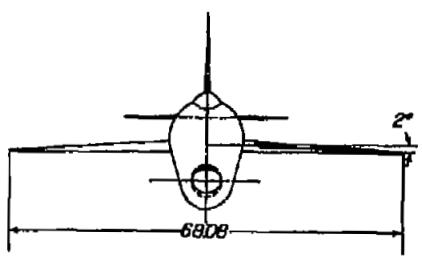

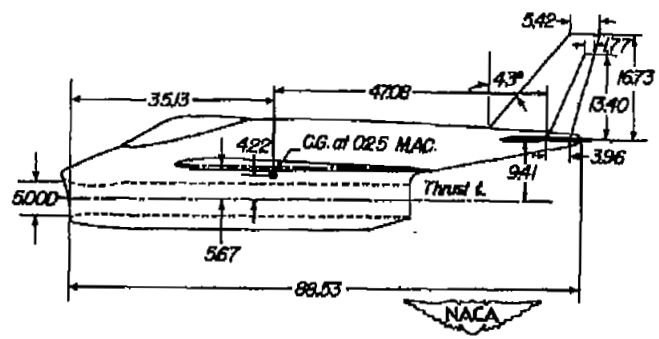

Figure 2.- General arrangement of test model.

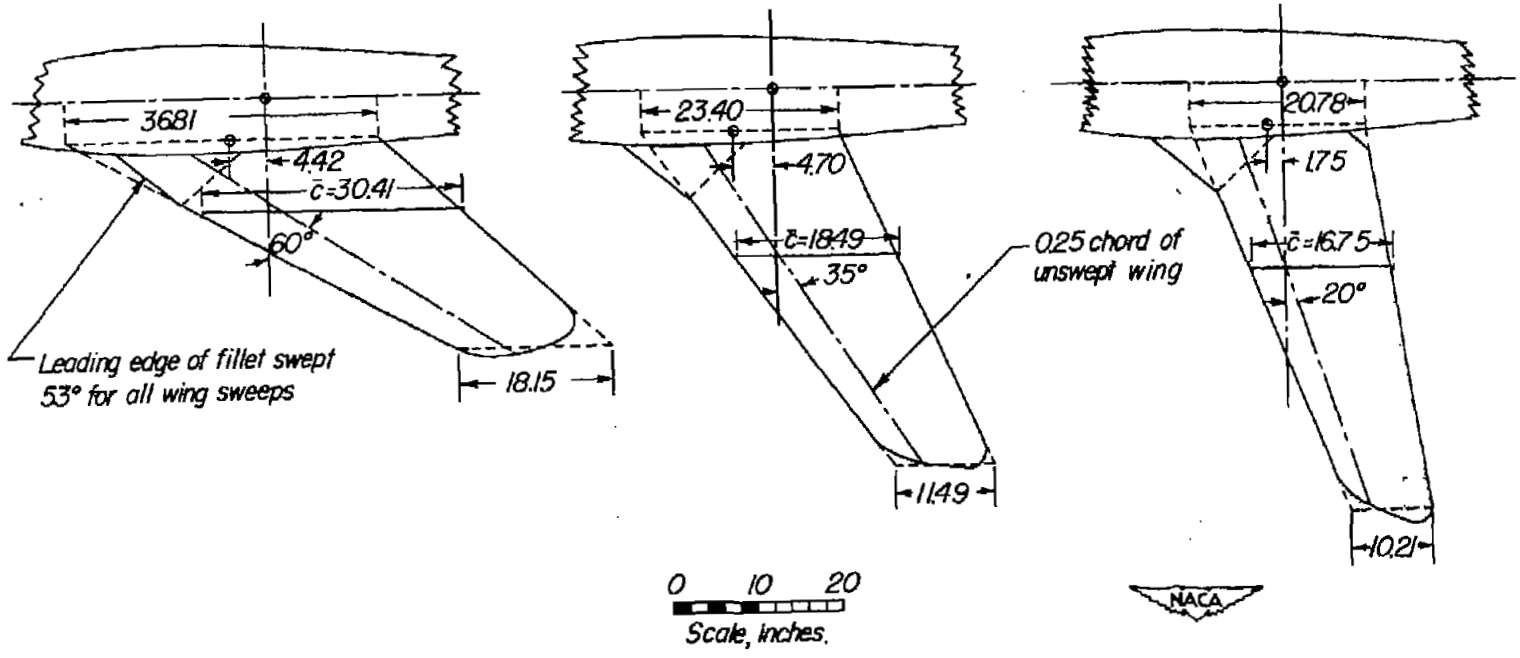

Figure 2.- Concluded.

(a) Slat extended; flap B; $\Lambda = 20^{\circ}$.

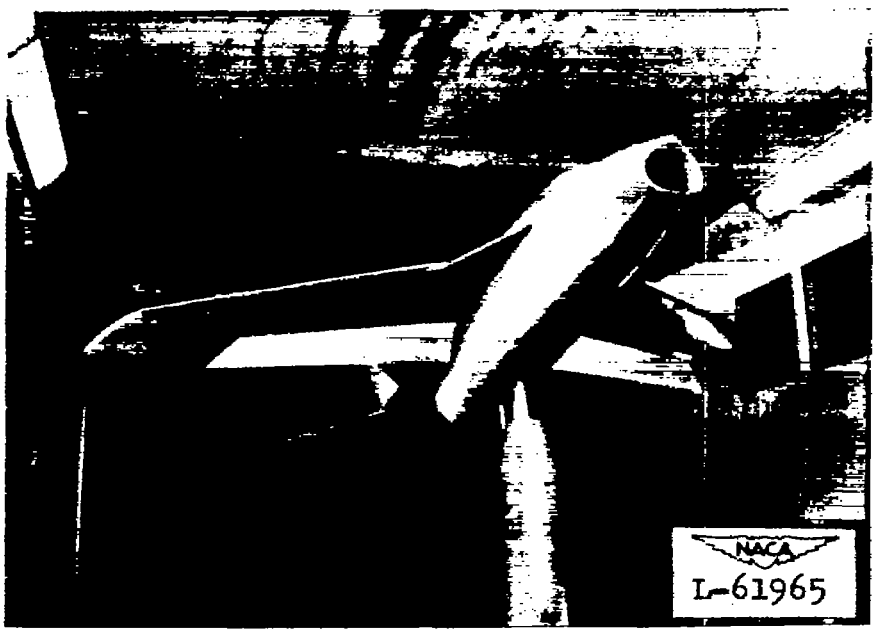

(b) Slat extended; flap C; $\Lambda = 20^{\circ}$.

Figure 3.- Views of test model mounted in tunnel.

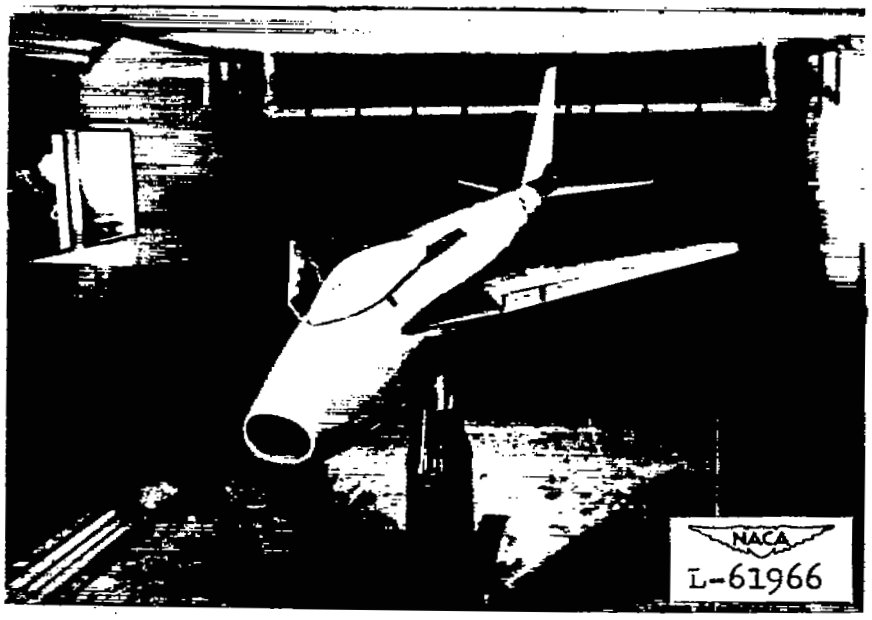

(c) Slat extended; flap B; $\Lambda = 20^{\circ}$.

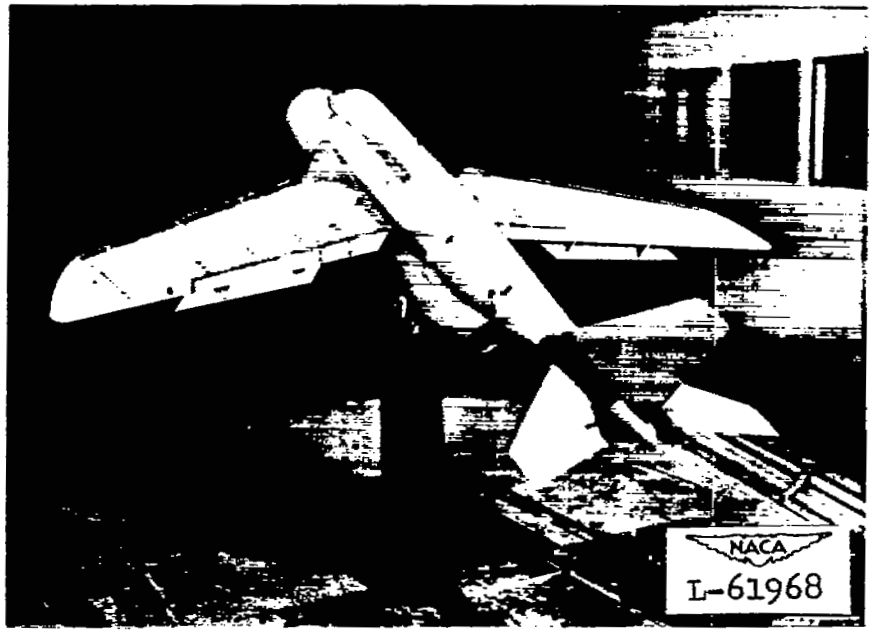

(d) Slats retracted; $\delta_f = 0$; $\Lambda = 60^{\circ}$.

Figure 3.- Concluded.

[redacted]

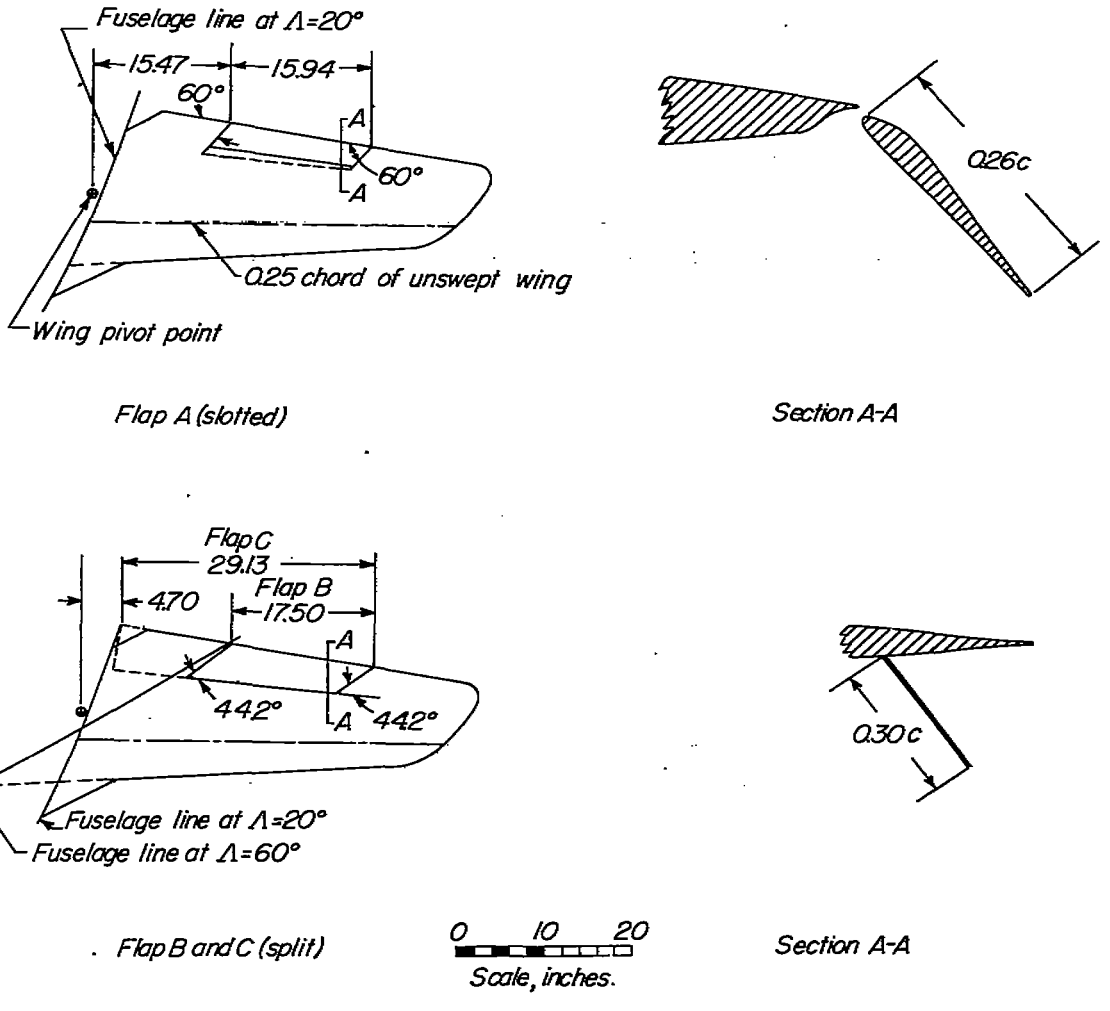

Figure 4.- Details of flaps, slats, and spoilers.

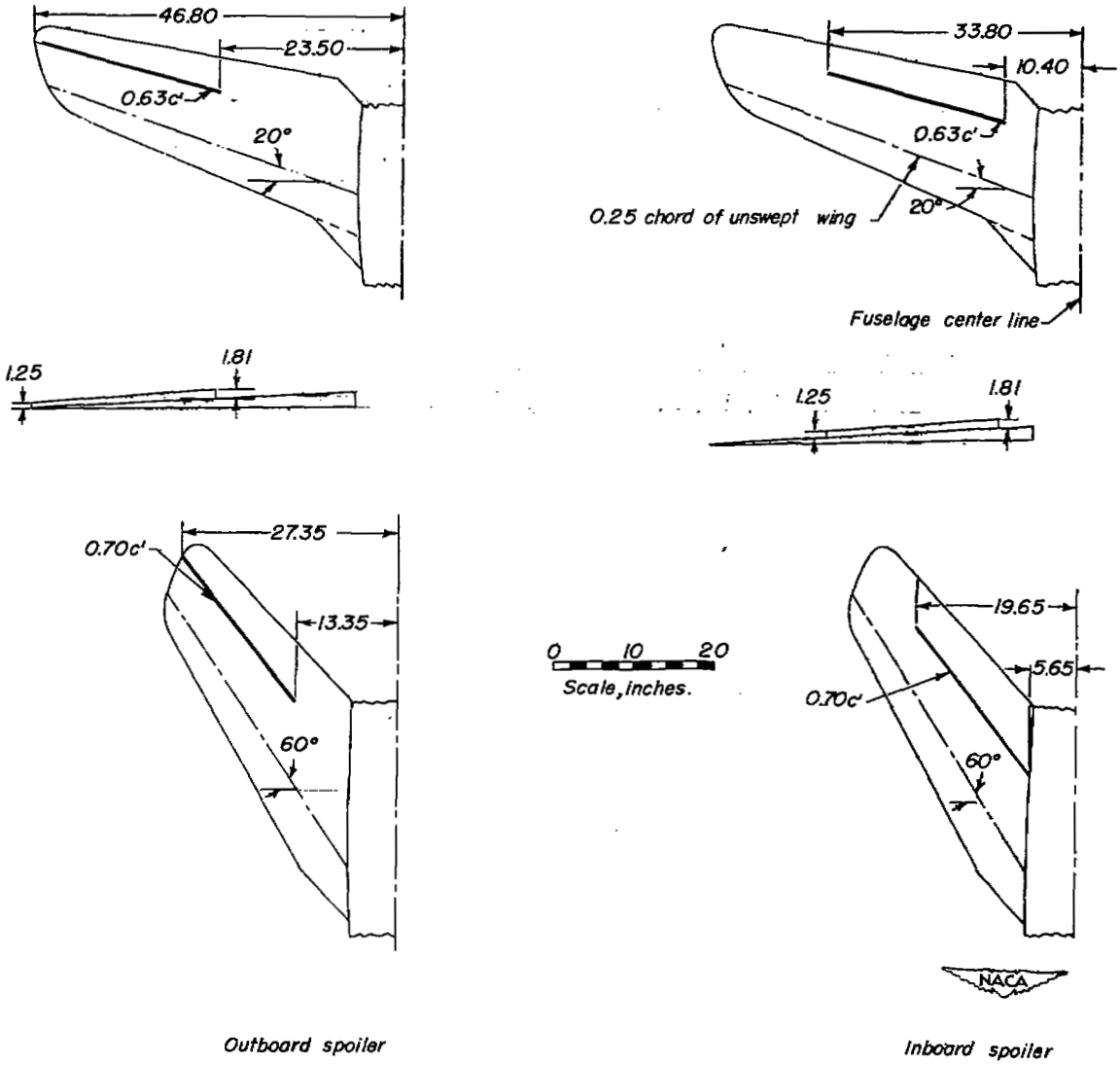

Figure 4.- Concluded.

[redacted]

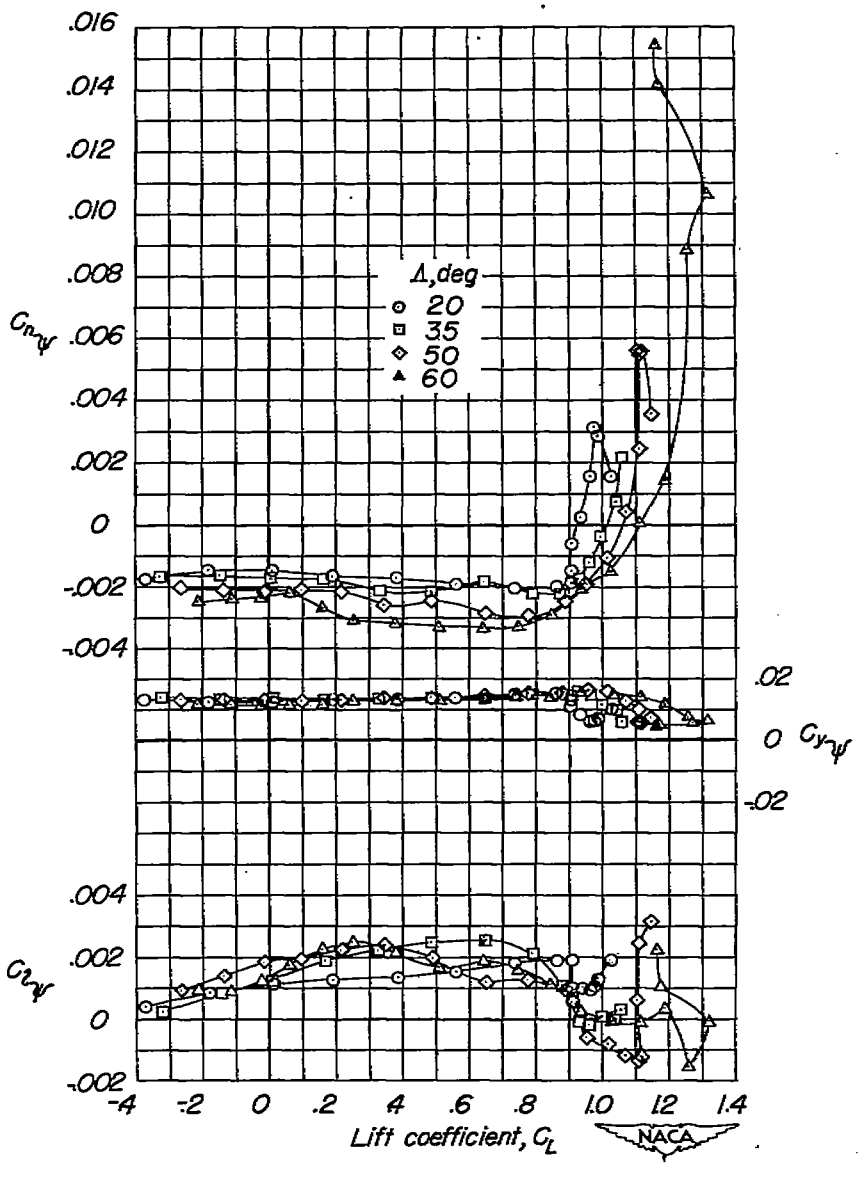

Figure 5.- The effect of sweep on the lateral-stability parameters of the test model. Slats retracted; $\delta_f = 0^\circ$; $i_t = -\frac{3^\circ}{4}$.

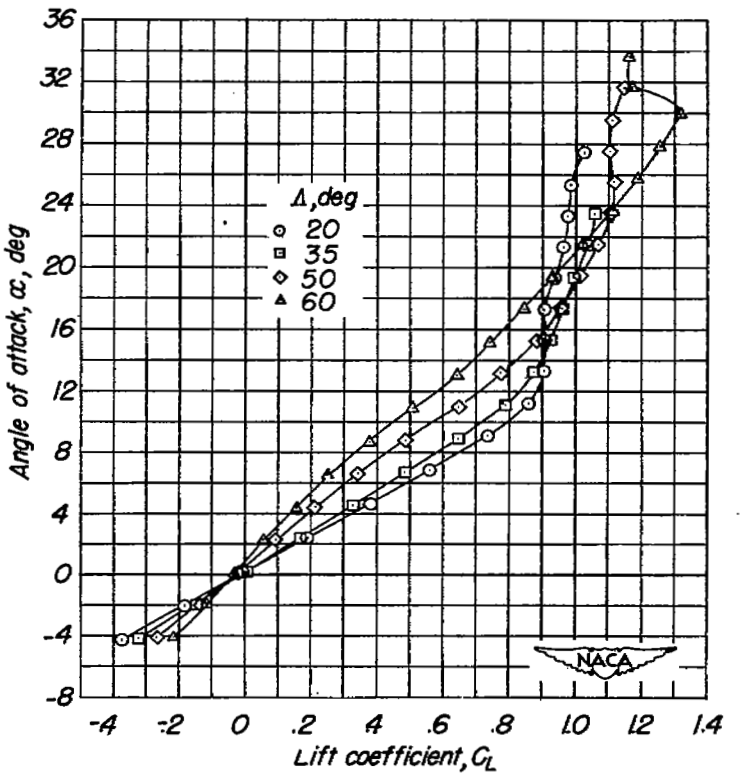

Figure 6.- The effect of sweep on the lift curves for the test model. Slats retracted; $\delta_f = 0^\circ$; $i_t = -\frac{3^\circ}{4}$.

[redacted]

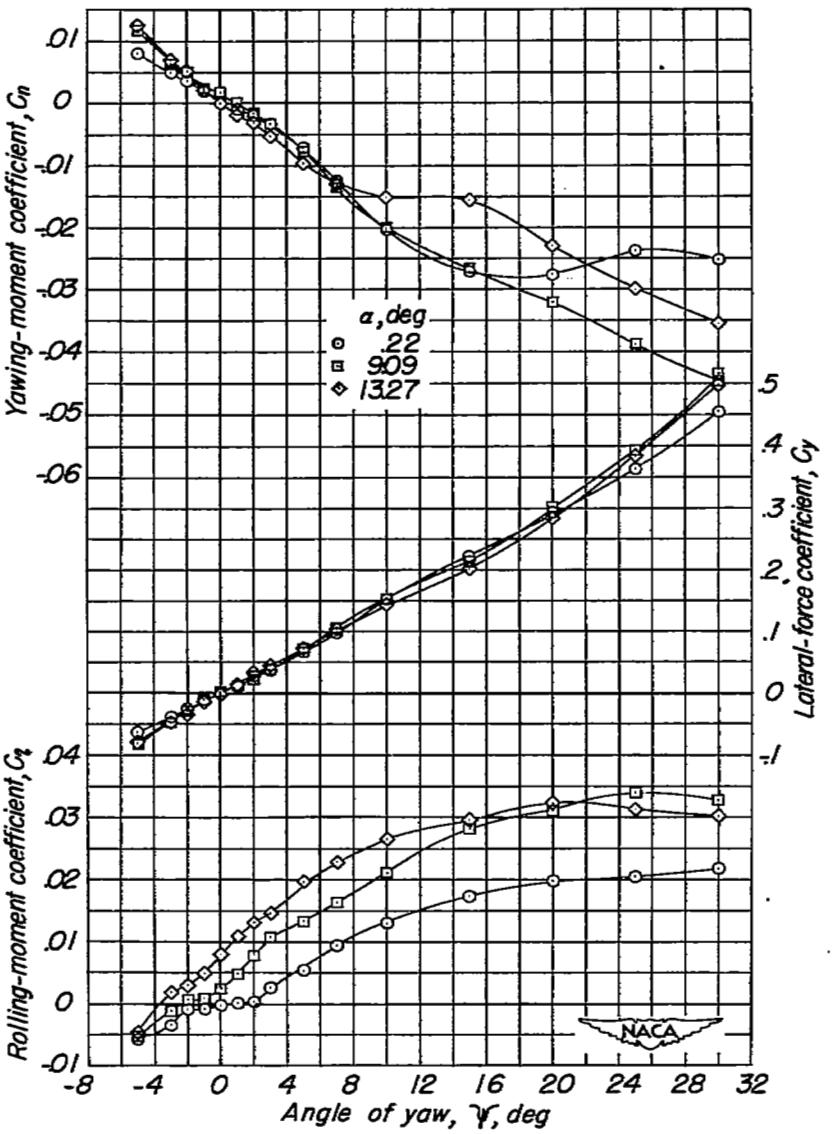

(a) $\Lambda = 20^\circ$.

Figure 7.- The effect of angle of attack on the aerodynamic characteristics in yaw of the test model. Slats retracted; $\delta_f = 0^\circ$; $i_t = -\frac{3}{4}^\circ$.

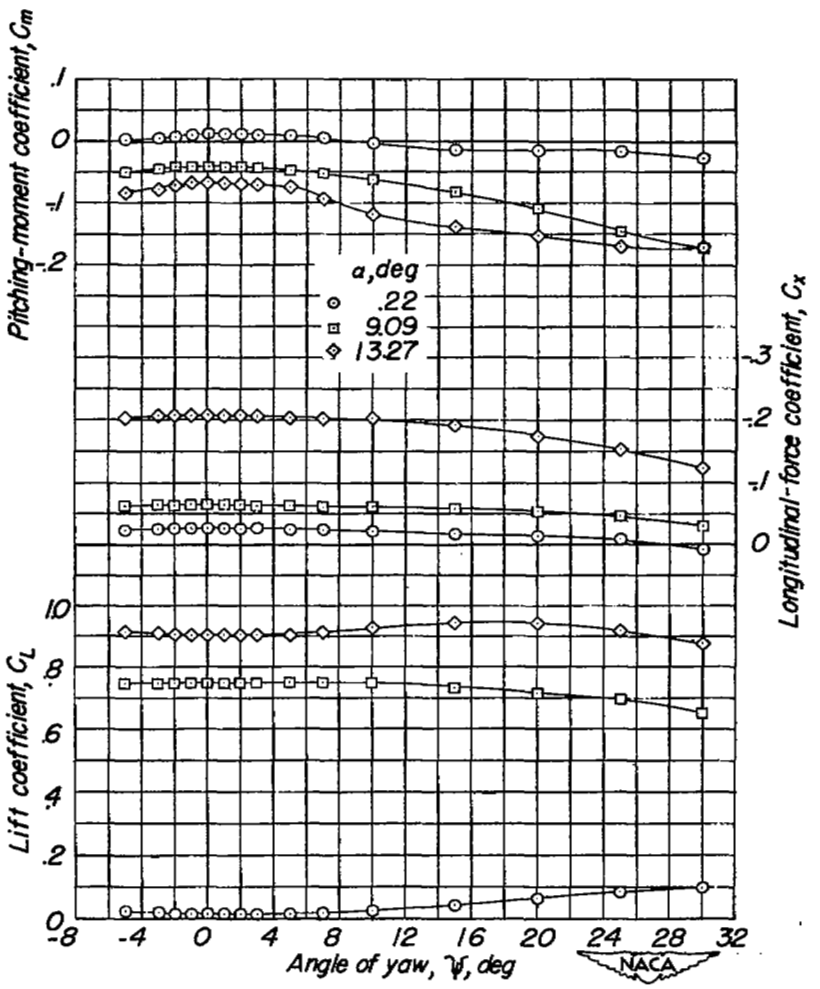

(a) Concluded.

Figure 7.- Continued.

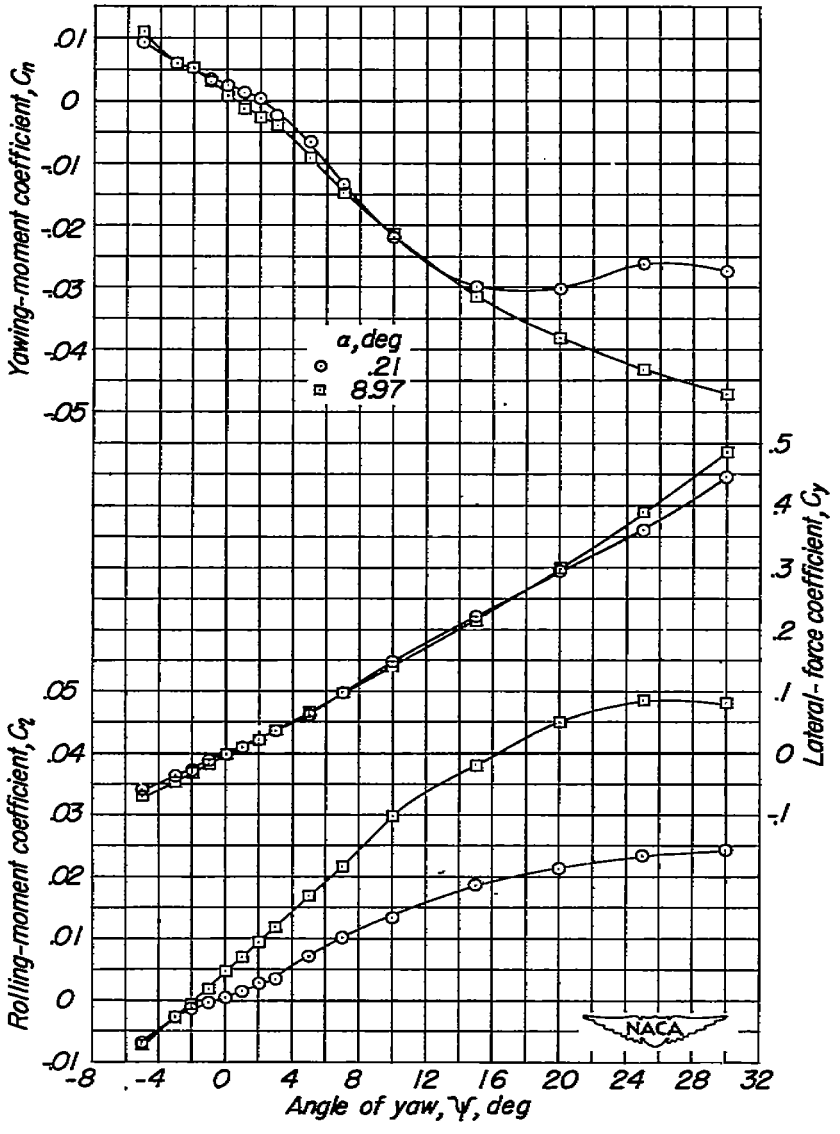

(b) $\Lambda = 35^{\circ}$.

Figure 7.- Continued.

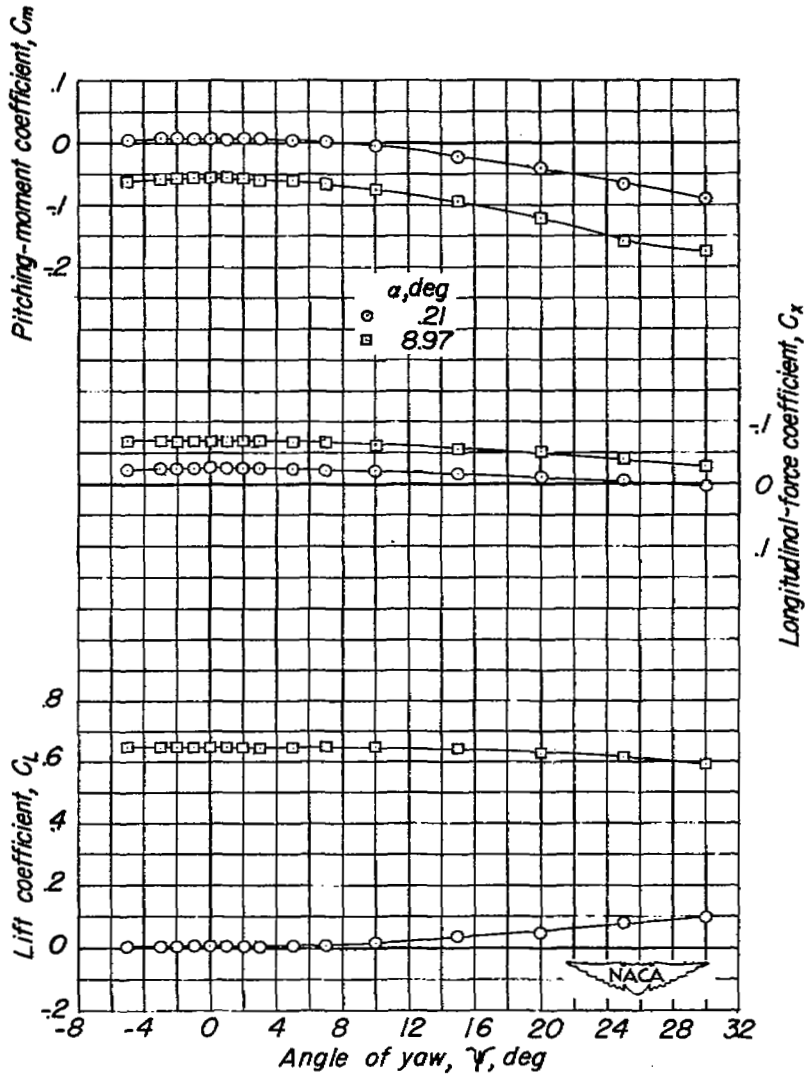

(b) Concluded.

Figure 7.- Continued.

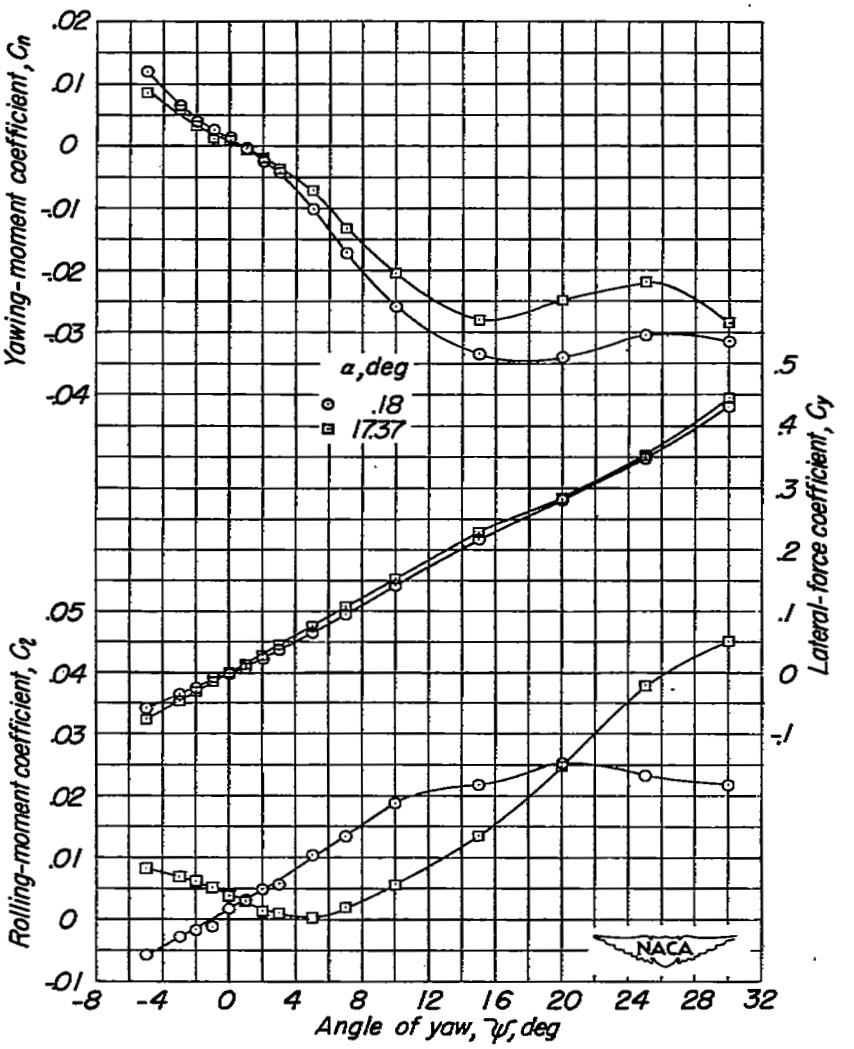

(c) $\Lambda = 50^\circ$.

Figure 7.- Continued.

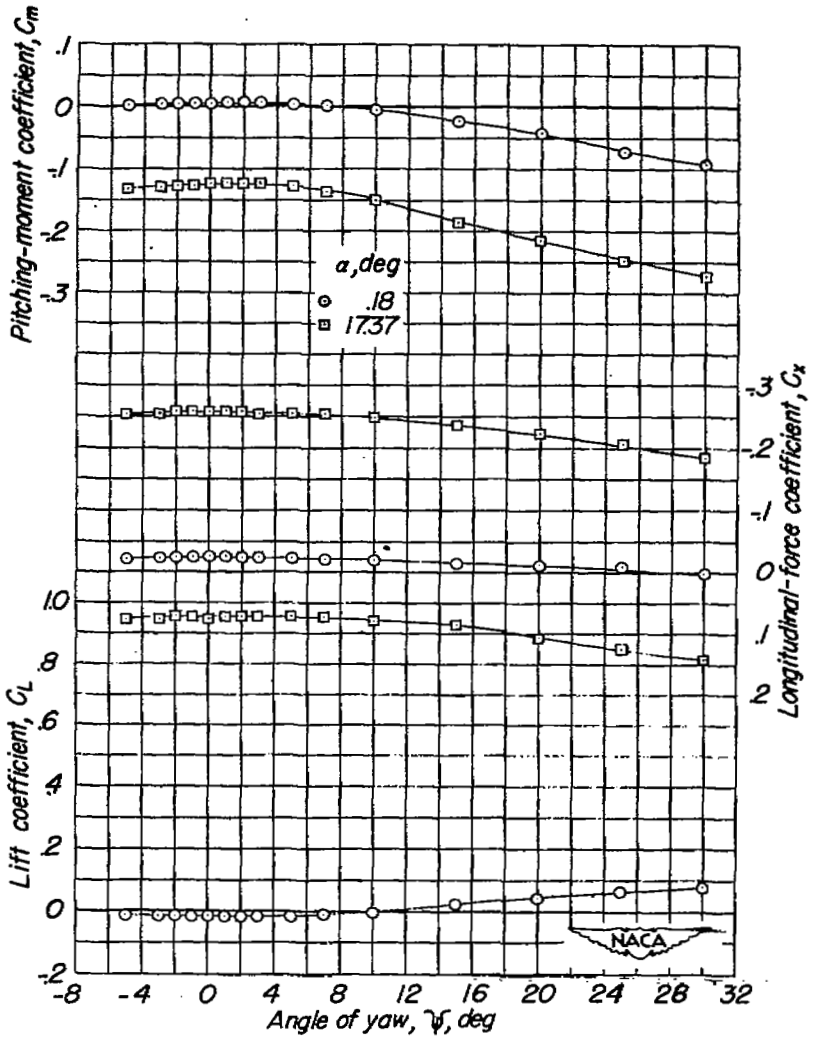

(c) Concluded.

Figure 7.- Continued.

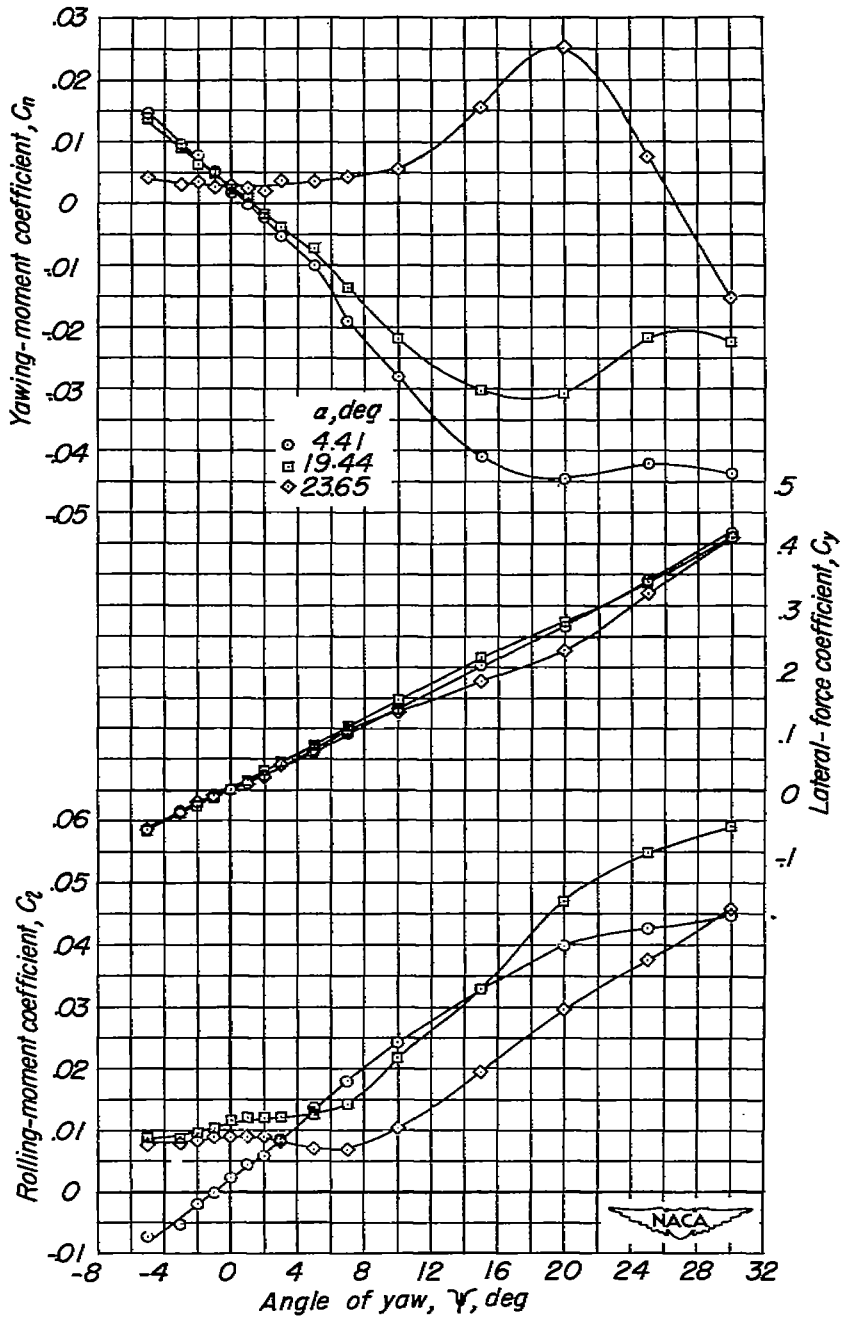

(d) $\Lambda = 60^{\circ}$.

Figure 7.- Continued.

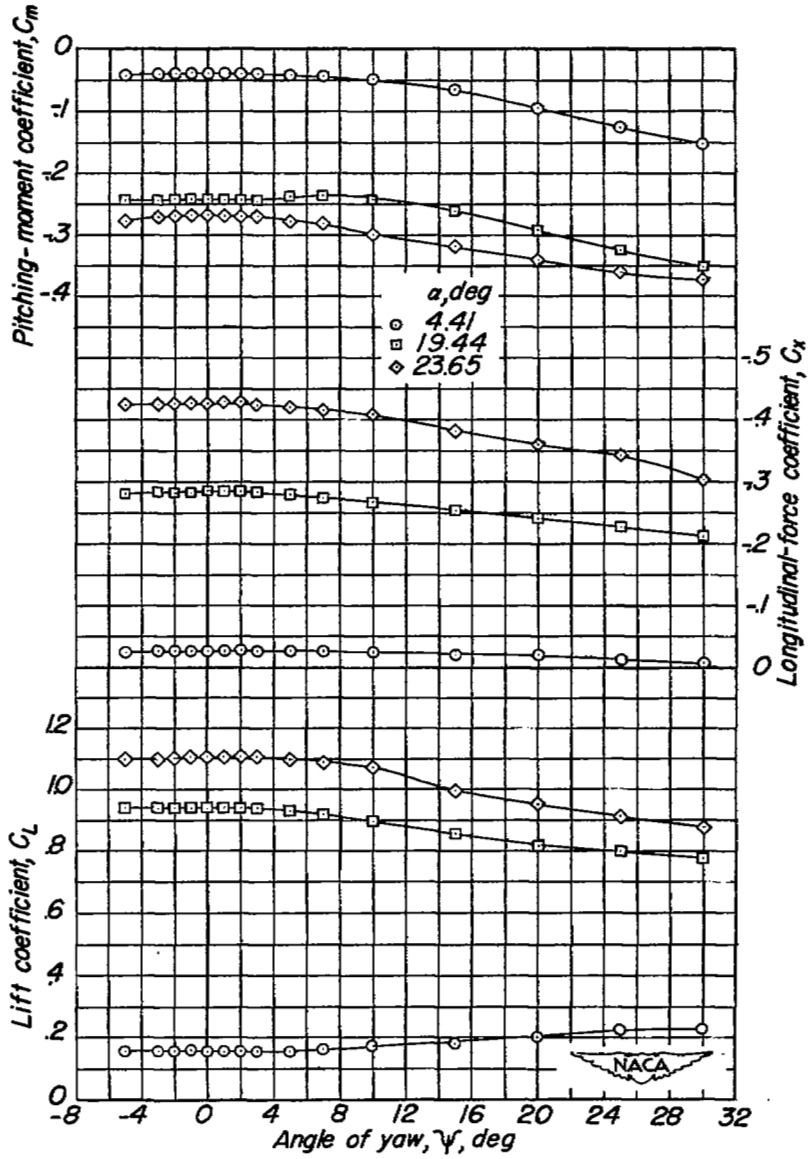

(d) Concluded.

Figure 7.- Concluded.

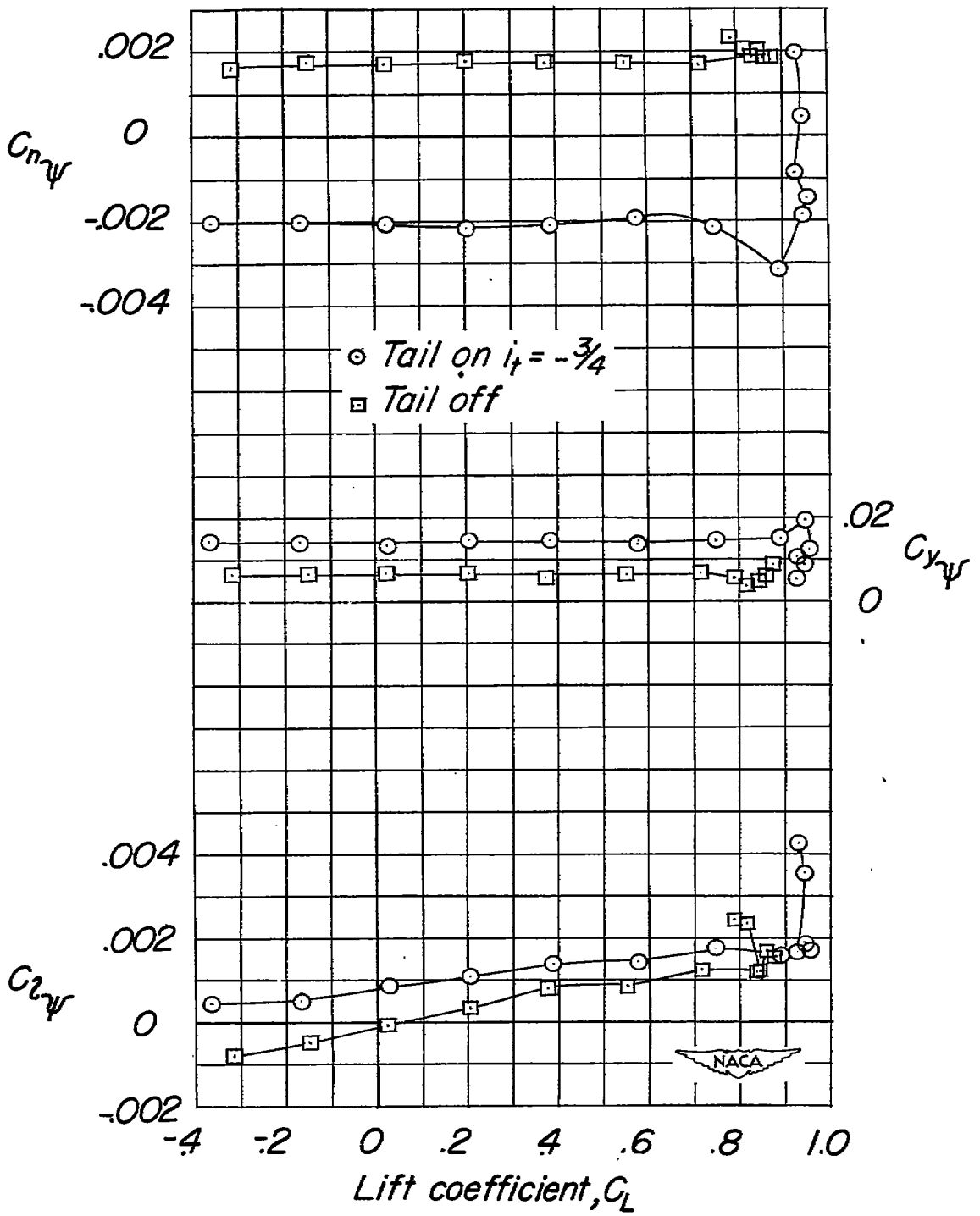

Figure 8.- The effect of the tail on the lateral-stability parameters of the test model. $\Lambda = 20^\circ$; slats retracted; $\delta_f = 0^\circ$.

[redacted]

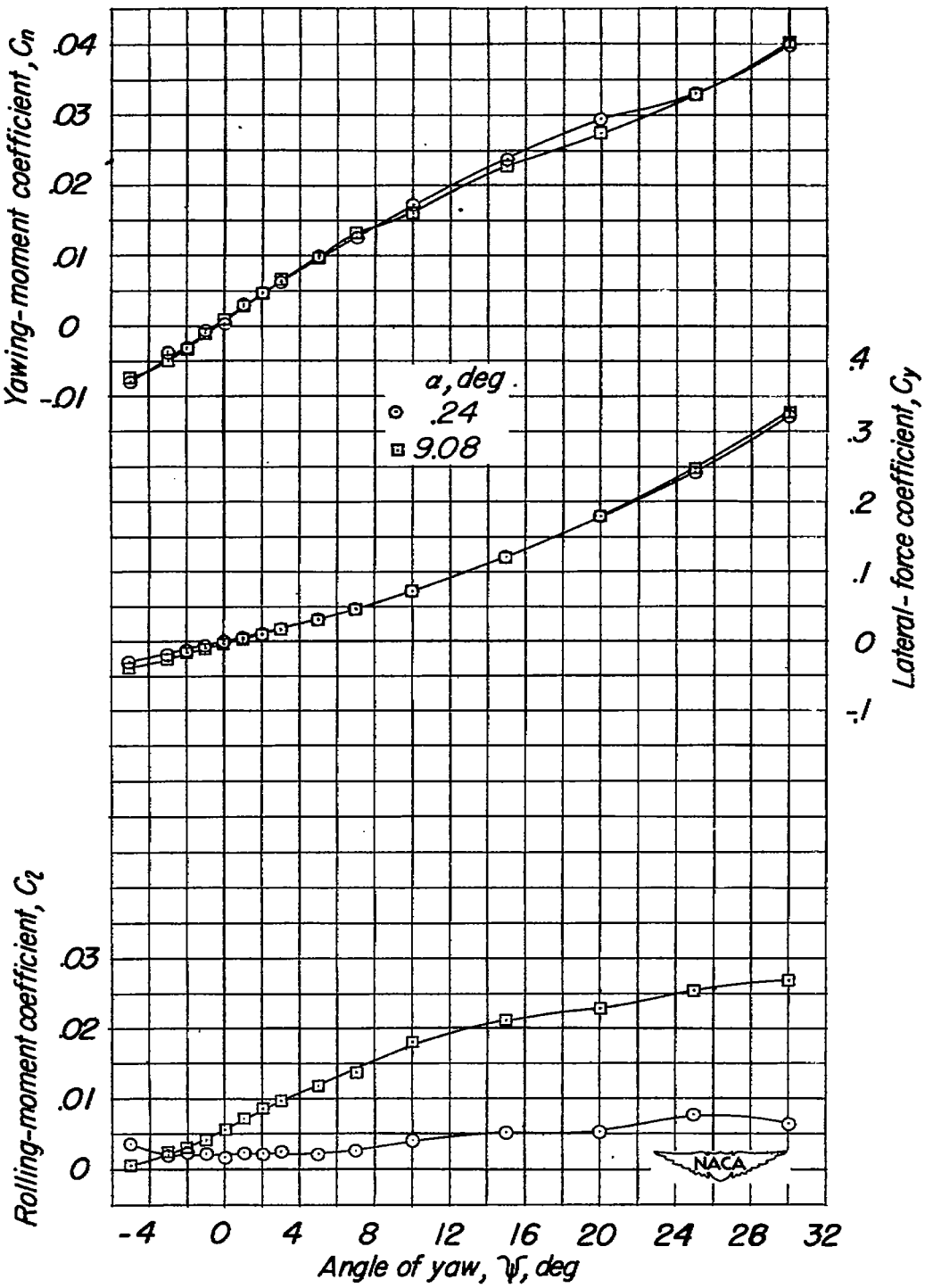

Figure 9.- The effect of angle of attack on the aerodynamic characteristics in yaw of the test model. $\Lambda = 20^\circ$; slats retracted; $\delta_f = 0^\circ$; tail off.

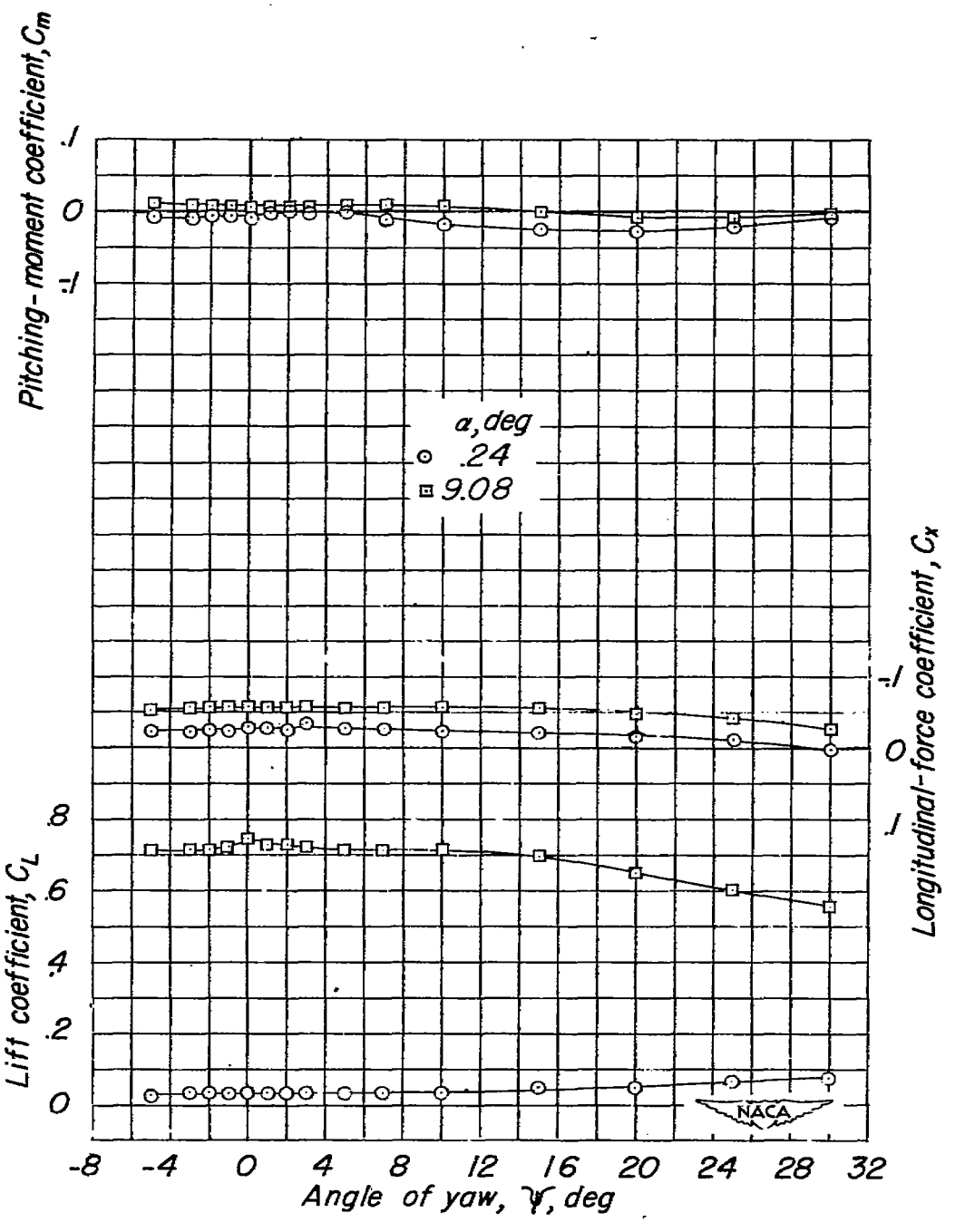

Figure 9.- Concluded.

[redacted]

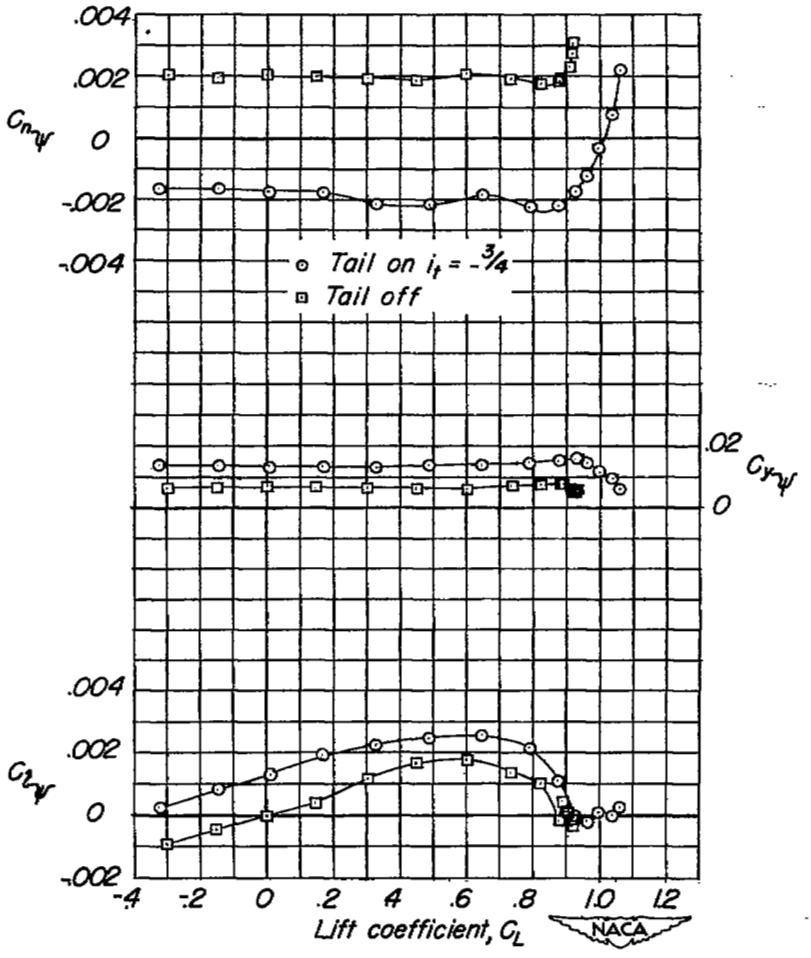

Figure 10.- The effect of the tail on the lateral-stability parameters of the test model. $\Lambda = 35^\circ$; slats retracted; $\delta_f = 0^\circ$.

[redacted]

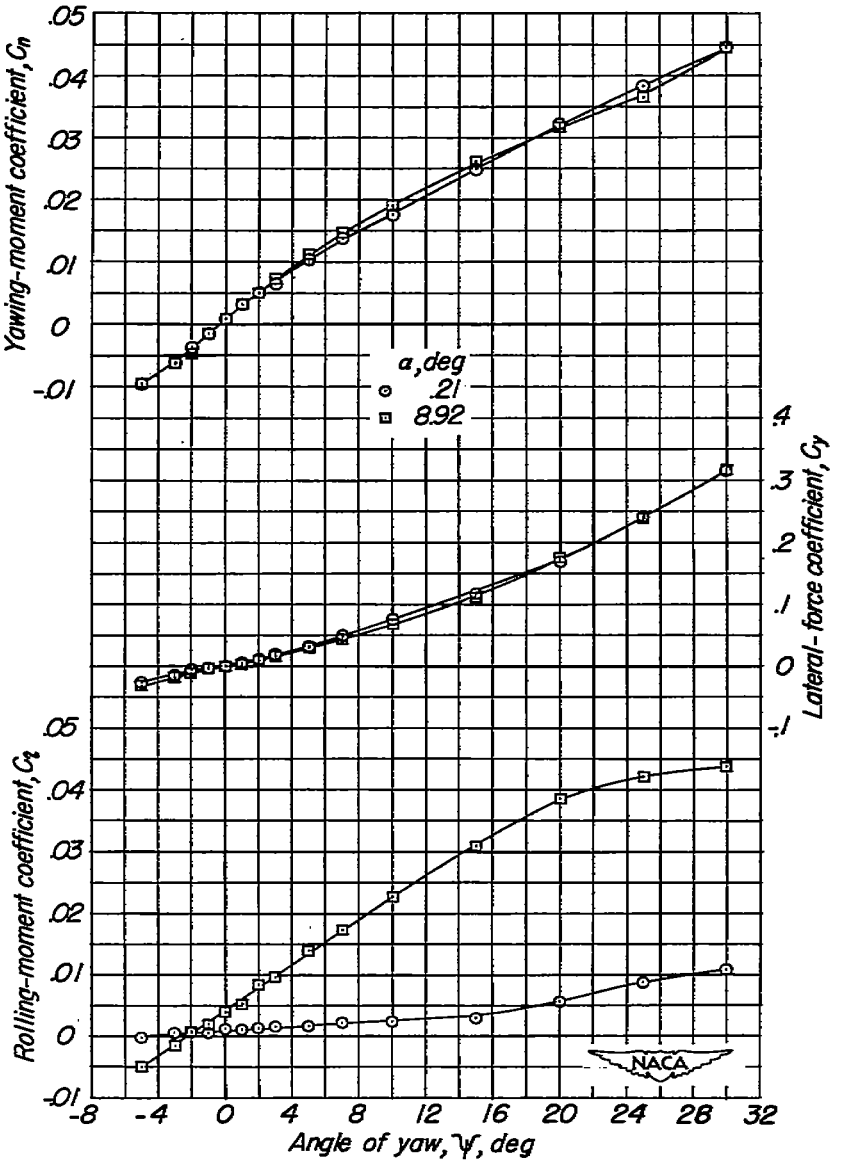

Figure 11.- The effect of angle of attack on the aerodynamic characteristics in yaw of the test model. $\Lambda = 35^\circ$; slats retracted; $\delta_f = 0^\circ$; tail off.

[redacted]

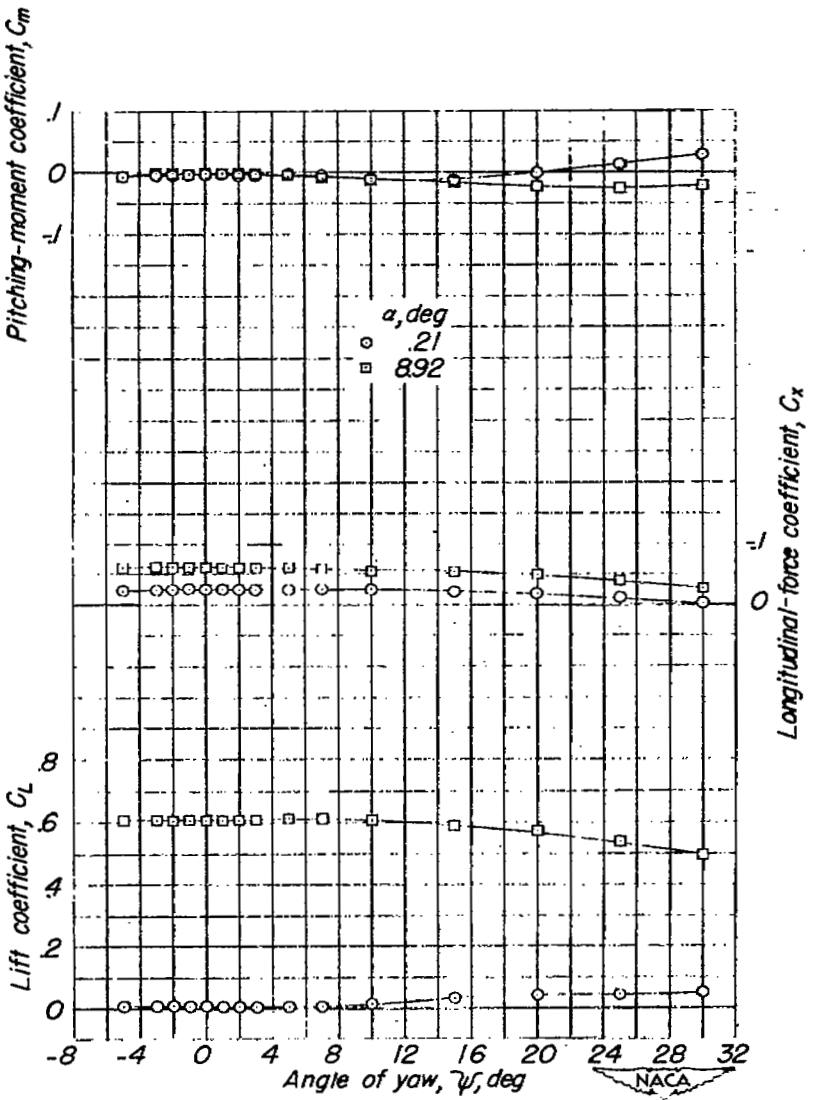

Figure 11.- Concluded.

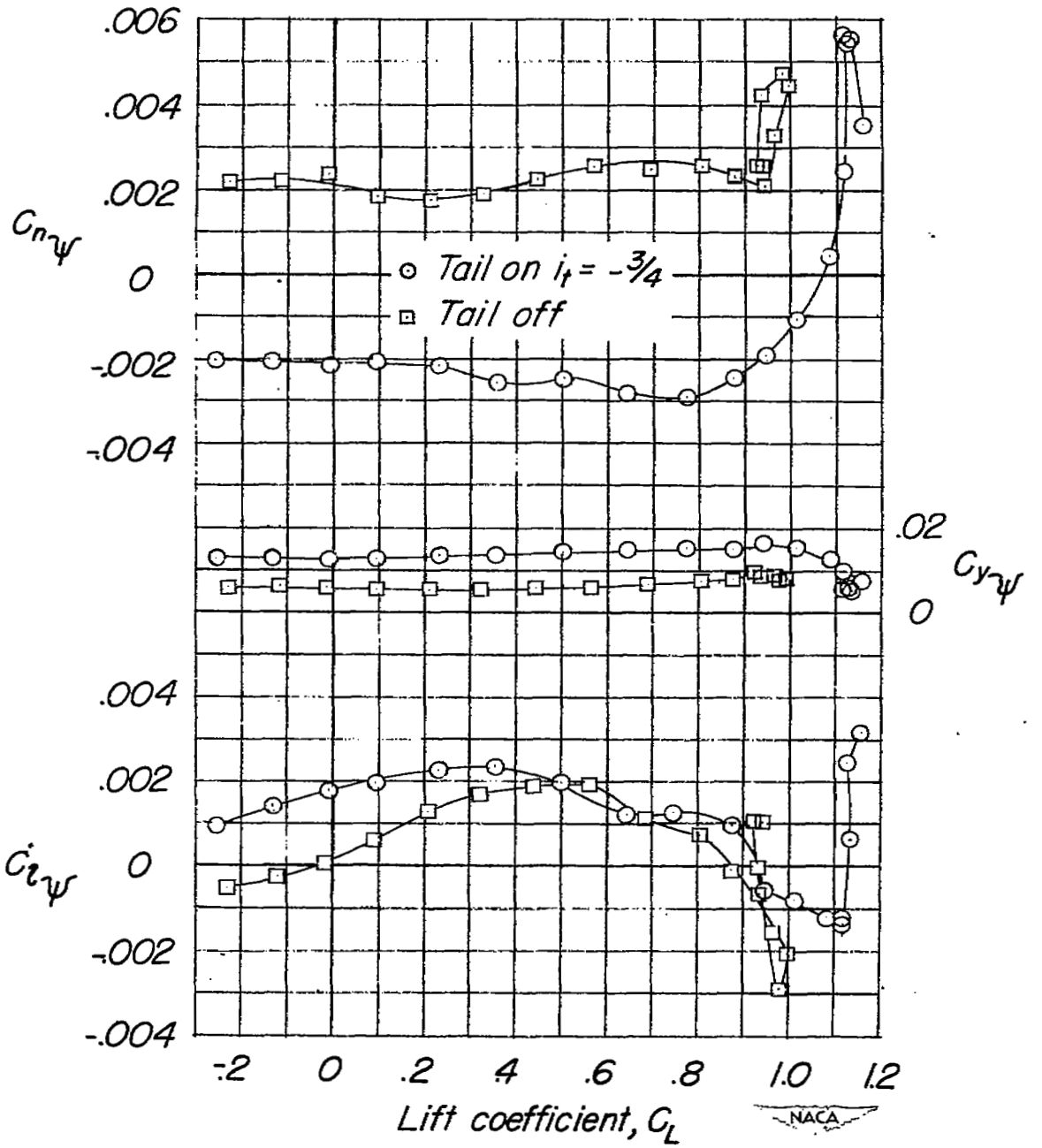

Figure 12.- The effect of the tail on the lateral-stability parameters of the test model. $\Lambda = 50^\circ$; slats retracted; $\delta_f = 0^\circ$.

[redacted]

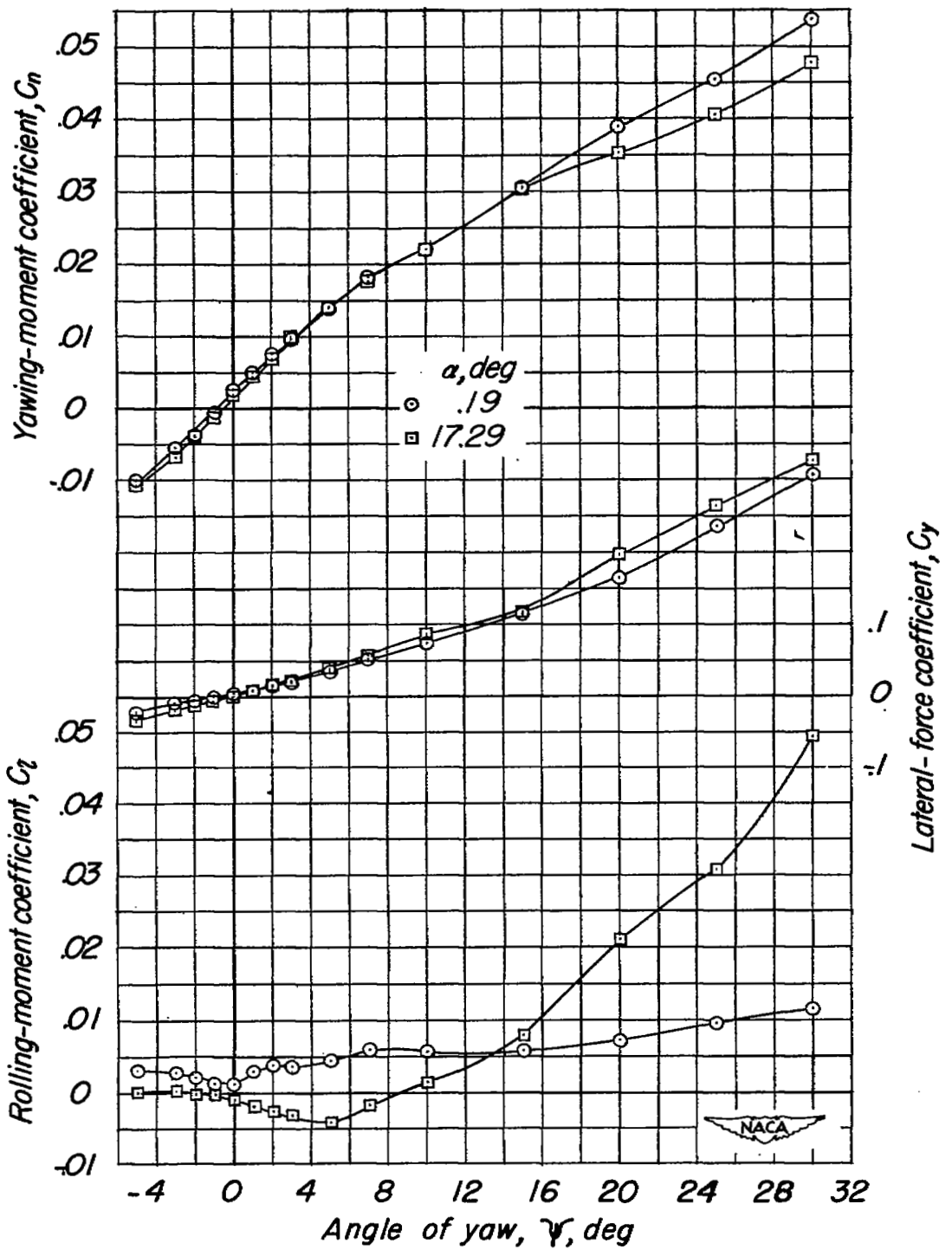

Figure 13.- The effect of angle of attack on the aerodynamic characteristics in yaw of the test model. $\Lambda = 50^\circ$; slats retracted; $\delta_f = 0^\circ$; tail off.

[redacted]

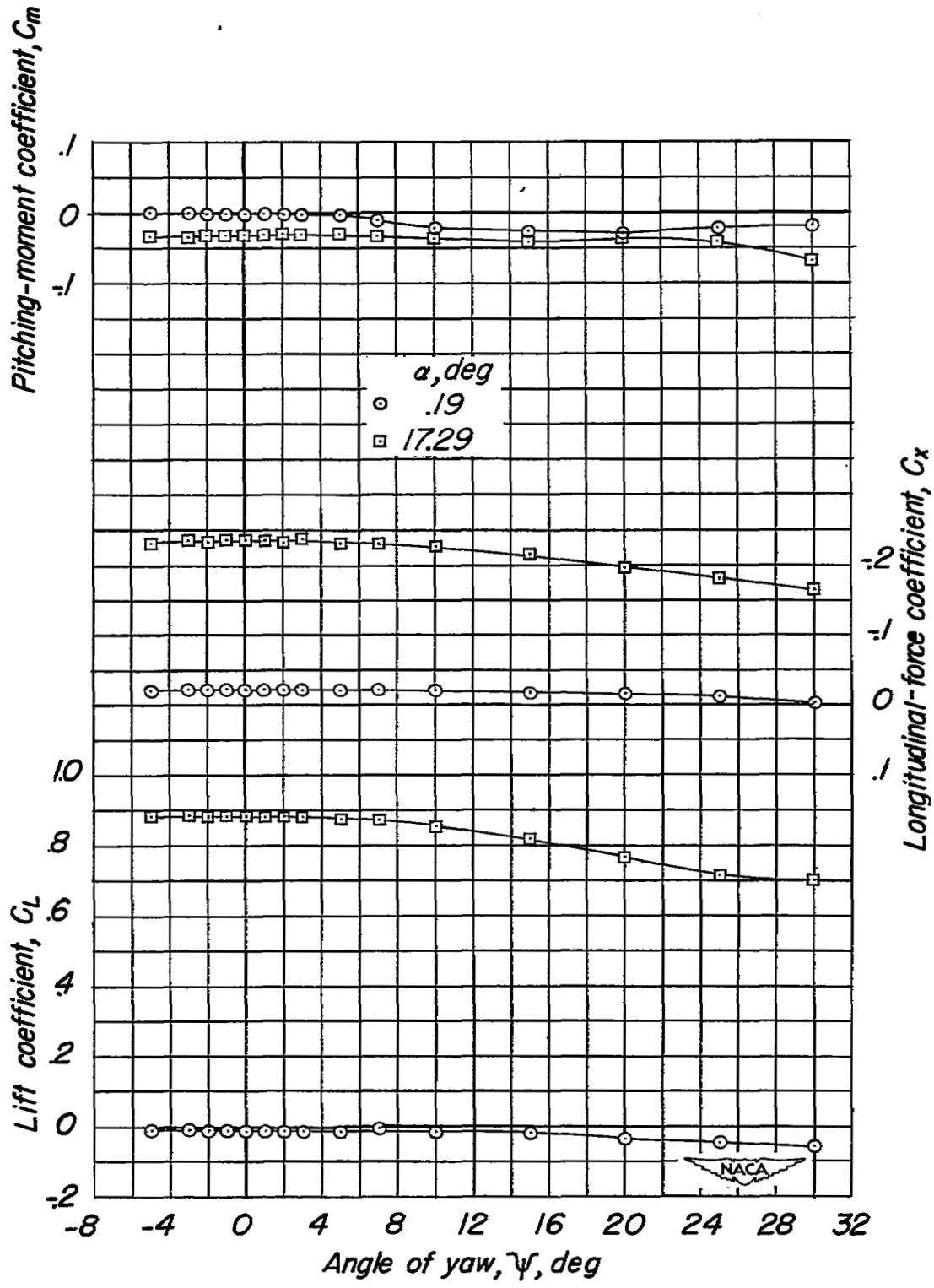

Figure 13.- Concluded.

[redacted]

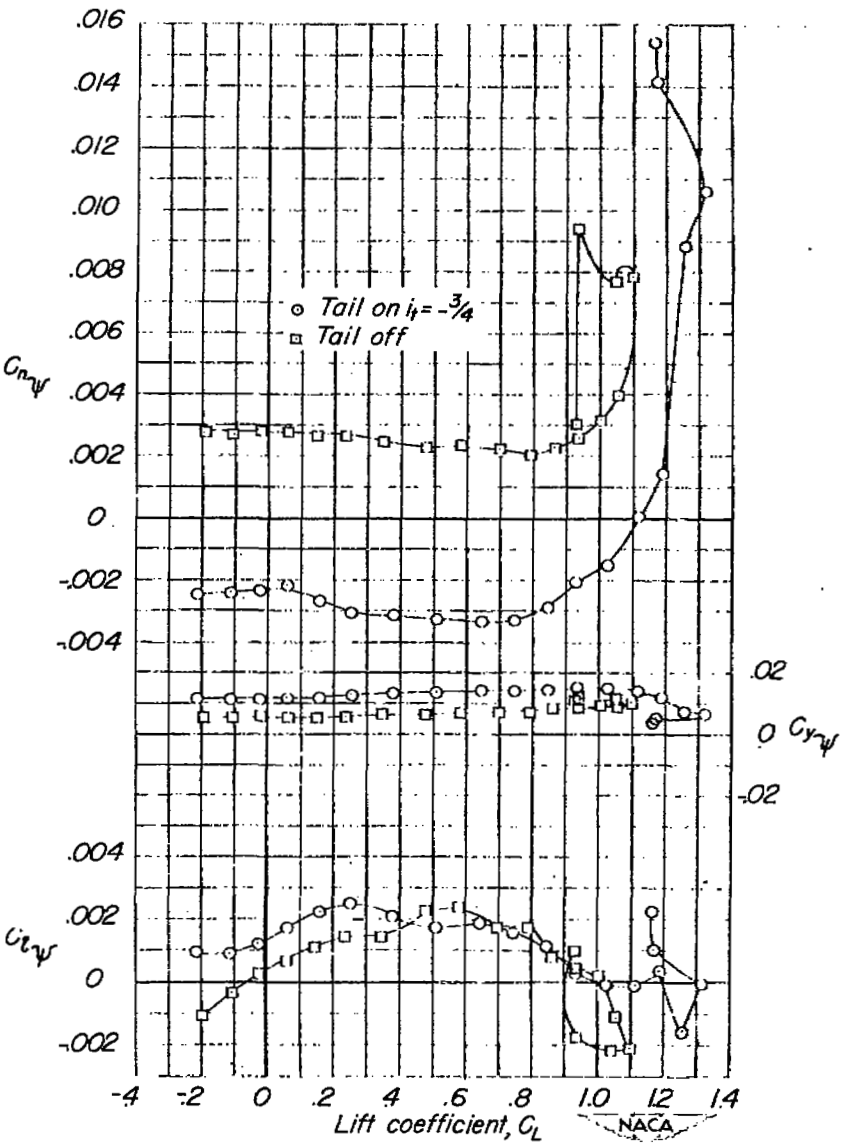

Figure 14.- The effect of the tail on the lateral-stability parameters of the test model. $\Lambda = 60^\circ$; slats retracted; $\delta_f = 0^\circ$.

[redacted]

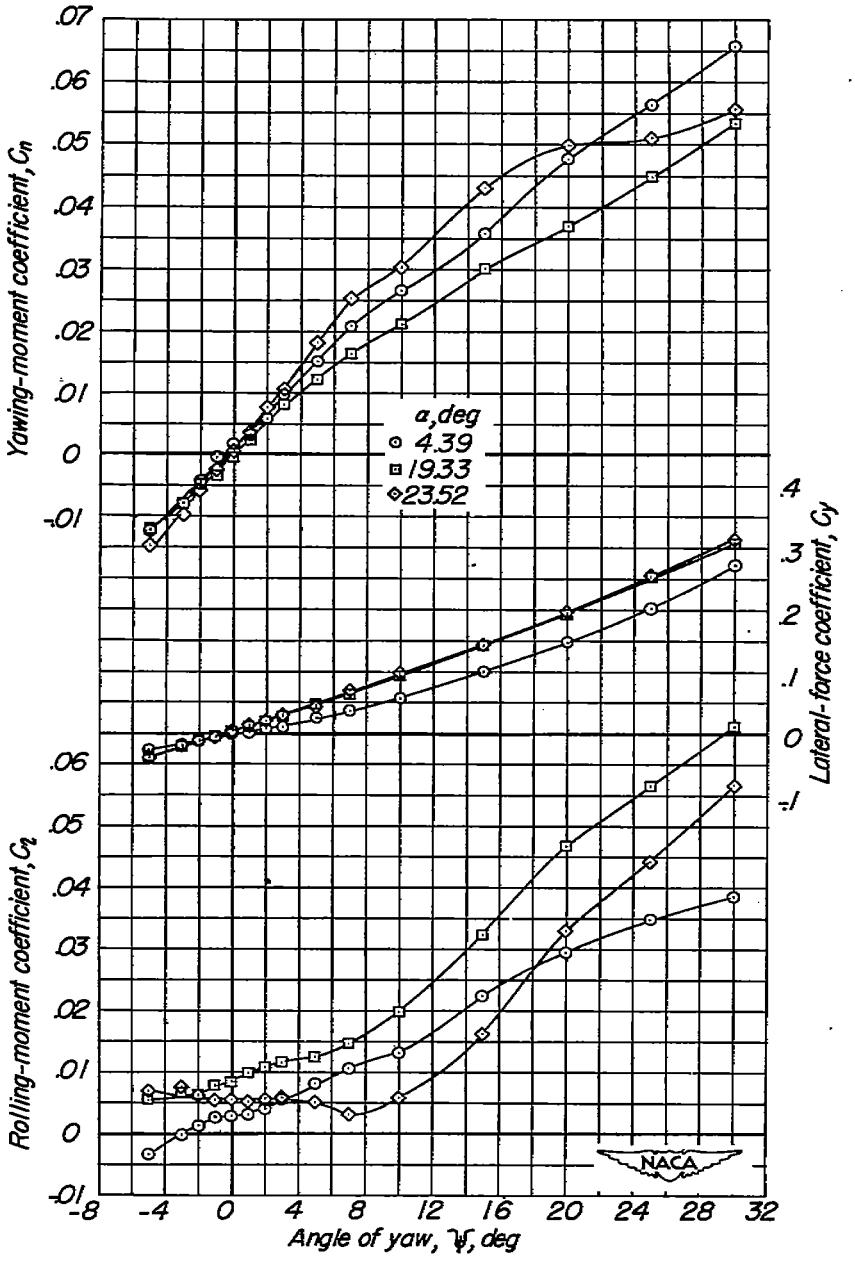

Figure 15.- The effect of angle of attack on the aerodynamic characteristics in yaw of the test model. $\Lambda = 60^\circ$; slats retracted; $\delta_f = 0^\circ$; tail off.

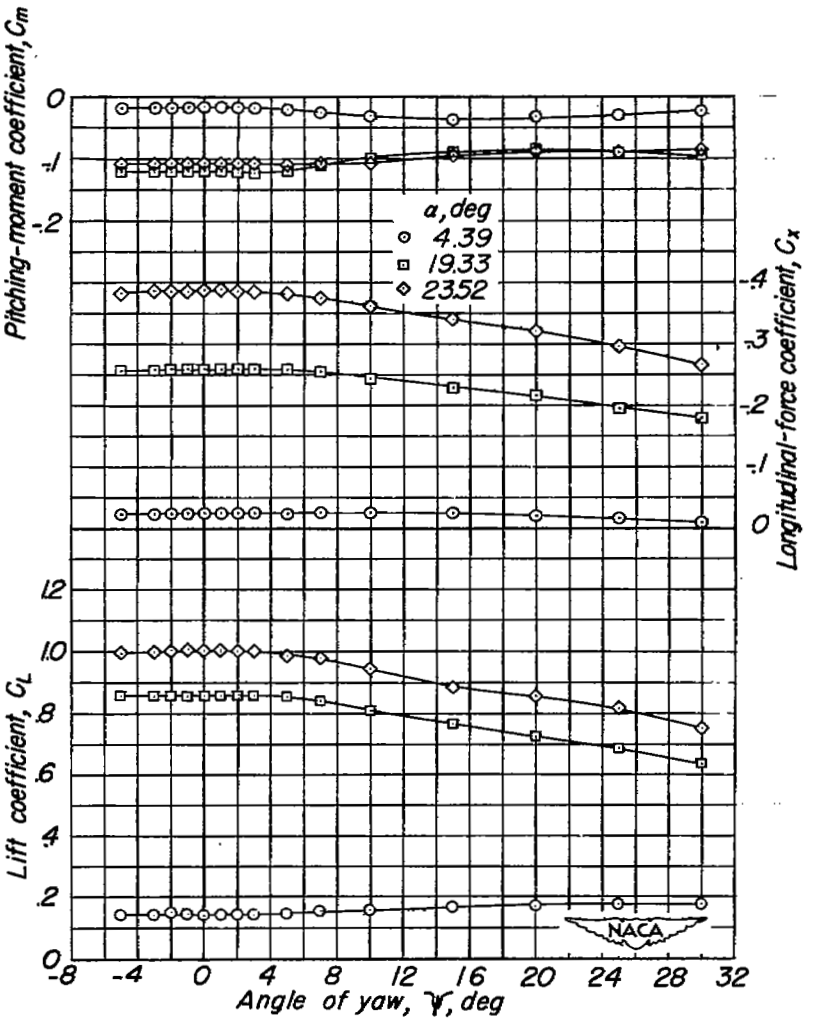

Figure 15.- Concluded.

[redacted]

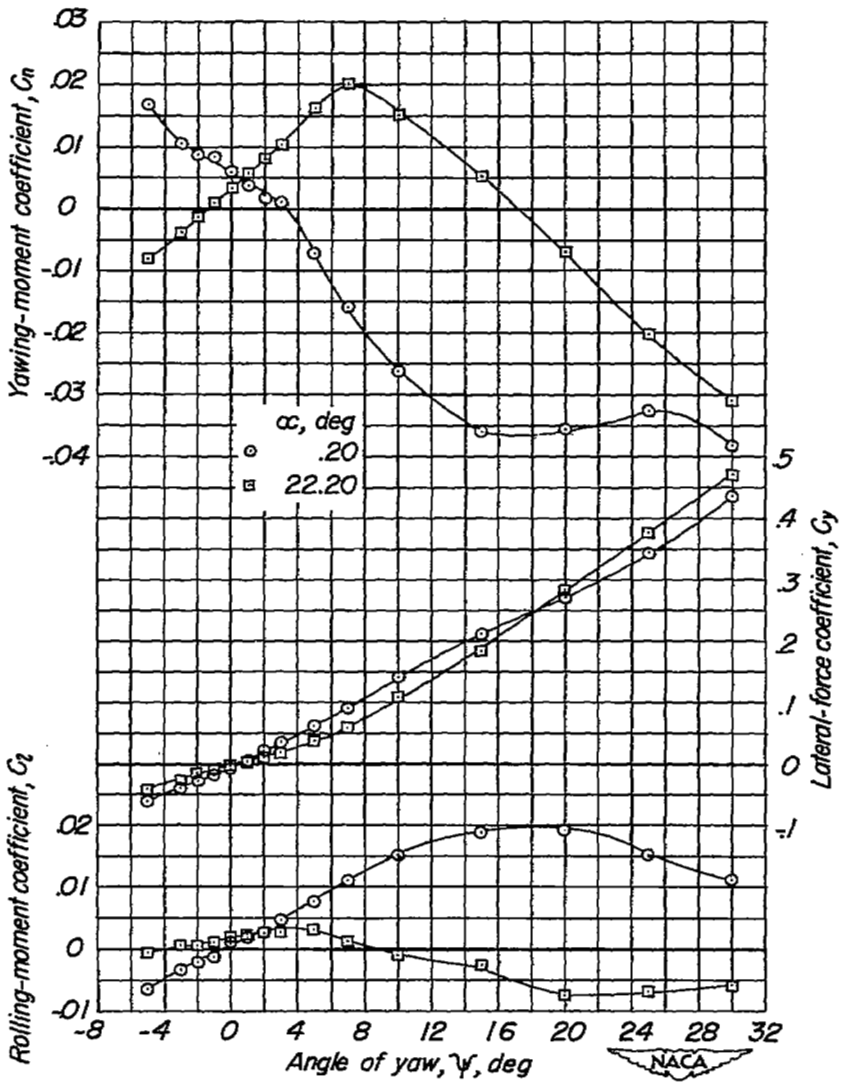

Figure 16.- The effect of angle of attack on the aerodynamic characteristics in yaw of the fuselage and tail of the test model. $i_t = -\frac{3^\circ}{4}$.

[redacted]

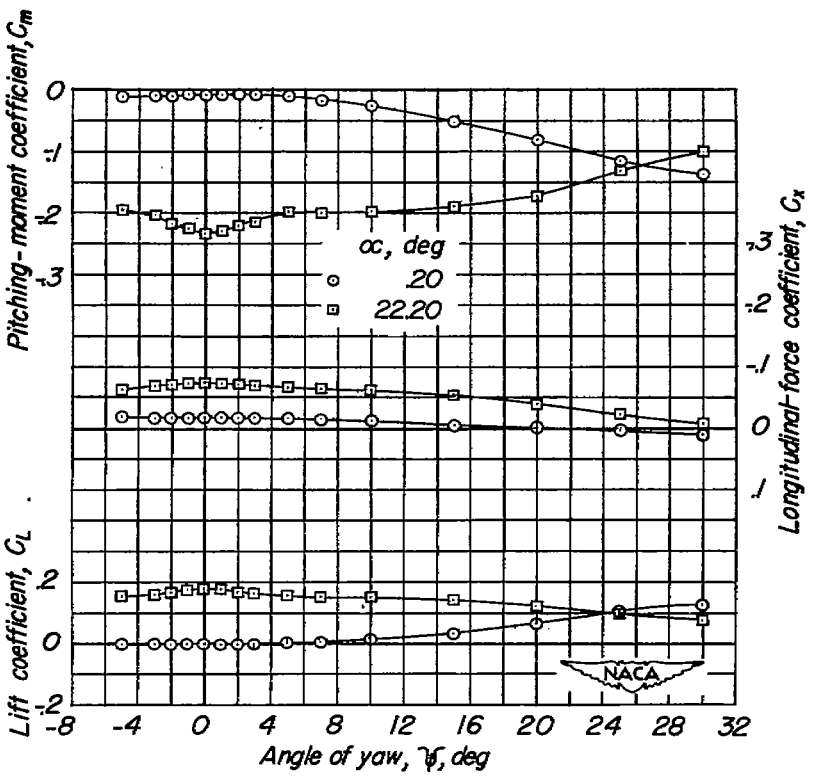

Figure 16.- Concluded.

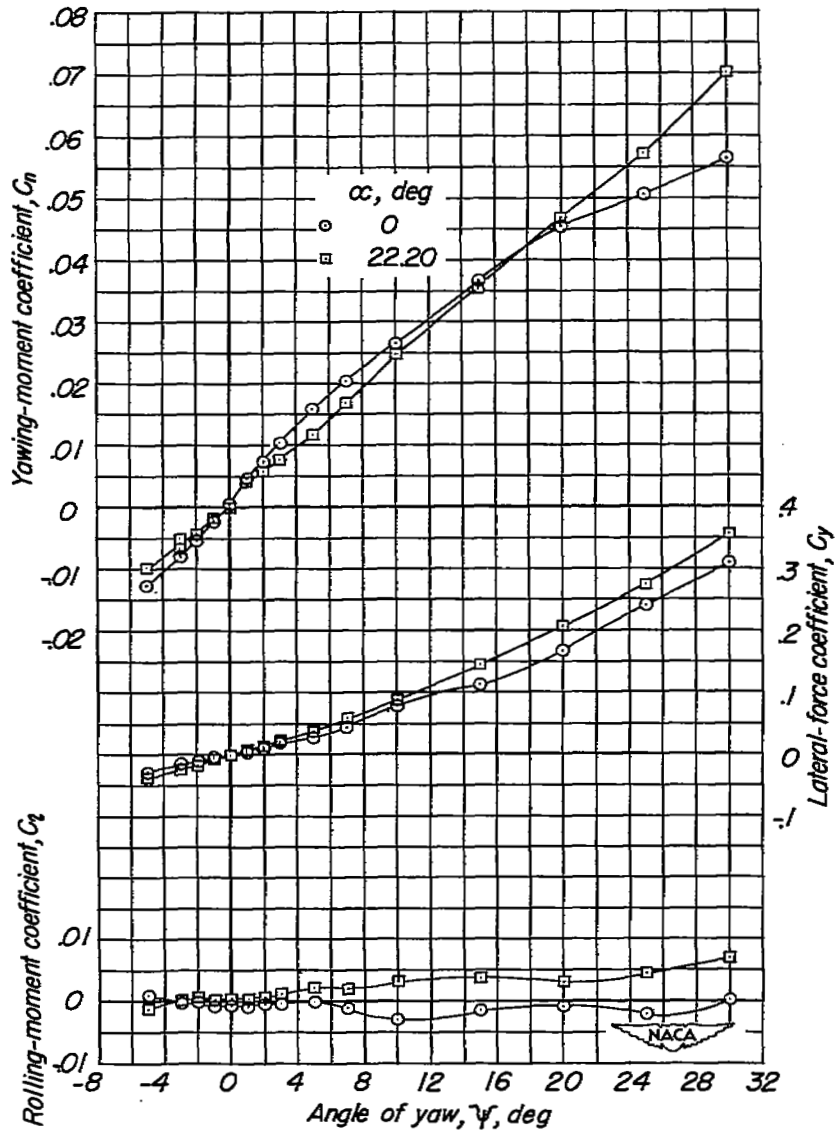

Figure 17.- The effect of angle of attack on the aerodynamic characteristics in yaw of the fuselage of the test model.

[redacted]

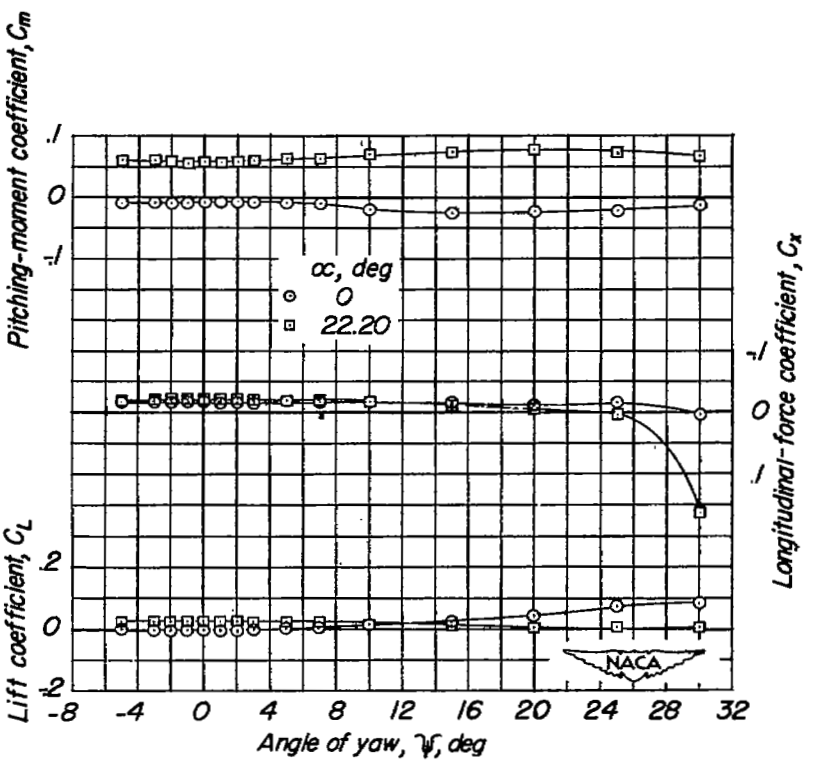

Figure 17.- Concluded.

[redacted]

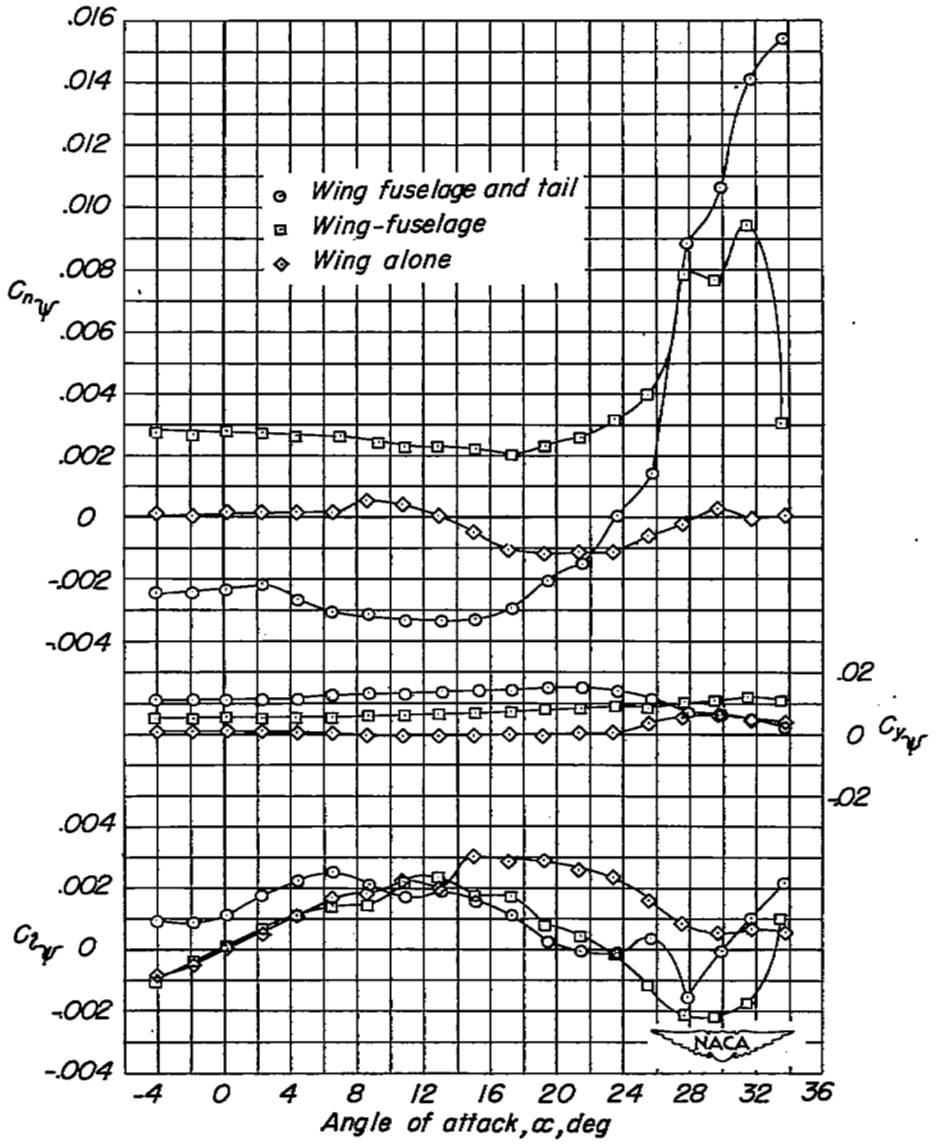

Figure 18.- The effect of the component model parts on the lateral-stability parameters. $\Lambda = 60^\circ$; slats retracted; $\delta_f = 0^\circ$; $i_t = -\frac{3^\circ}{4}$.

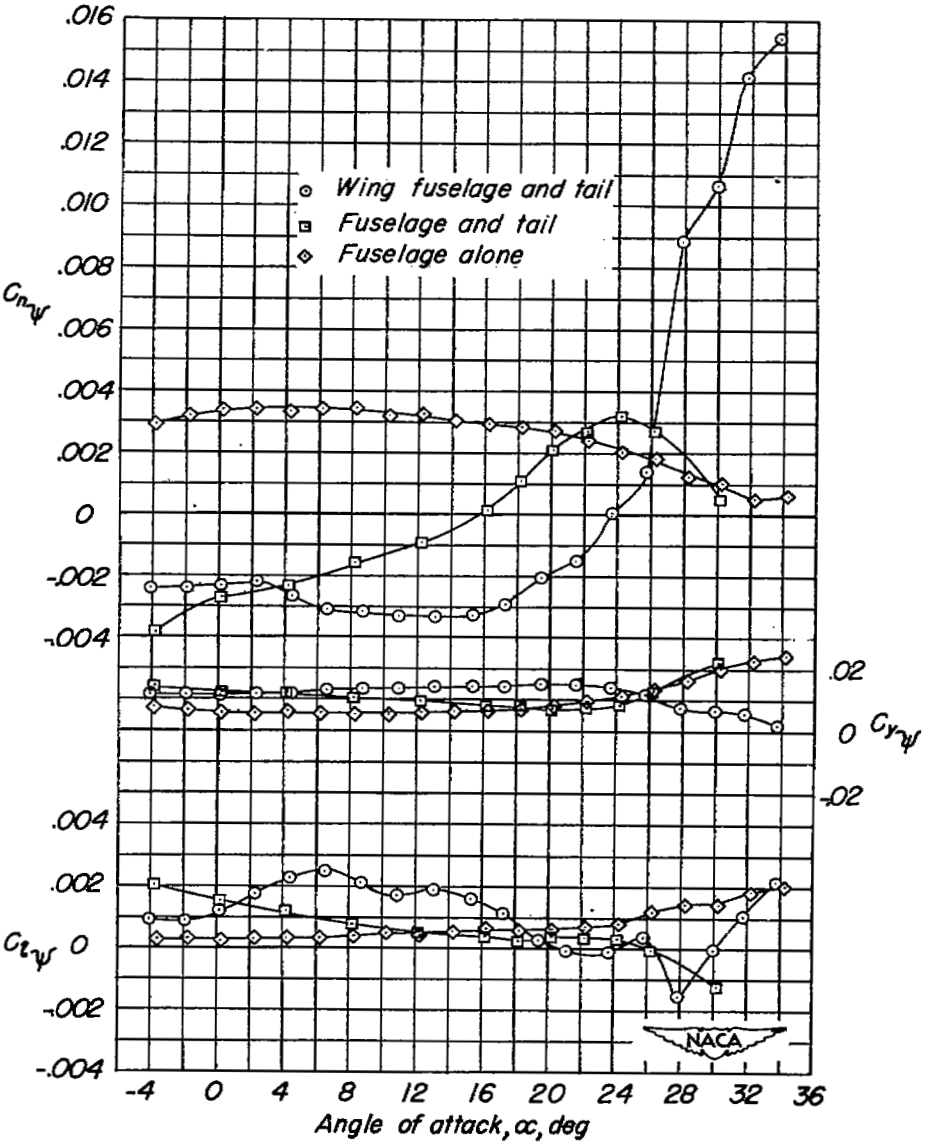

Figure 18.- Concluded.

[redacted]

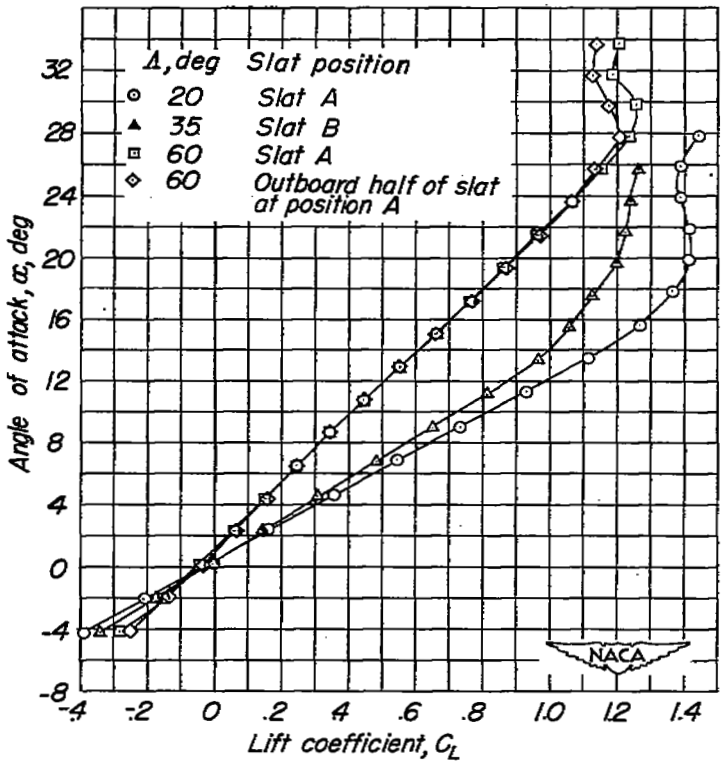

Figure 19.- The effect of sweep on the lift curves for the test model. Slats extended; $\delta_f = 0^\circ$; $i_t = -\frac{3^\circ}{4}$.

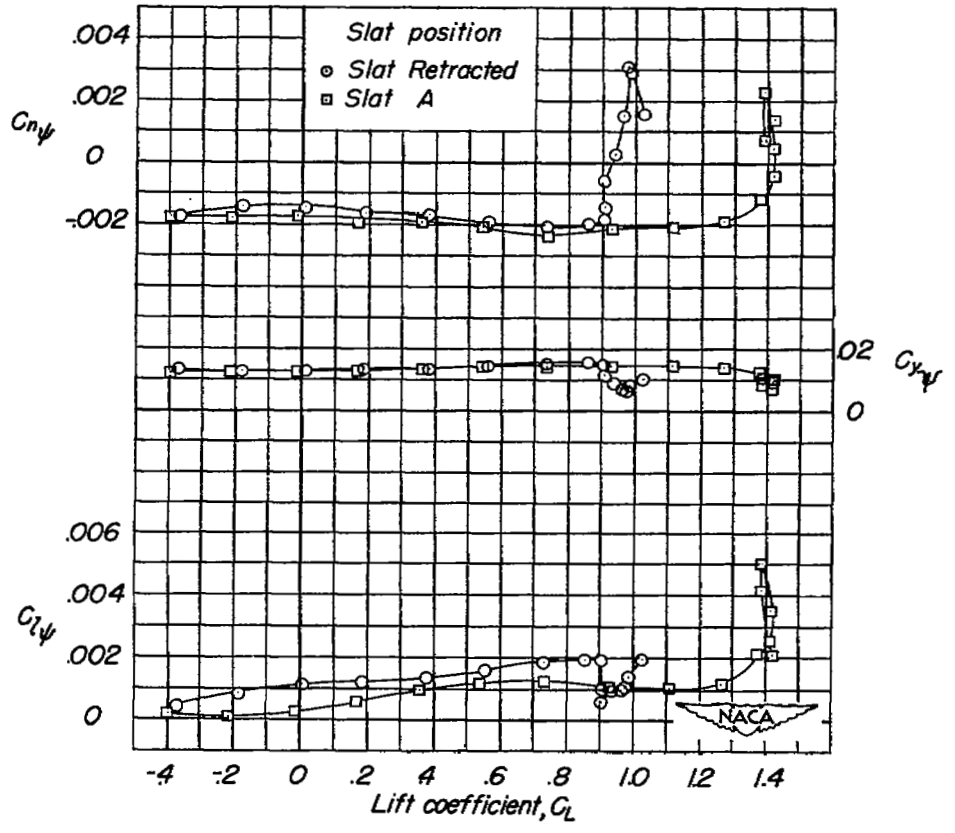

Figure 20.- The effect of slat position on the lateral-stability parameters of the test model. $\Lambda = 20^\circ$; $\delta_f = 0^\circ$; $i_t = -\frac{3^\circ}{4}$.

[redacted]

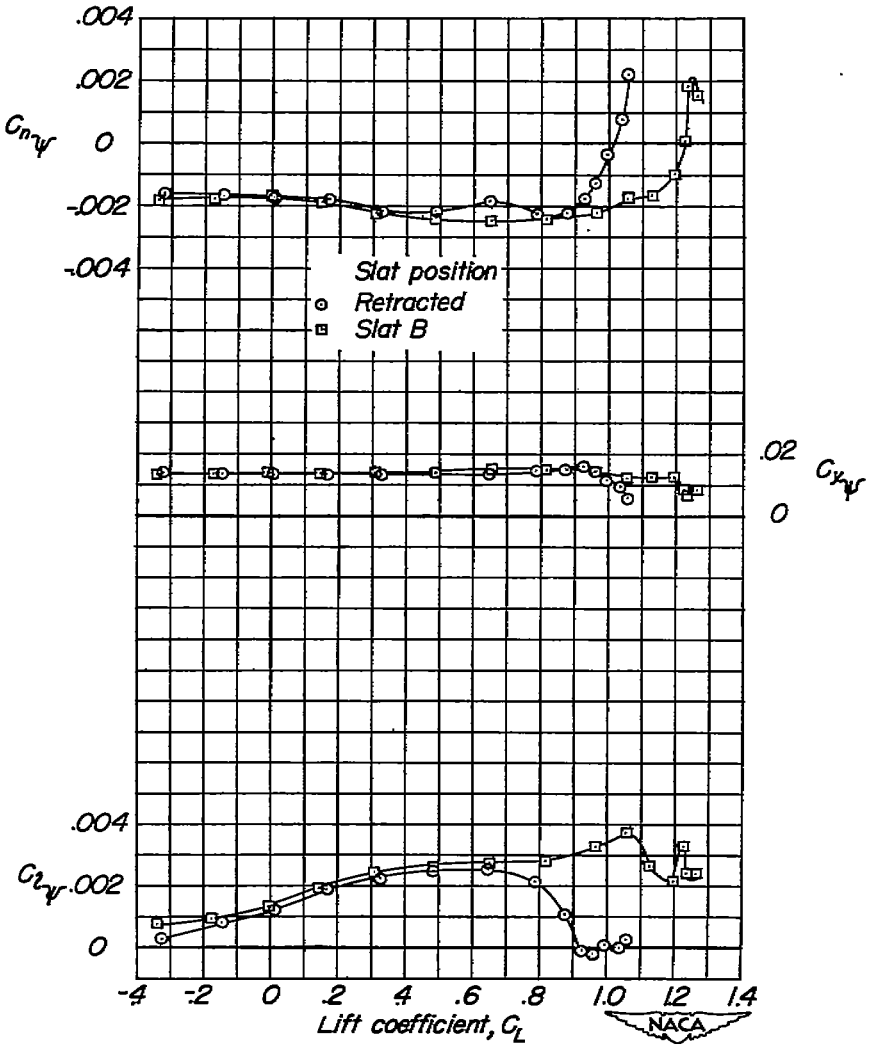

Figure 21.- The effect of slat position on the lateral-stability parameters of the test model. $\Lambda = 35^\circ$; $\delta_f = 0^\circ$; $i_t = -\frac{3^\circ}{4}$.

[redacted]

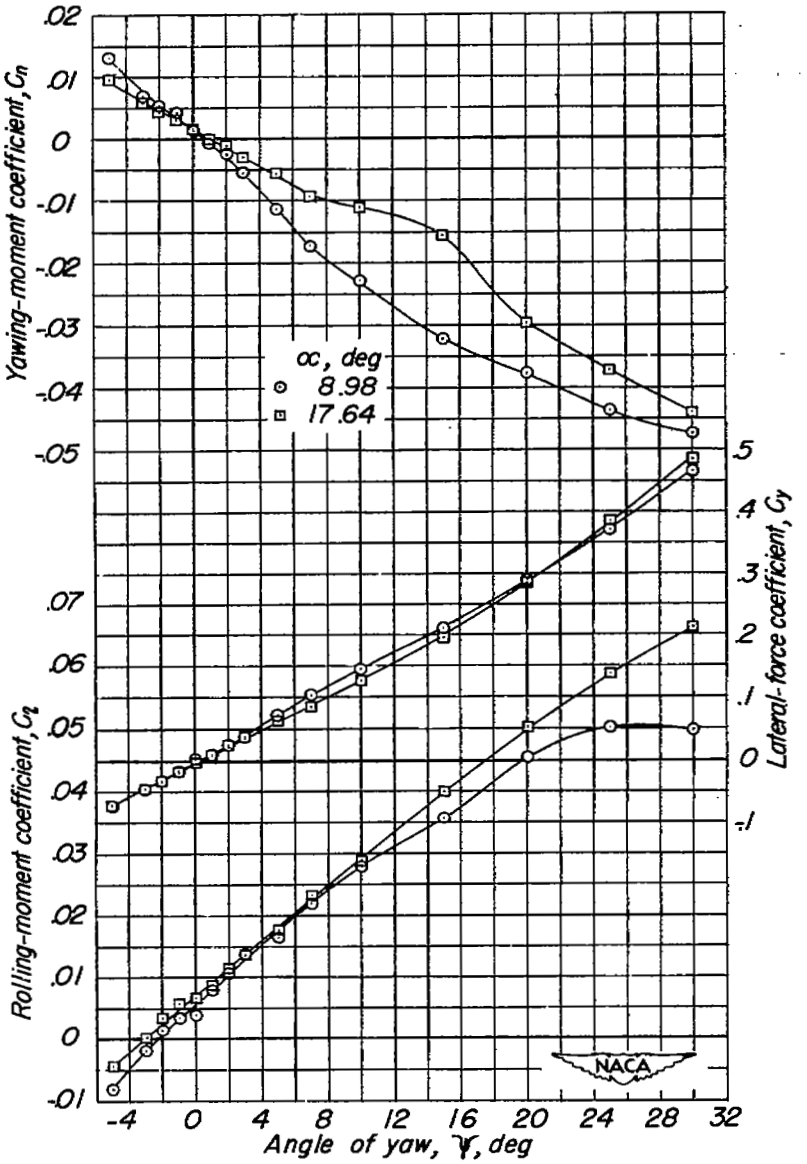

Figure 22.- The effect of angle of attack on the aerodynamic characteristics in yaw of the test model. $\Lambda = 35^\circ$; slat B; $\delta_f = 0^\circ$; $i_t = -\frac{3^\circ}{4}$.

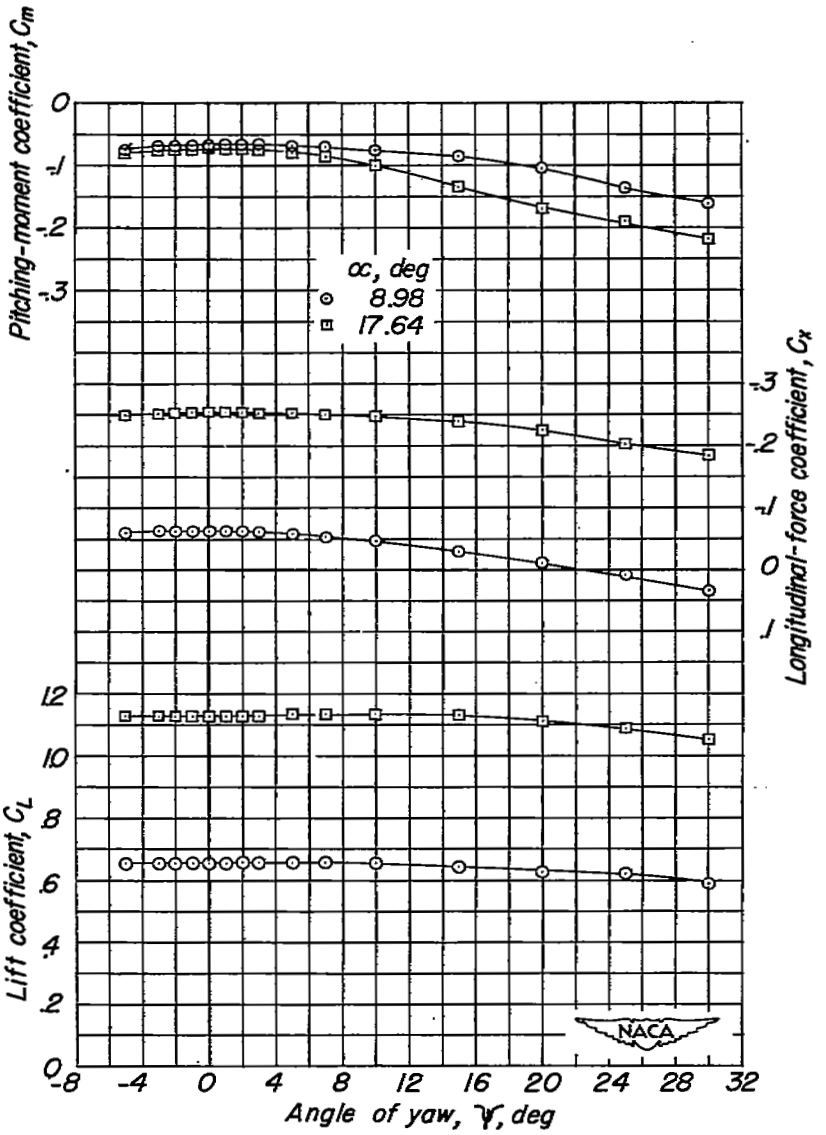

Figure 22.- Concluded.

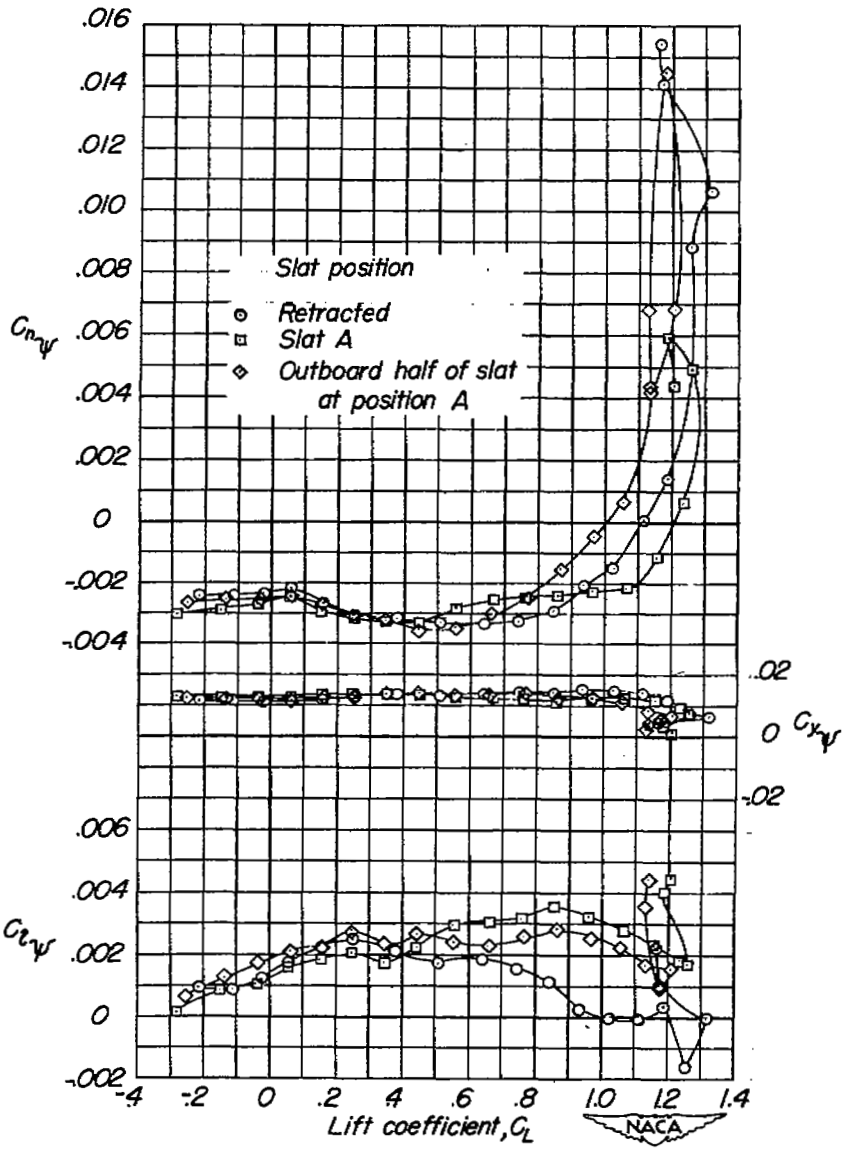

Figure 23.- The effect of slat position on the lateral-stability parameters of the test model. $\Lambda = 60^\circ$; $\delta_f = 0^\circ$; $i_t = -\frac{3^\circ}{4}$.

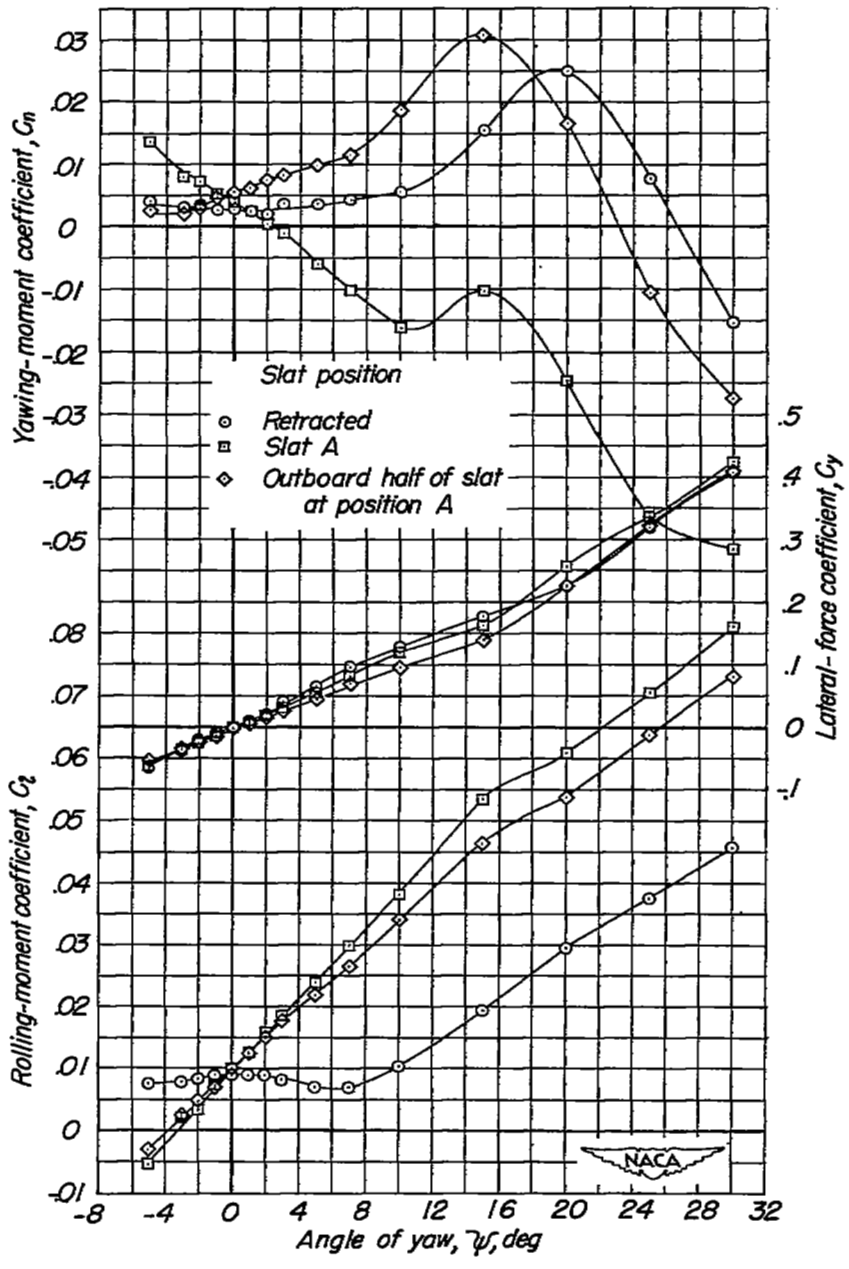

Figure 24.- The effect of slat position on the aerodynamic characteristics in yaw of the test model. $\Lambda = 60°$; $\delta_f = 0°$; $i_t = -\frac{3}{4}°$; $\alpha = 23.61°$.

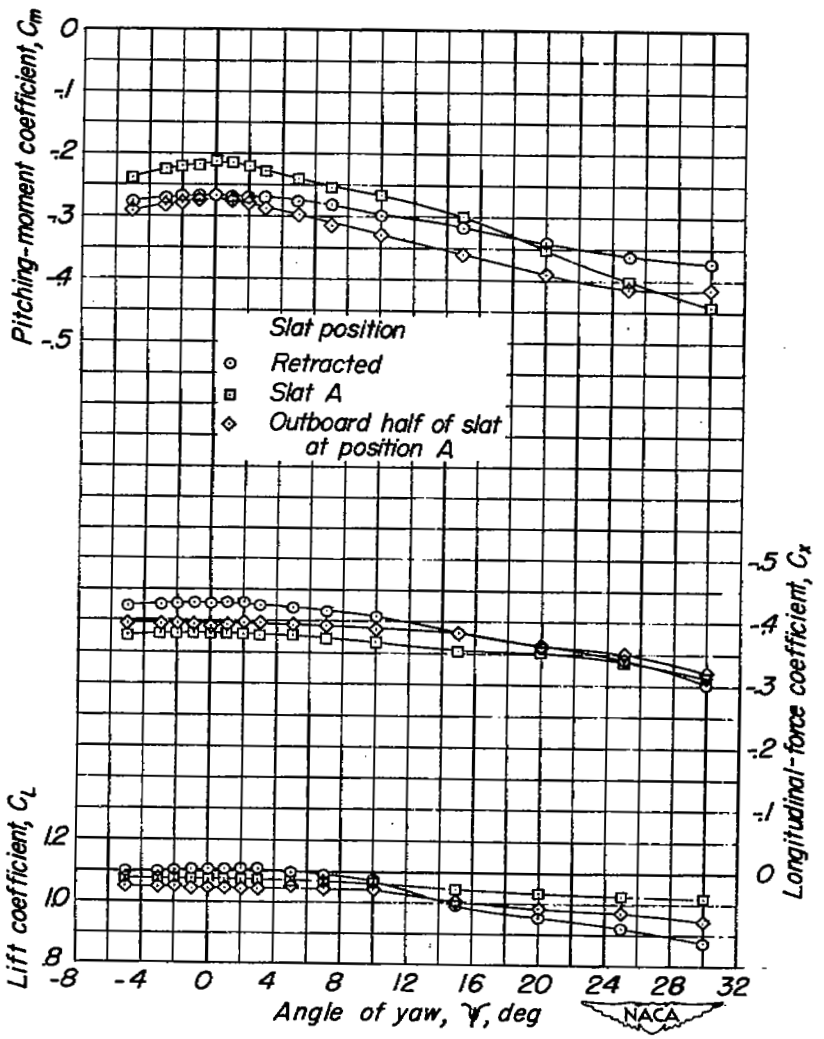

Figure 24.- Concluded.

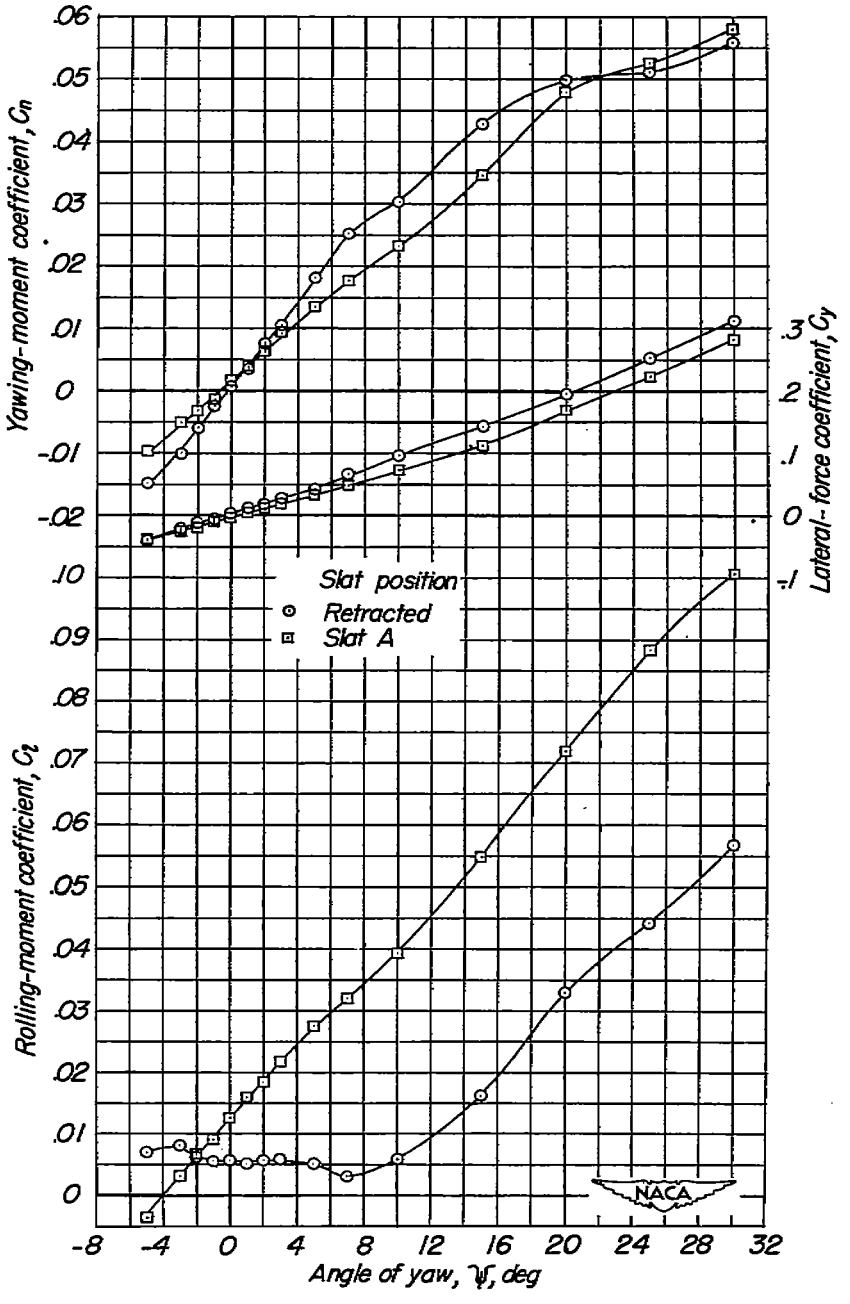

Figure 25.- The effect of slat position on the aerodynamic characteristics in yaw of the test model. $\Lambda = 60^\circ$; $\delta_f = 0^\circ$; tail off; $\alpha = 23.50^\circ$.

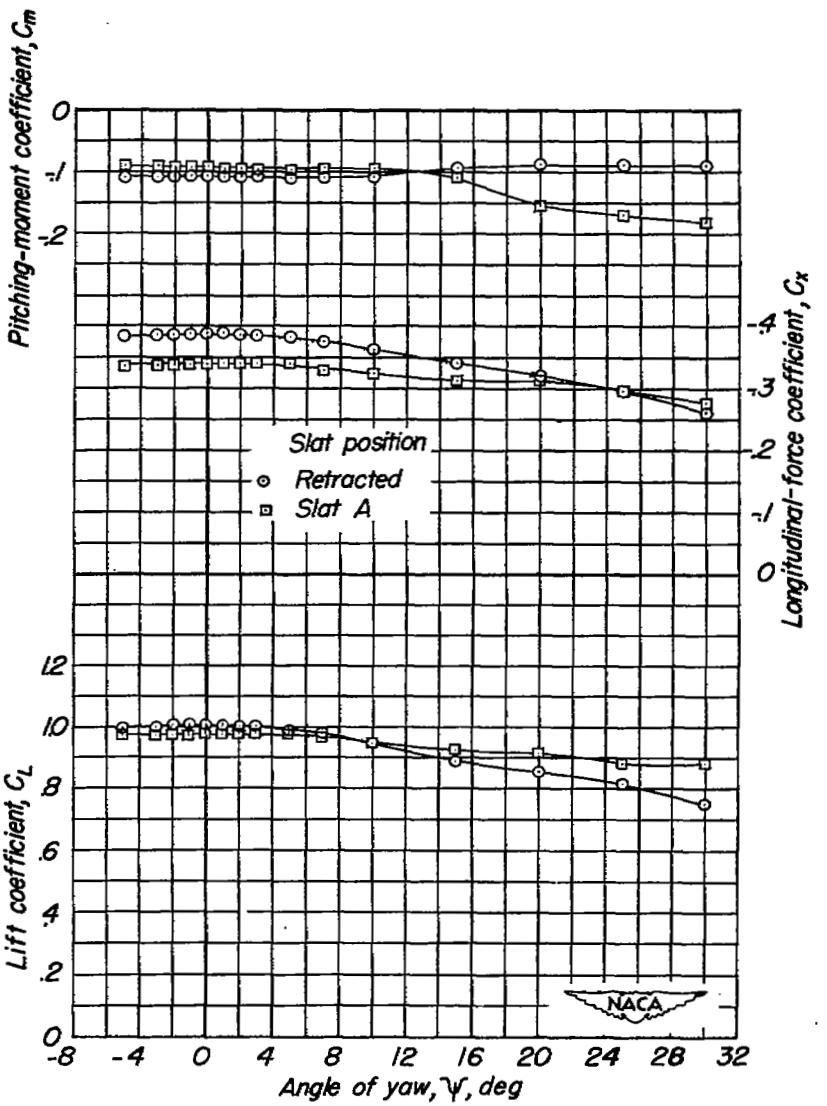

Figure 25.- Concluded.

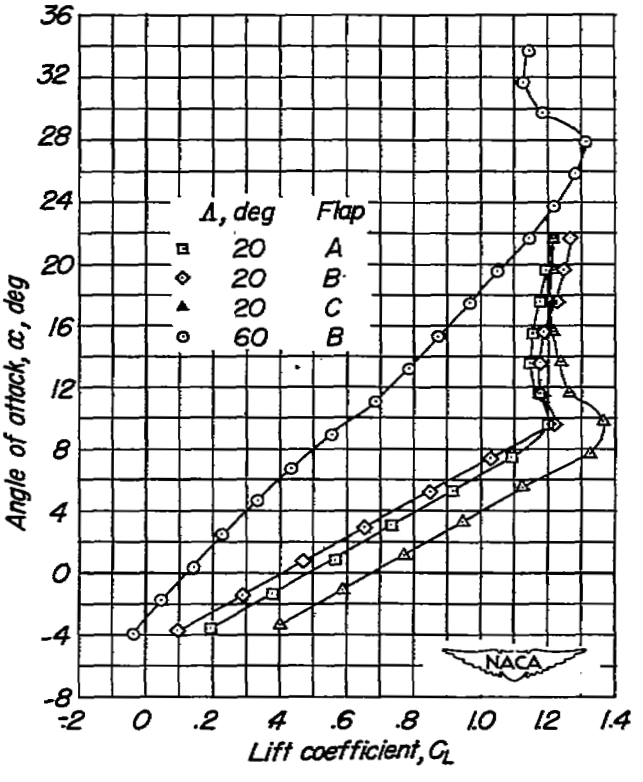

Figure 26.- The effect of sweep and flap configuration on the lift curves for the test model. Slats retracted; $\delta_f = 50^\circ$; $i_t = -\frac{3}{4}^\circ$.

[redacted]

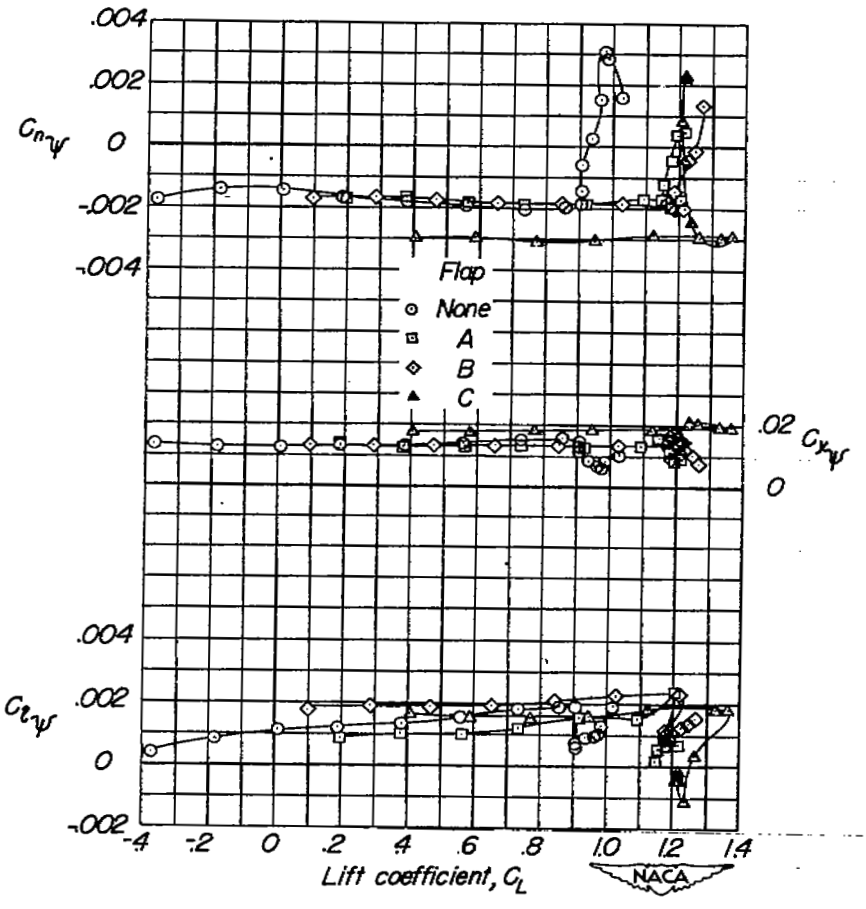

Figure 27.- The effect of flap configuration on the lateral-stability parameters of the test model. $\Lambda = 20^\circ$; slats retracted; $\delta_f = 50^\circ$; $i_t = -\frac{3^\circ}{4}$.

[redacted]

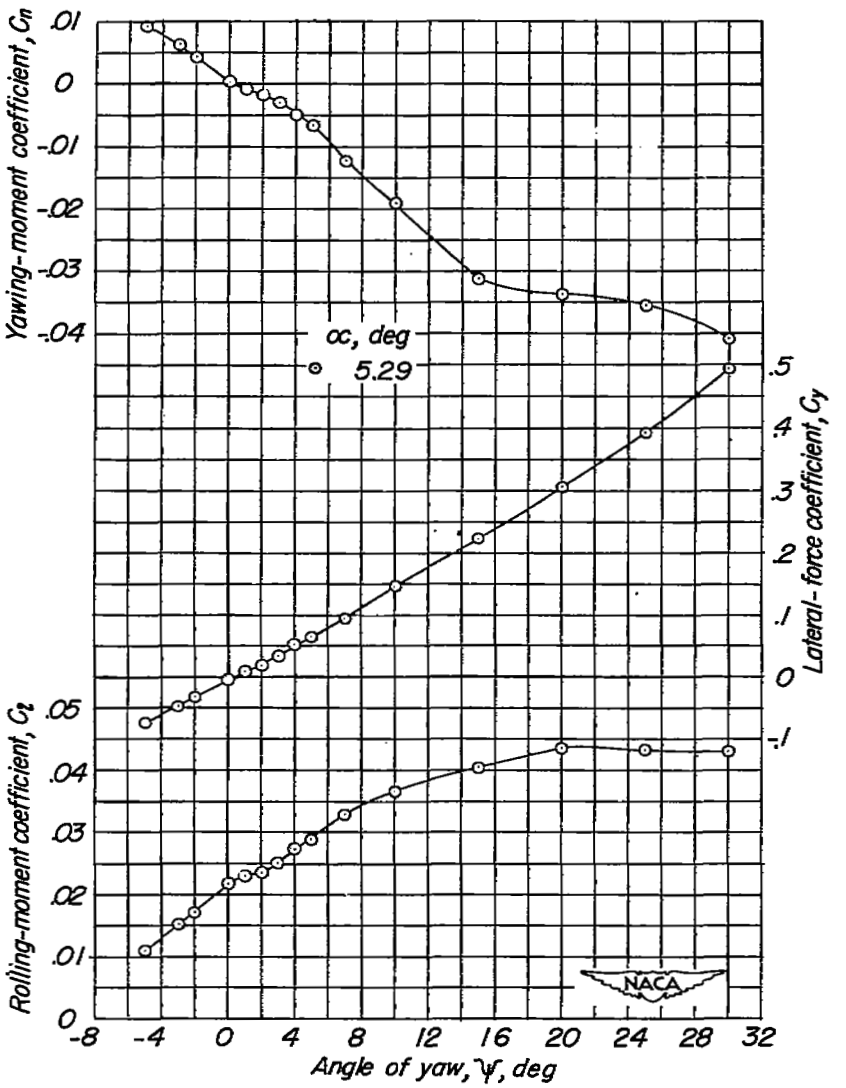

(a) Flap A.

Figure 28.- The effect of angle of attack on the aerodynamic characteristics in yaw of the test model. $\Lambda = 20°$; slats retracted; $\delta_f = 50°$; $i_t = -\frac{3°}{4}$.

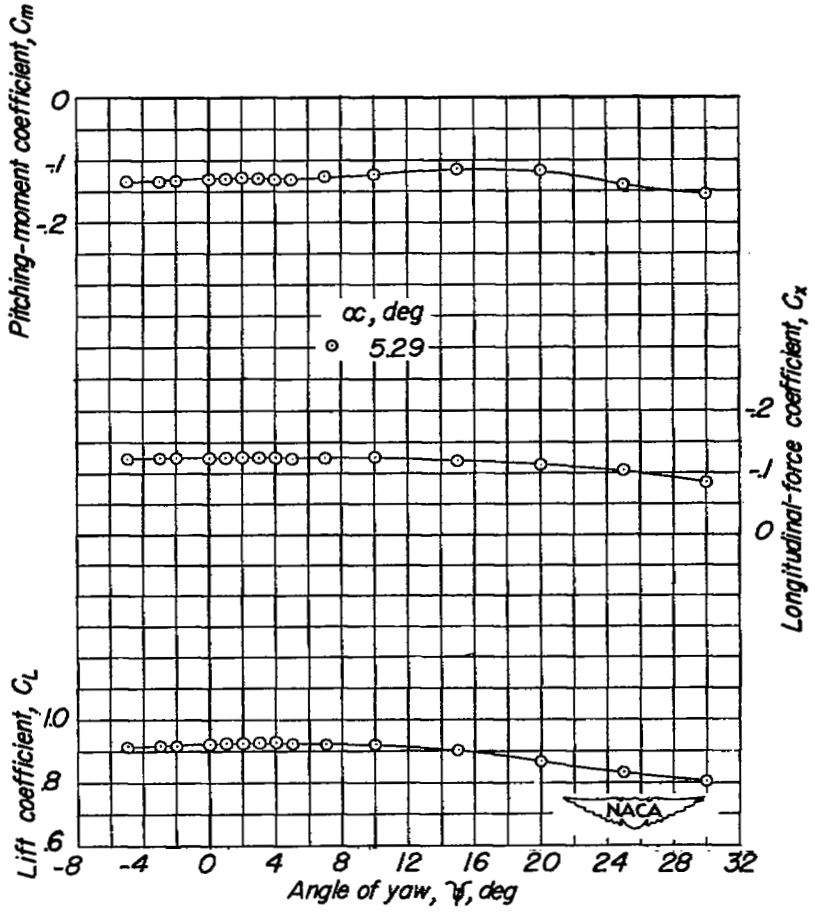

(a) Concluded.

Figure 28.- Continued.

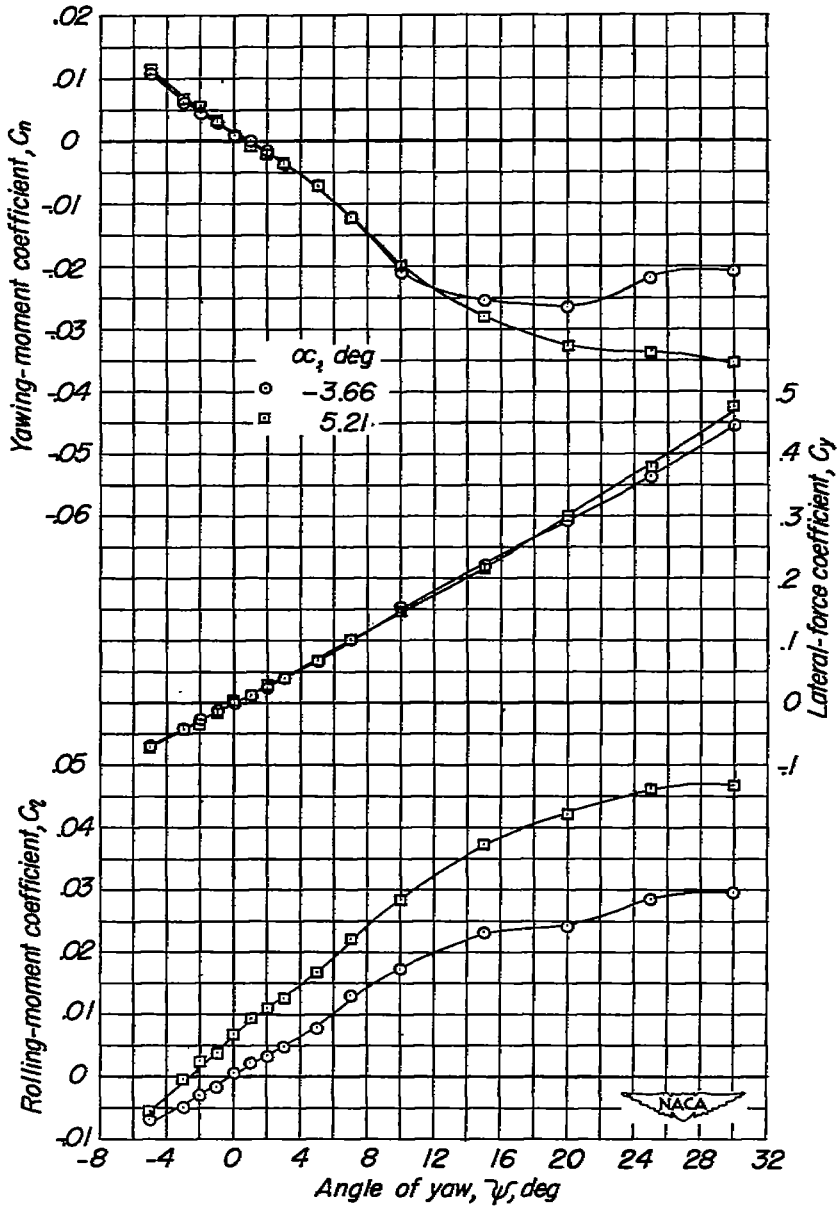

(b) Flap B.

Figure 28.- Continued.

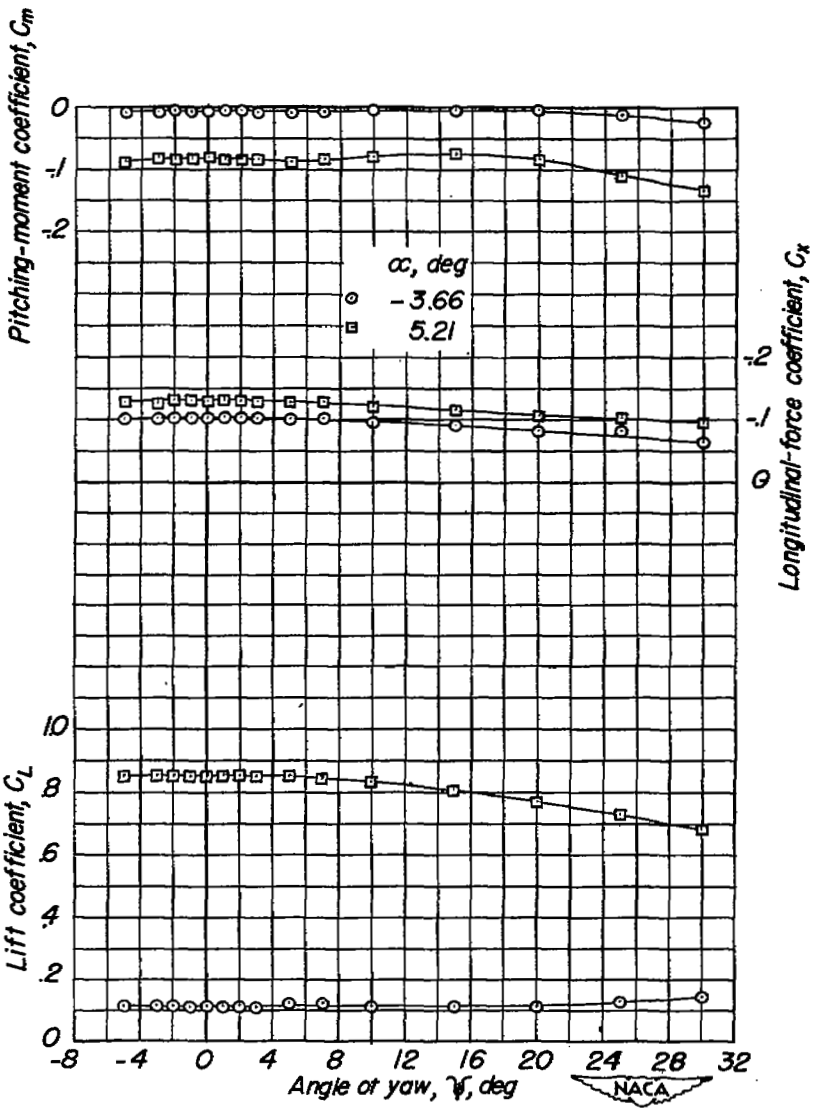

(b) Concluded.

Figure 28.- Continued.

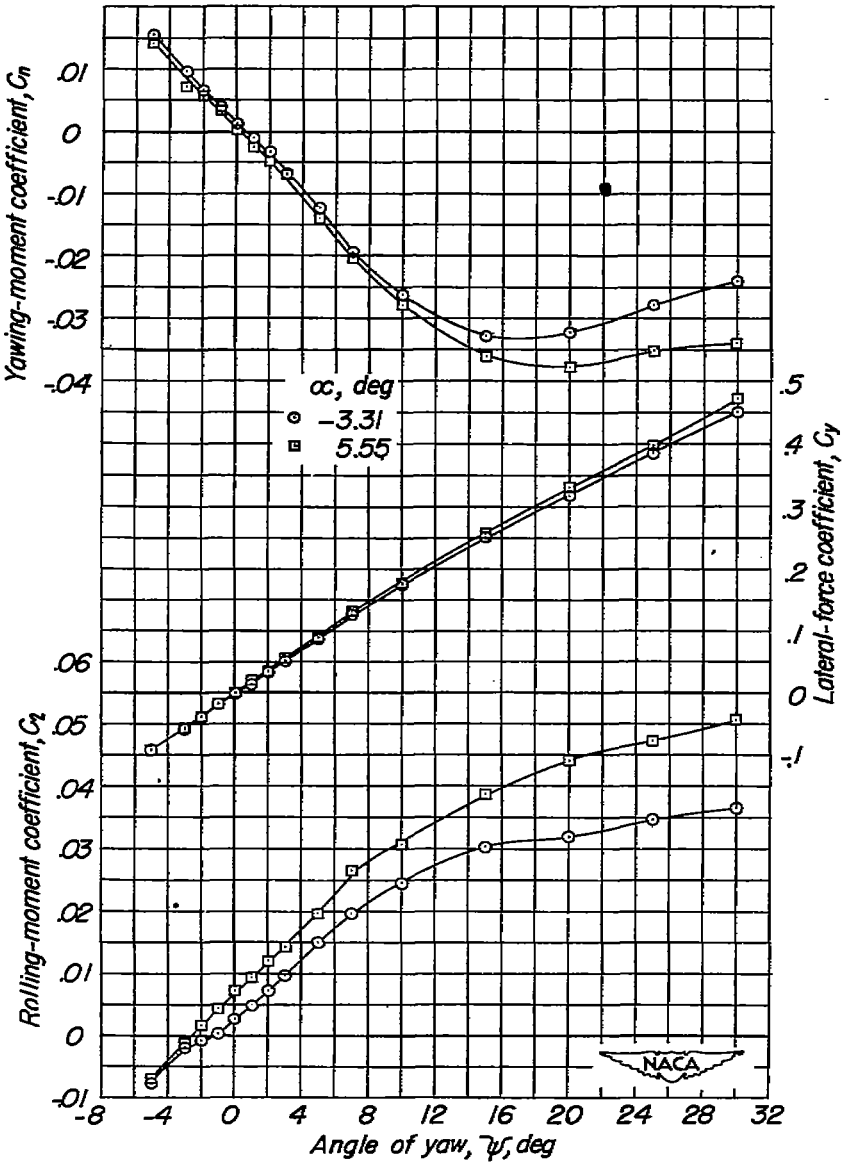

(c) Flap C.

Figure 28.- Continued.

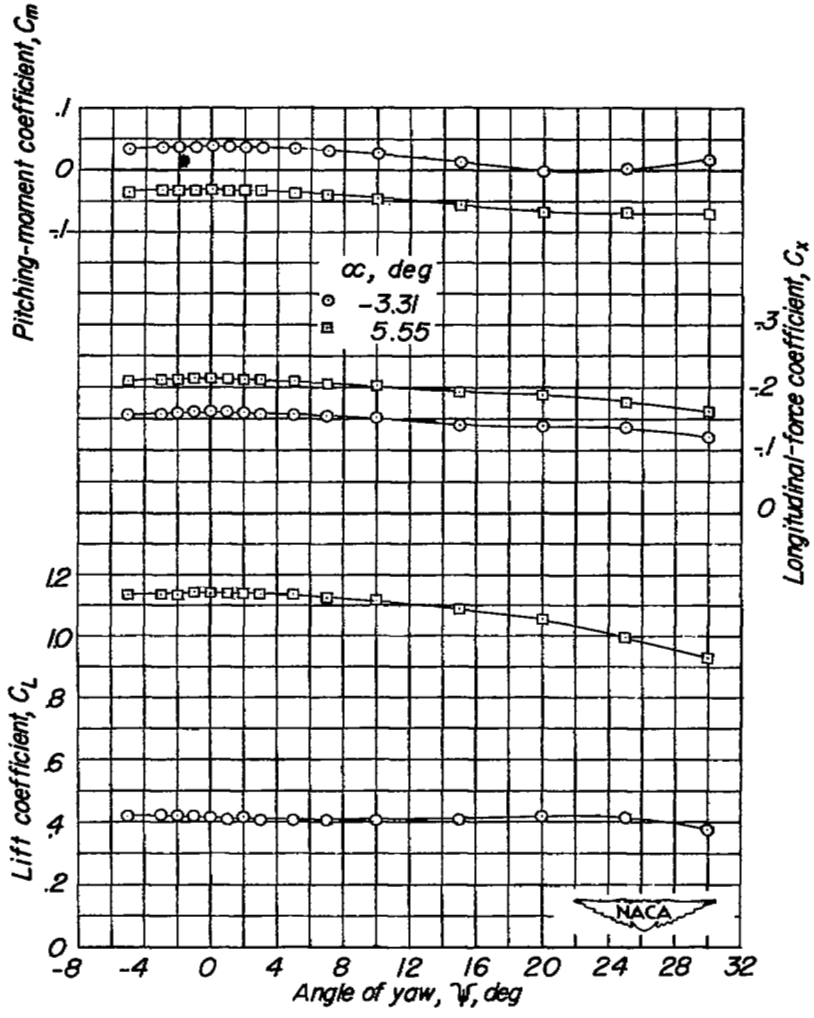

(c) Concluded.

Figure 28.- Concluded.

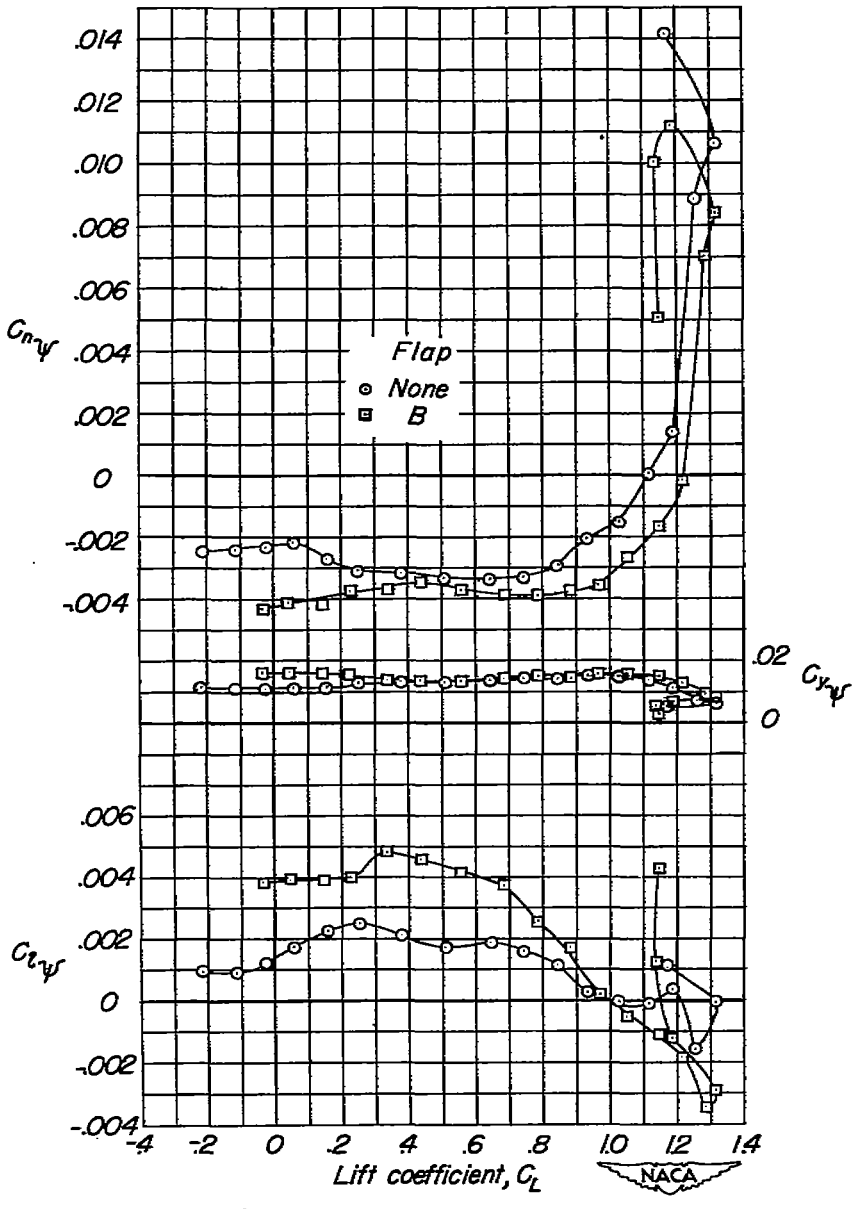

Figure 29.- The effect of flap B on the lateral-stability parameters of the test model. $\Lambda = 60^\circ$; slats retracted; $\delta_f = 50^\circ$; $i_t = -\frac{3^\circ}{4}$.

[redacted]

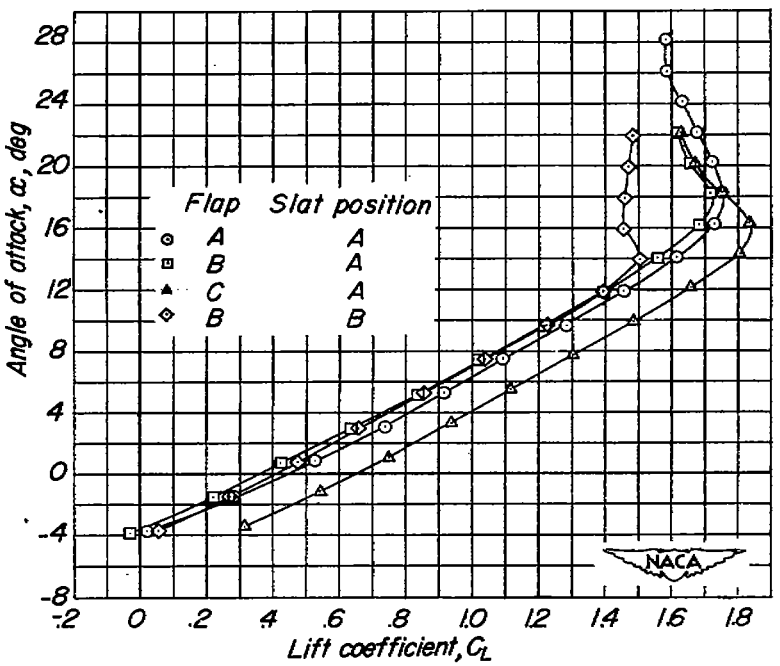

Figure 30.- The effect of flap configuration and slat position on the lift curves for the test model. $\Lambda = 20°$; $\delta_f = 50°$; $i_t = -\frac{3}{4}°$.

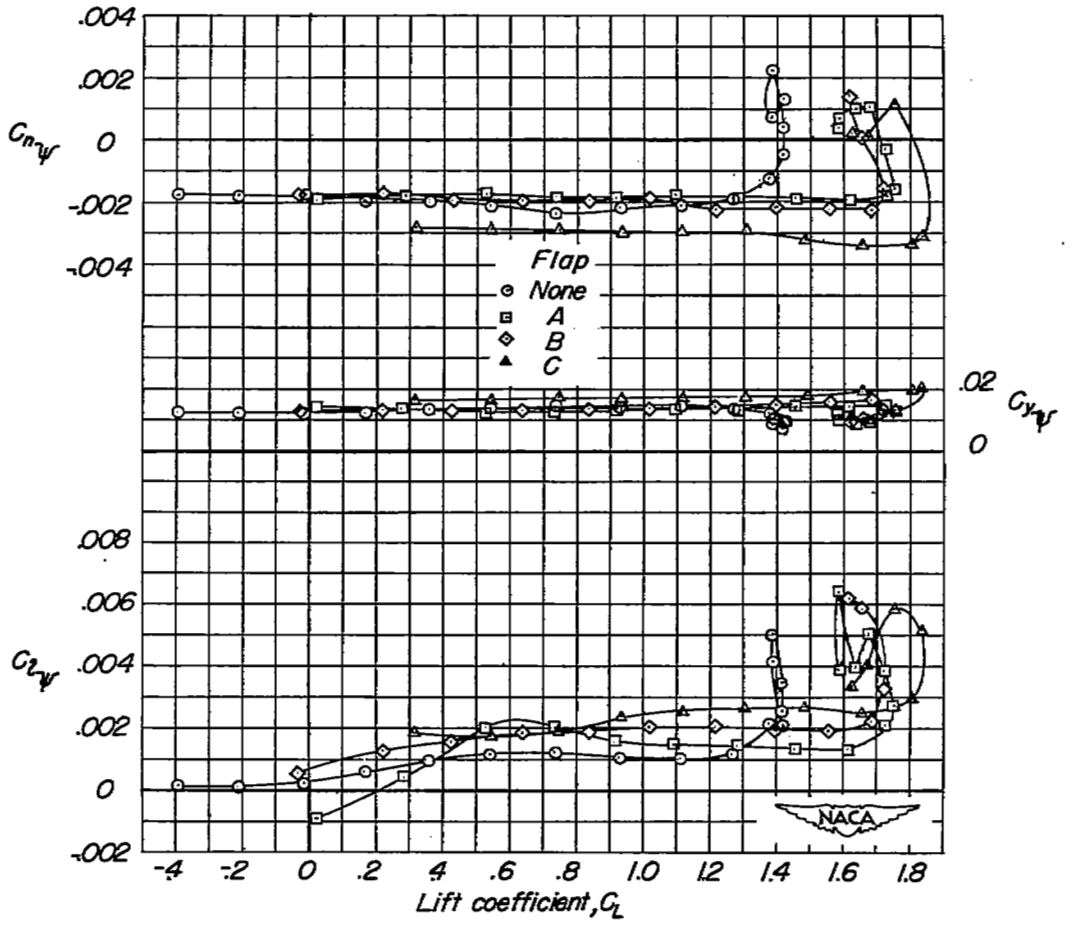

Figure 31.- The effect of flap configuration on the lateral-stability parameters of the test model. $\Lambda = 20°$; slat A; $\delta_f = 50°$; $i_t = -\frac{3}{4}^{8}$.

[redacted]

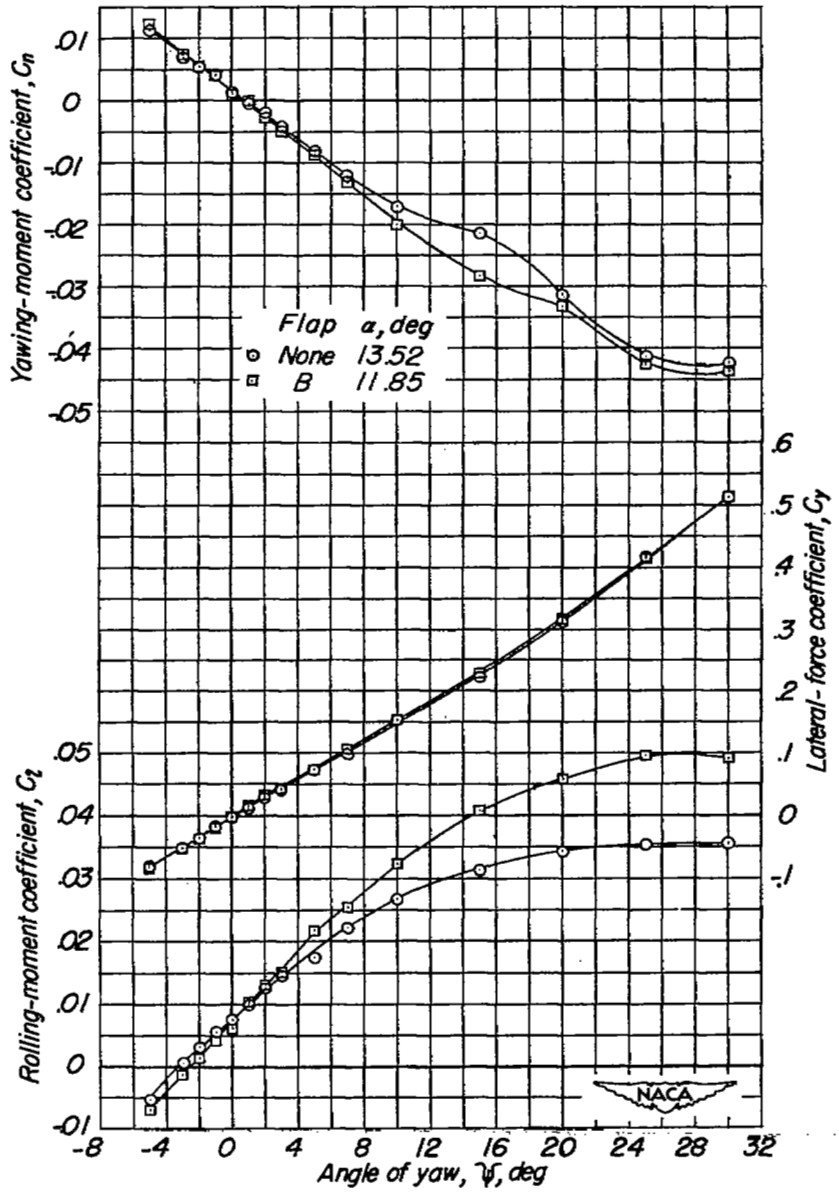

Figure 32.- The effect of flap B on the aerodynamic characteristics in yaw of the test model. $\Lambda = 20^\circ$; slat B; $\delta_f = 50^\circ$; $i_t = -\frac{3^\circ}{4}$.

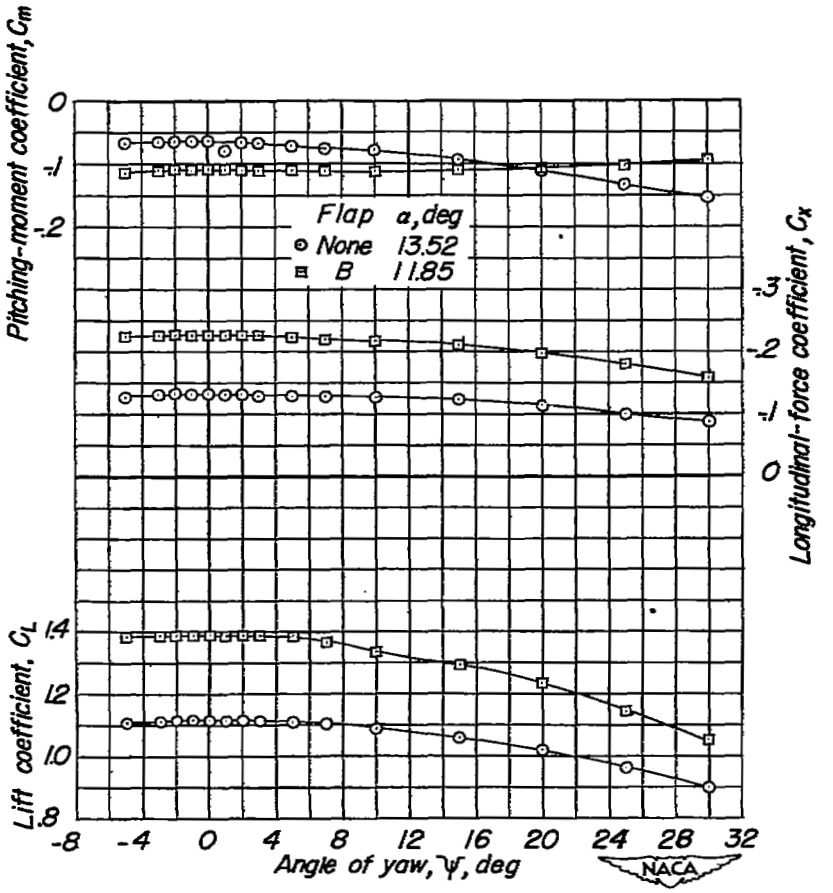

Figure 32.- Concluded.

[redacted]

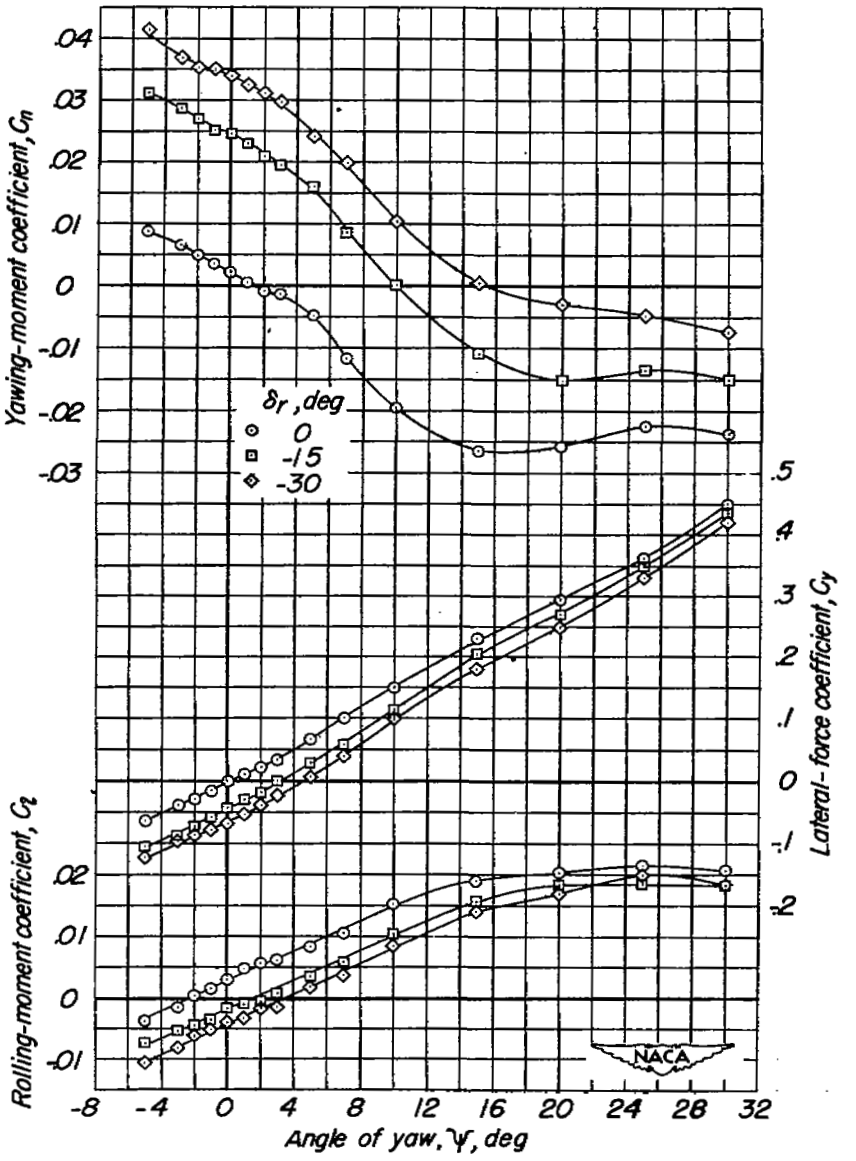

Figure 33.- The effect of rudder deflection on the aerodynamic characteristics in yaw of the test model. $\Lambda = 20^\circ$; slats retracted; $\delta_f = 0^\circ$; $i_t = -\frac{3^\circ}{4}$; $\alpha = 0.24^\circ$.

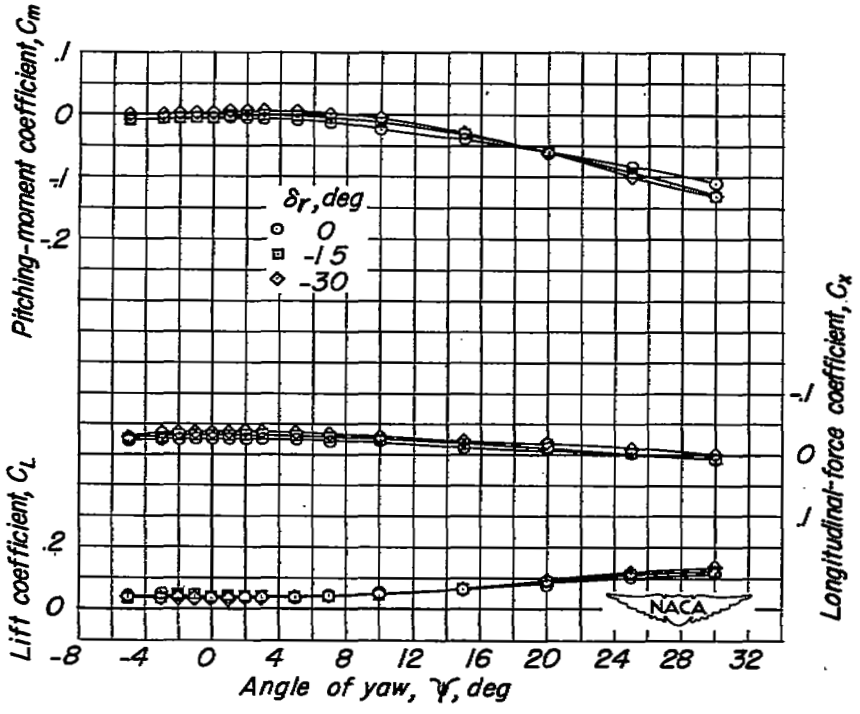

Figure 33.- Concluded.

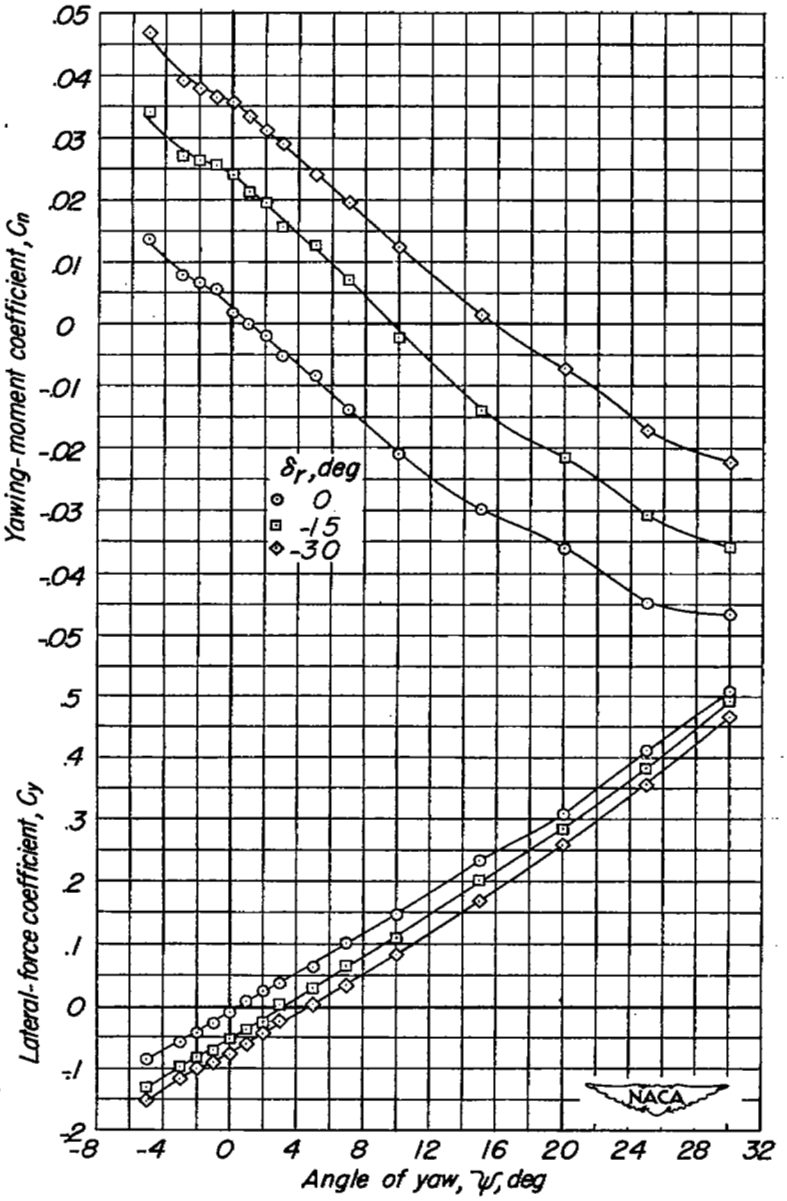

Figure 34.- The effect of rudder deflection on the aerodynamic characteristics in yaw of the test model. $\Lambda = 20°$; slat A; flap B; $\delta_f = 50°$; $i_t = -\frac{3°}{4}$; $\alpha = 11.88°$.

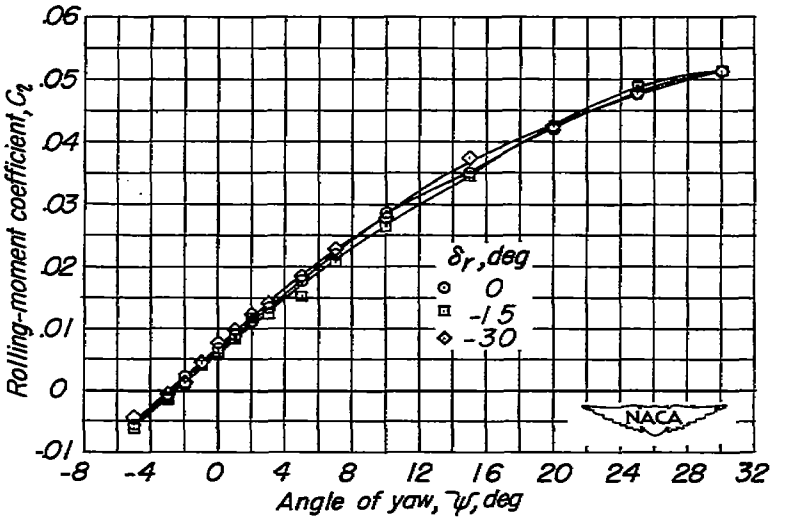

Figure 34.- Continued.

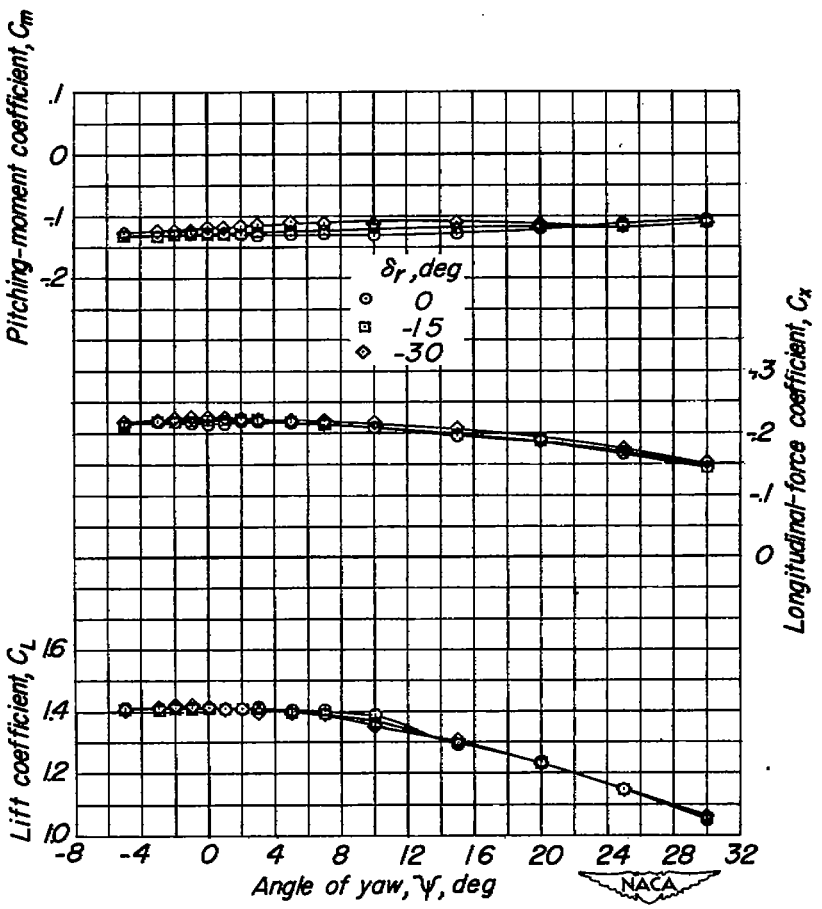

Figure 34.- Concluded.

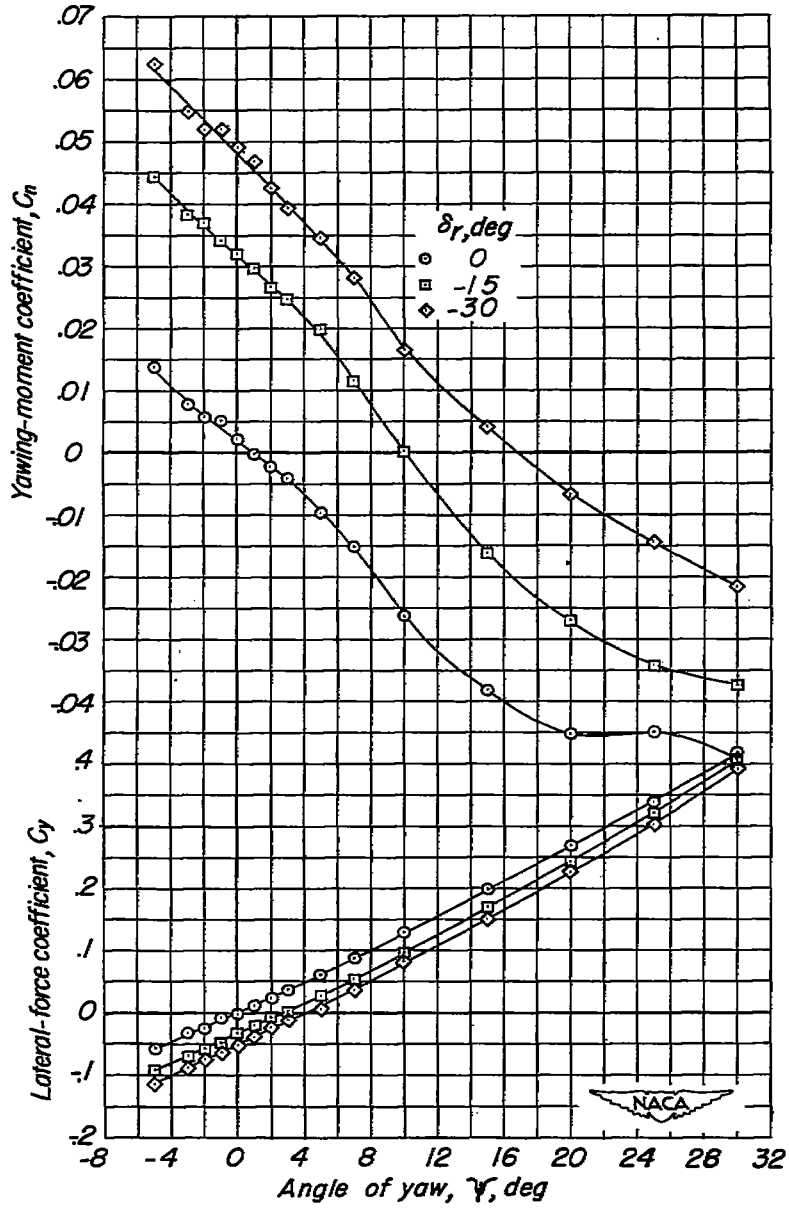

Figure 35.- The effect of rudder deflection on the aerodynamic characteristics in yaw of the test model. $\Lambda = 60°$; slats retracted; $\delta_f = 0°$; $i_t = -5°$; $\alpha = 4.36°$.

[redacted]

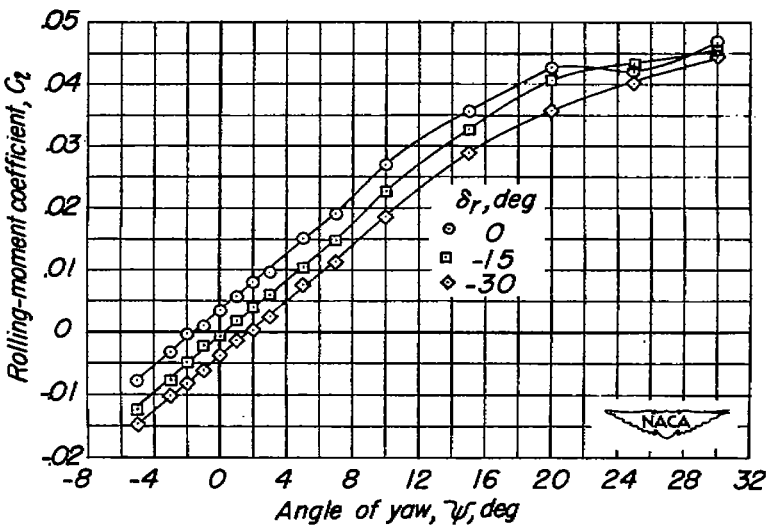

Figure 35.- Continued.

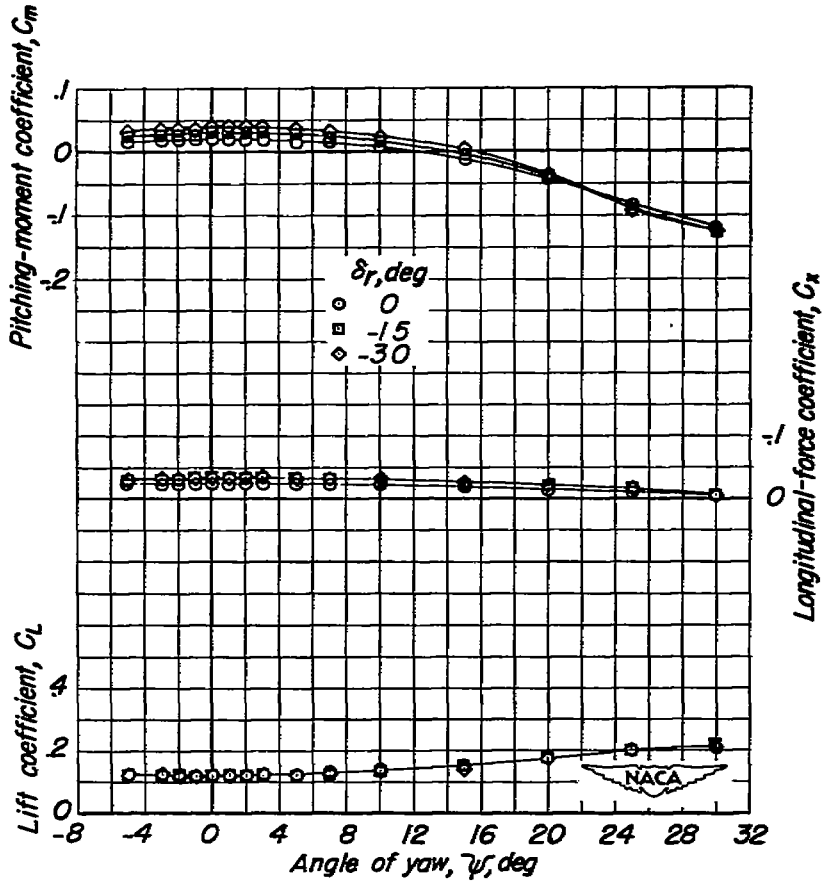

Figure 35.- Concluded.

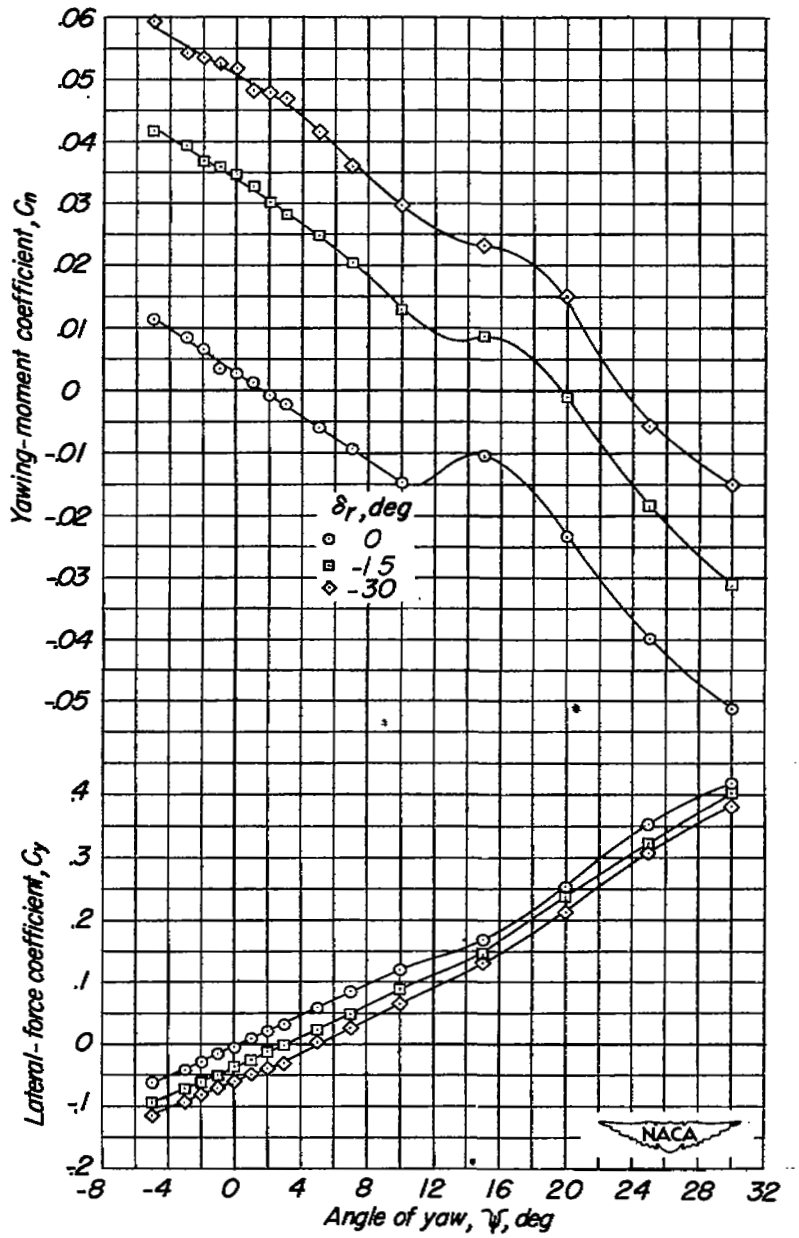

Figure 36.- The effect of rudder deflection on the aerodynamic characteristics in yaw of the test model. $\Lambda = 60^\circ$; slat A; $\delta_f = 0^\circ$; $i_t = -5^\circ$; $\alpha = 23.54^\circ$.

[redacted]

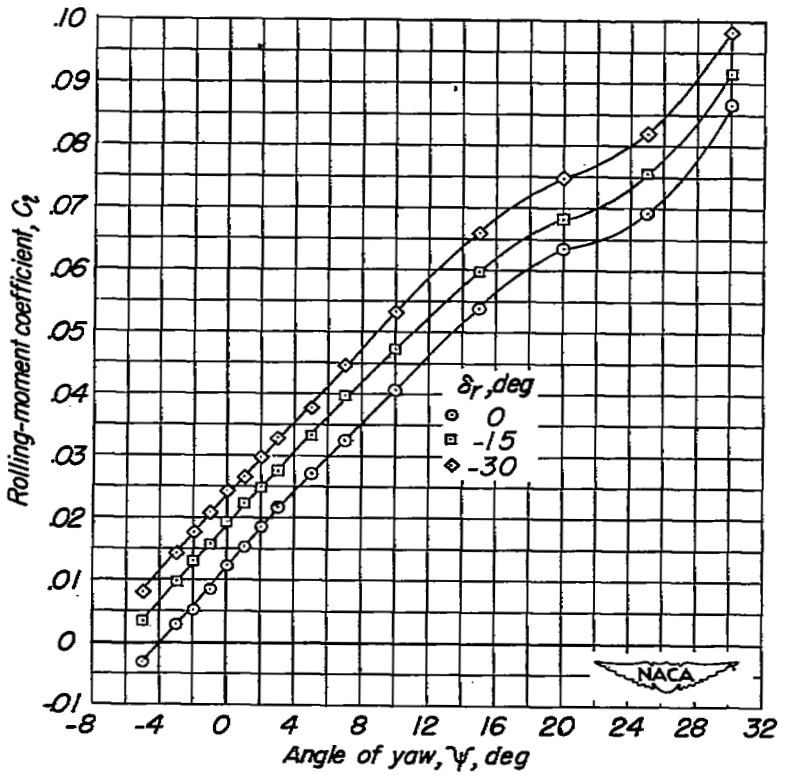

Figure 36.- Continued.

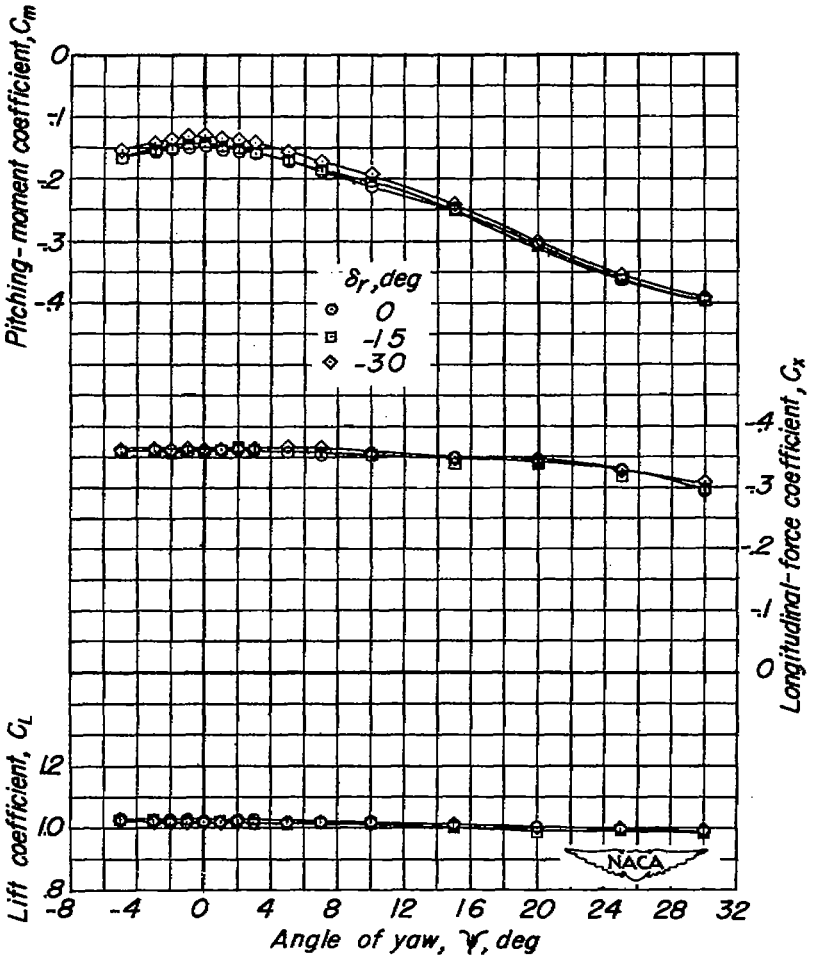

Figure 36.- Concluded.

[redacted]

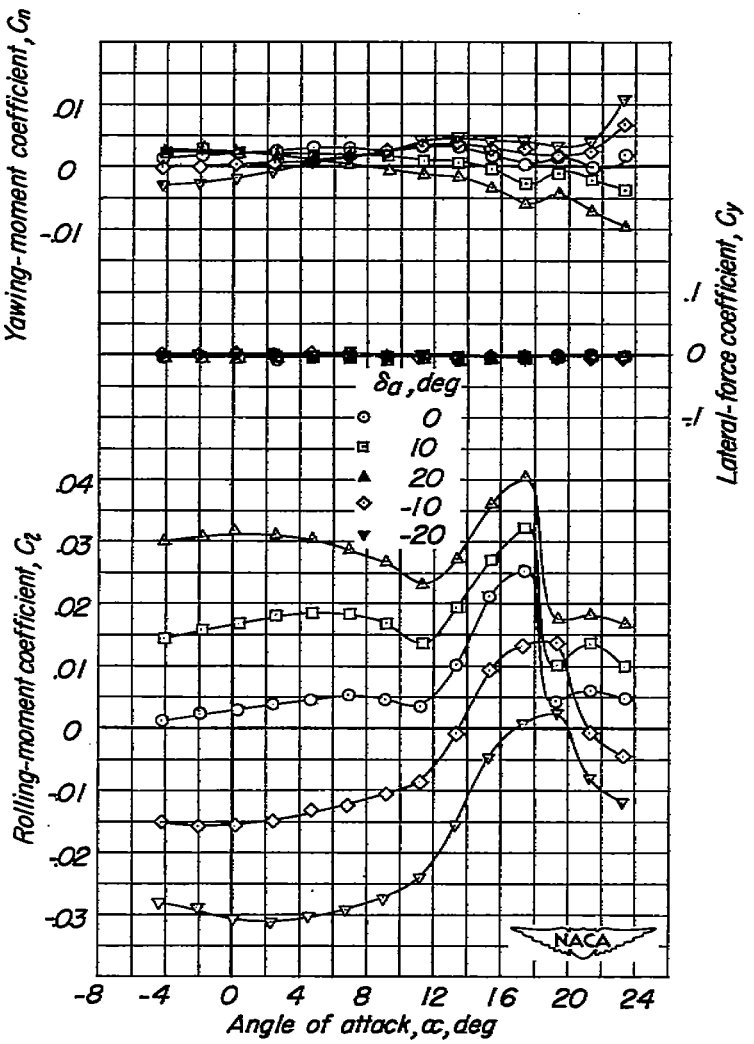

Figure 37.- The effect of left-aileron deflection on the aerodynamic characteristics in pitch of the test model. $\Lambda = 20^\circ$; slats retracted; $\delta_f = 0^\circ$; $i_t = -\frac{3^\circ}{4}$.

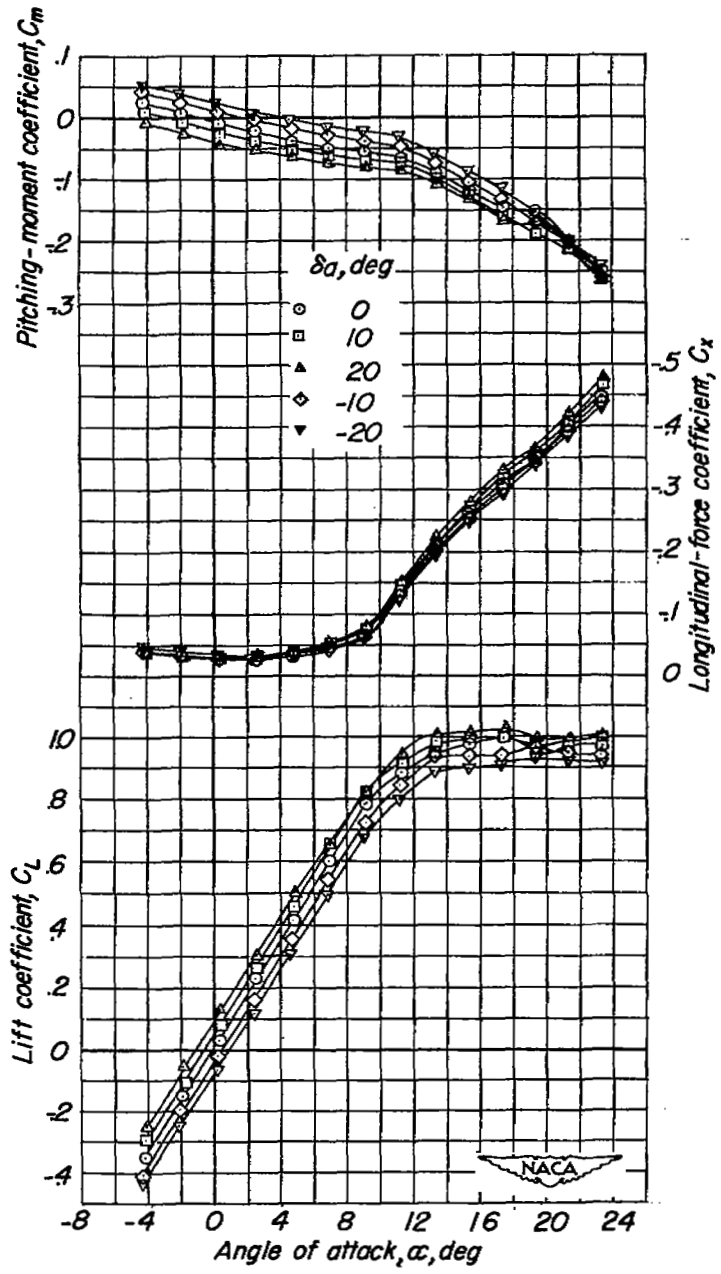

Figure 37.- Concluded.

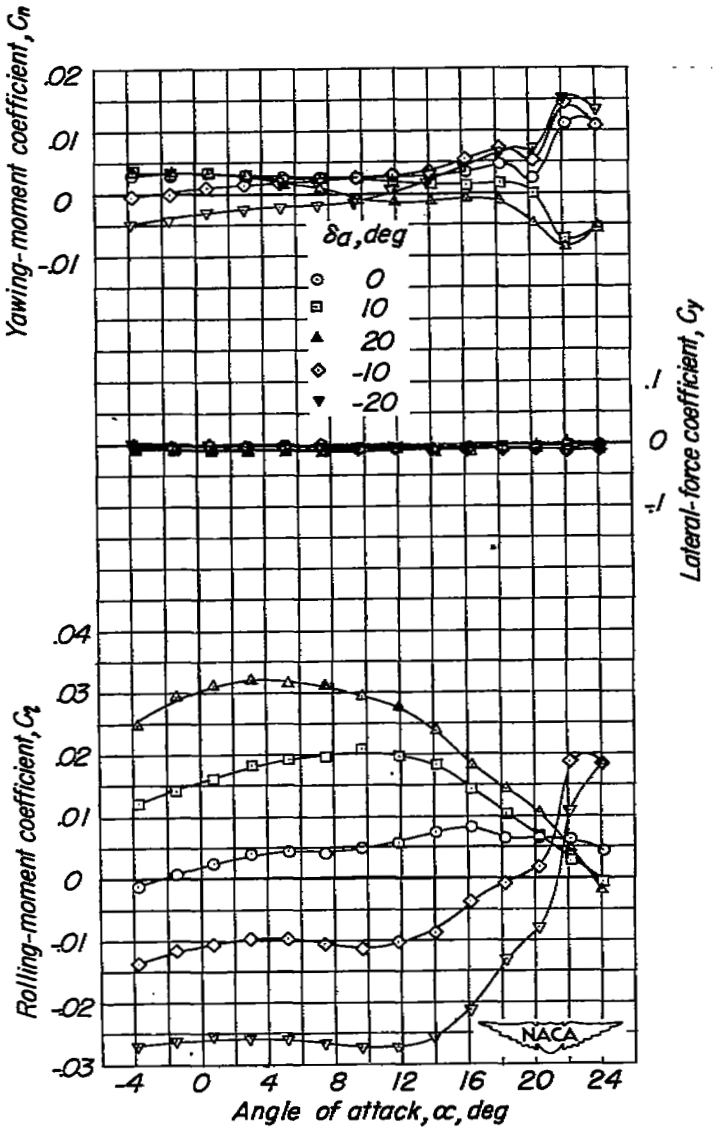

Figure 38.- The effect of left-aileron deflection on the aerodynamic characteristics in pitch of the test model. $\Lambda = 20^\circ$; slat A; flap B; $\delta_f = 50^\circ$; $i_t = -\frac{3^\circ}{4}$.

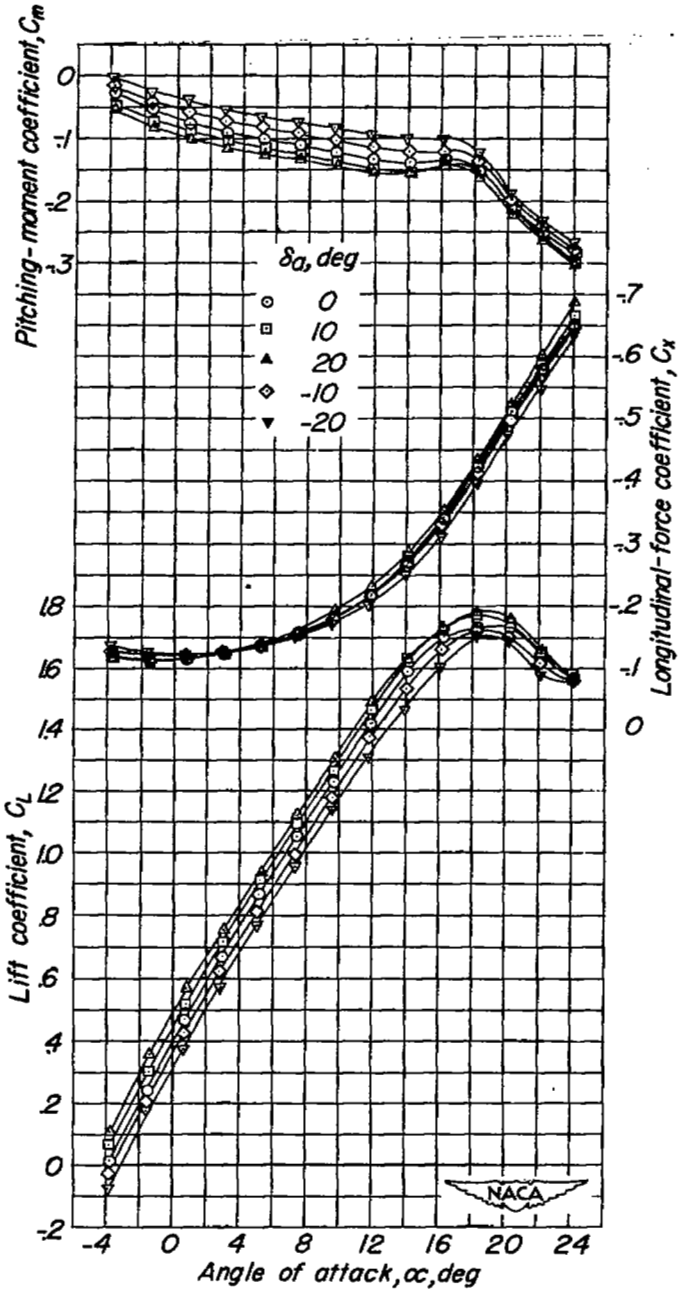

Figure 38.- Concluded.

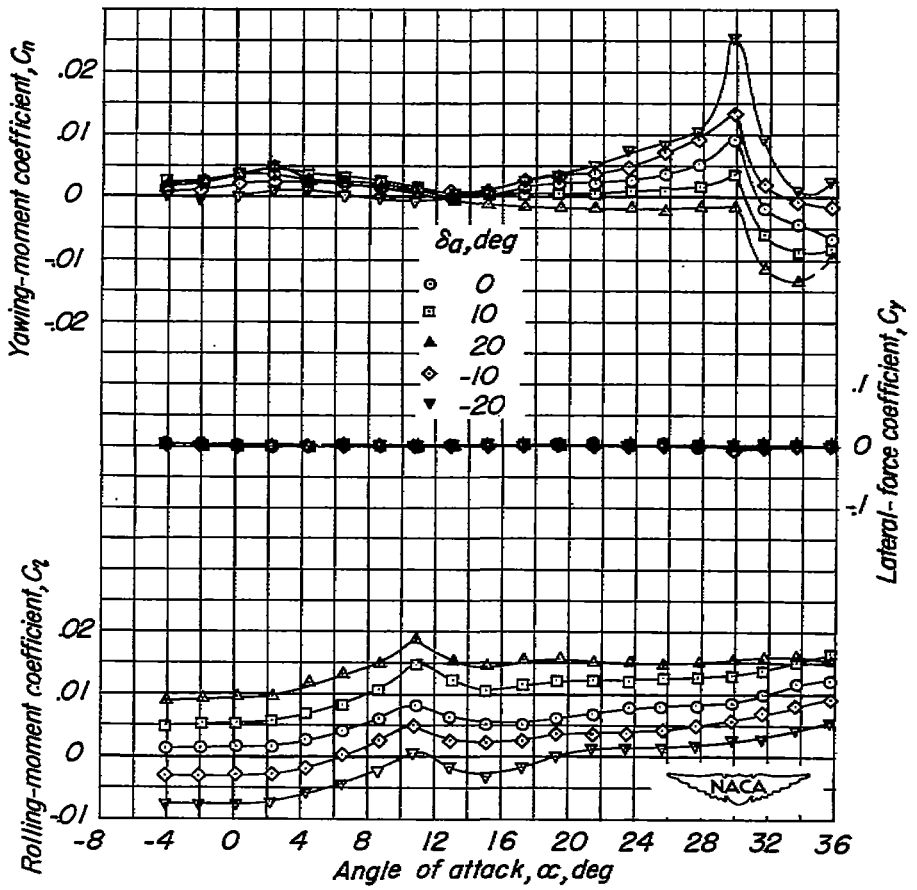

Figure 39.- The effect of left-aileron deflection on the aerodynamic characteristics in pitch of the test model. $\Lambda = 60^\circ$; slats retracted; $\delta_f = 0^\circ$; $i_t = -5^\circ$.

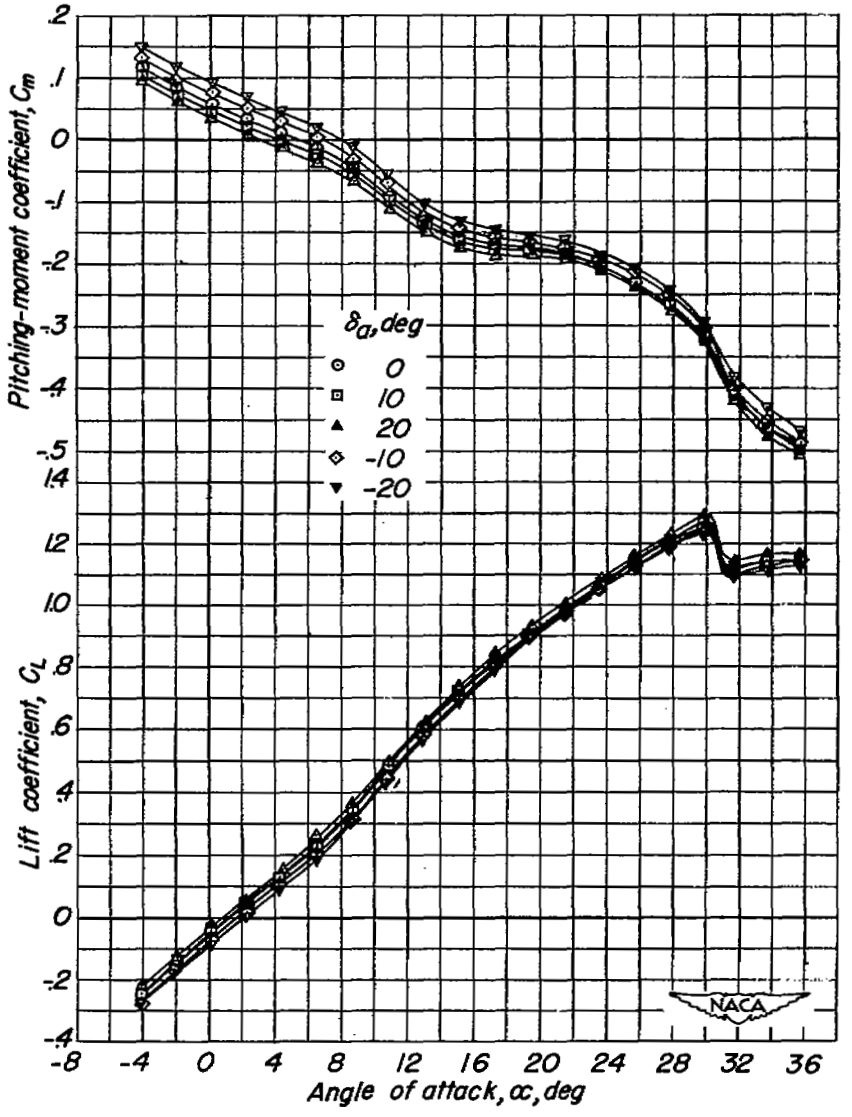

Figure 39.- Continued.

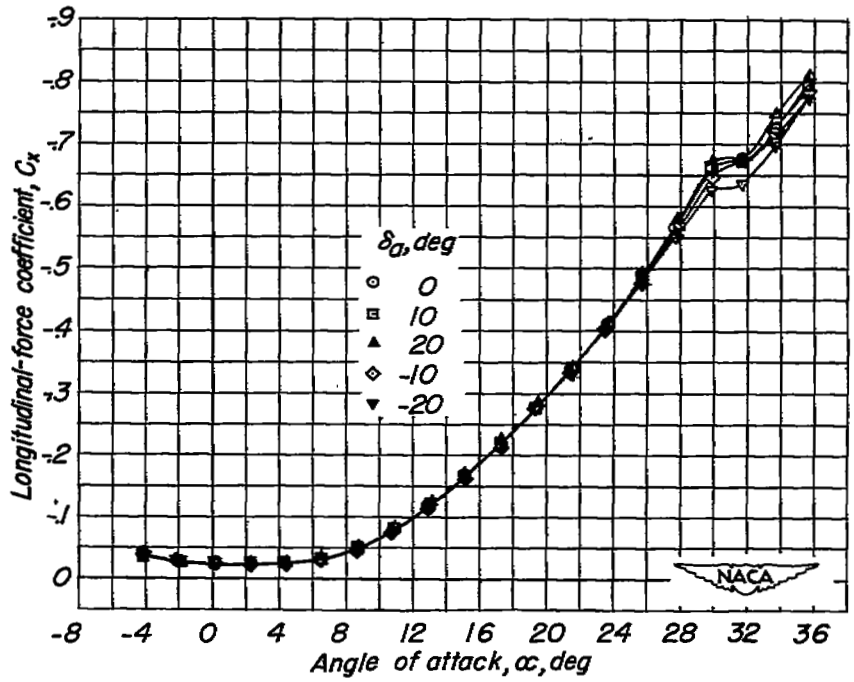

Figure 39.- Concluded.

[redacted]

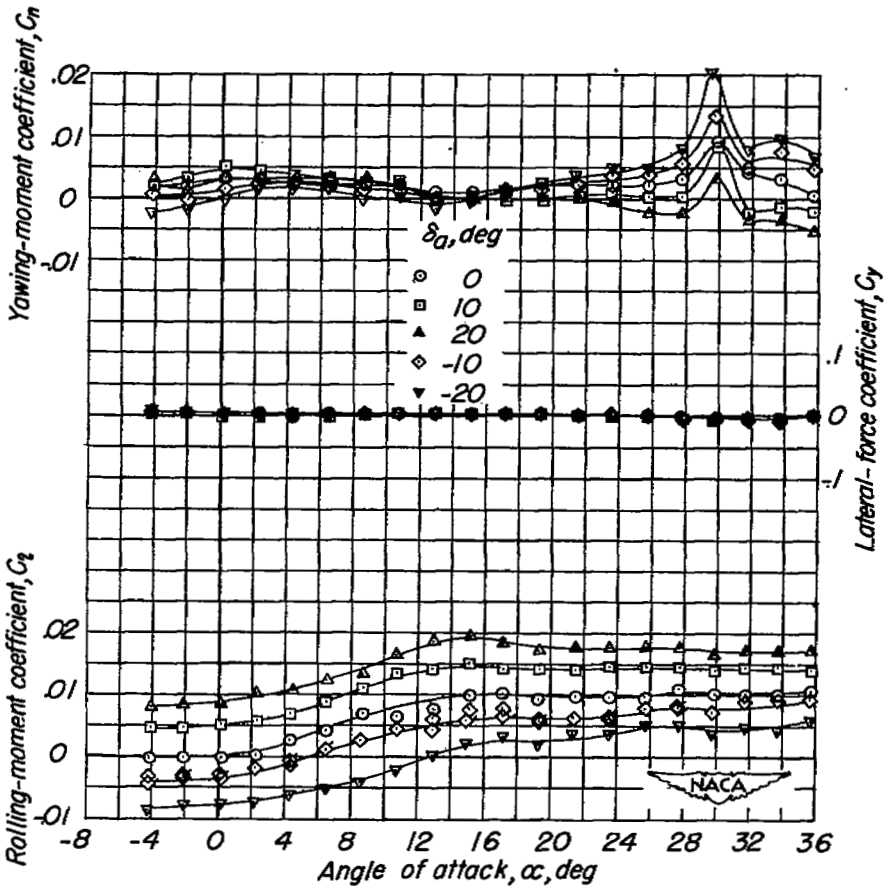

Figure 40.- The effect of left-aileron deflection on the aerodynamic characteristics in pitch of the test model. $\Lambda = 60^\circ$; slat A; $\delta_f = 0^\circ$; $i_t = -5^\circ$.

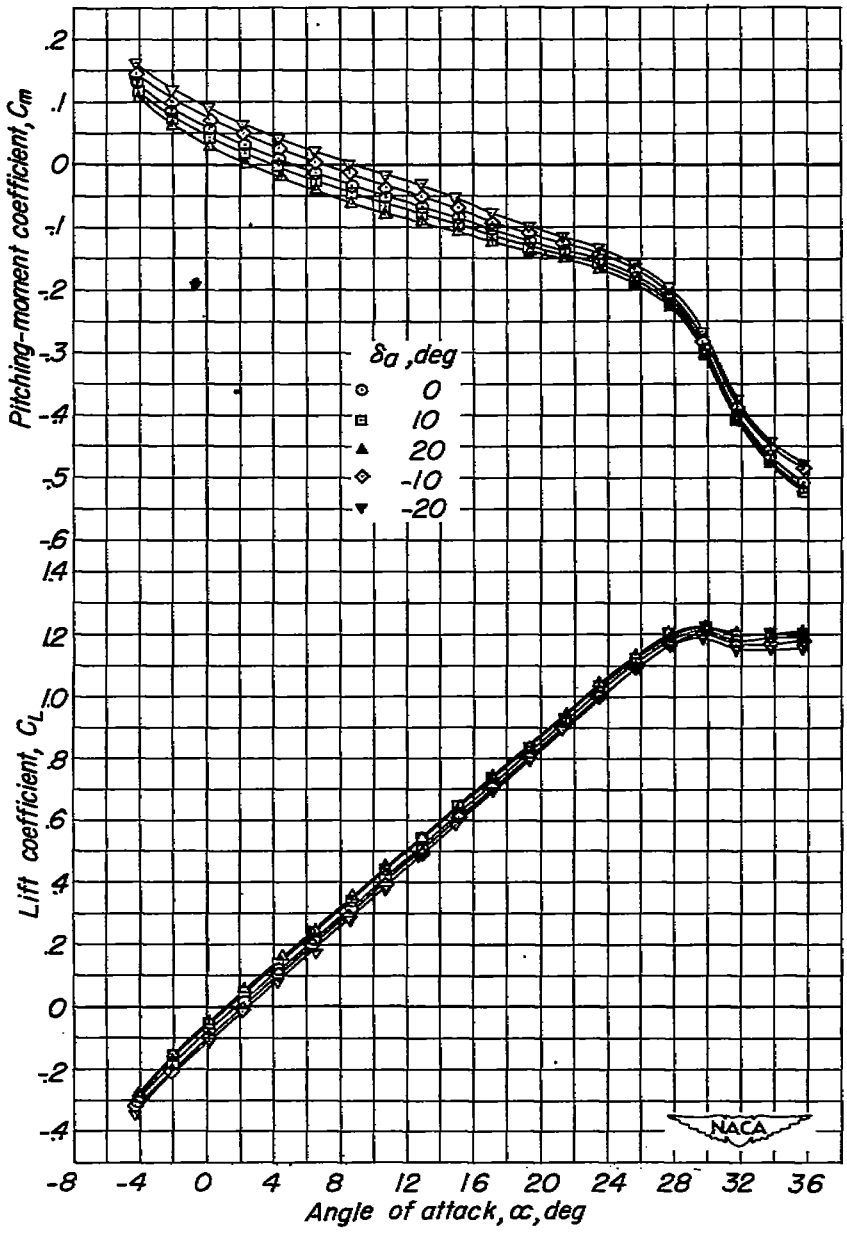

Figure 40.- Continued.

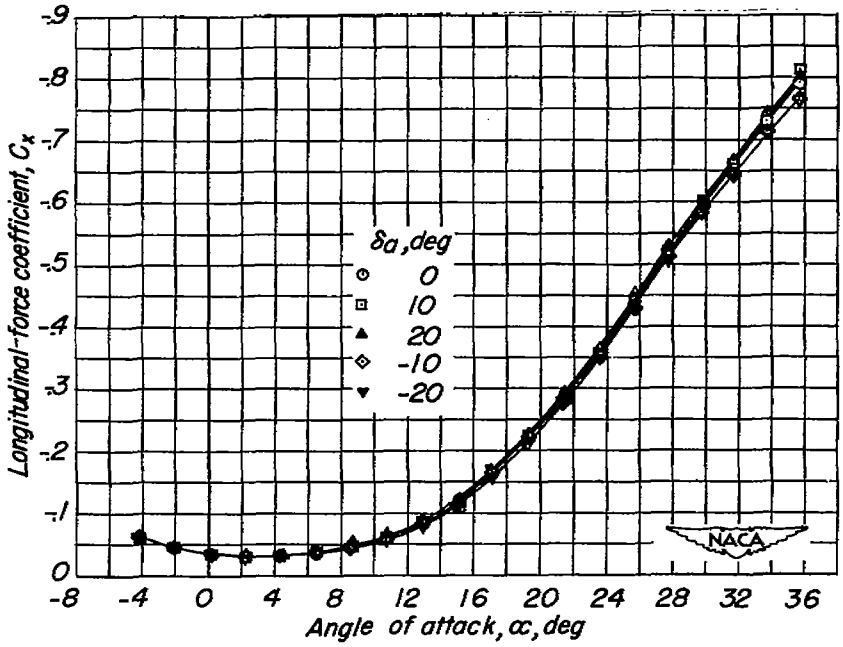

Figure 40.- Concluded.

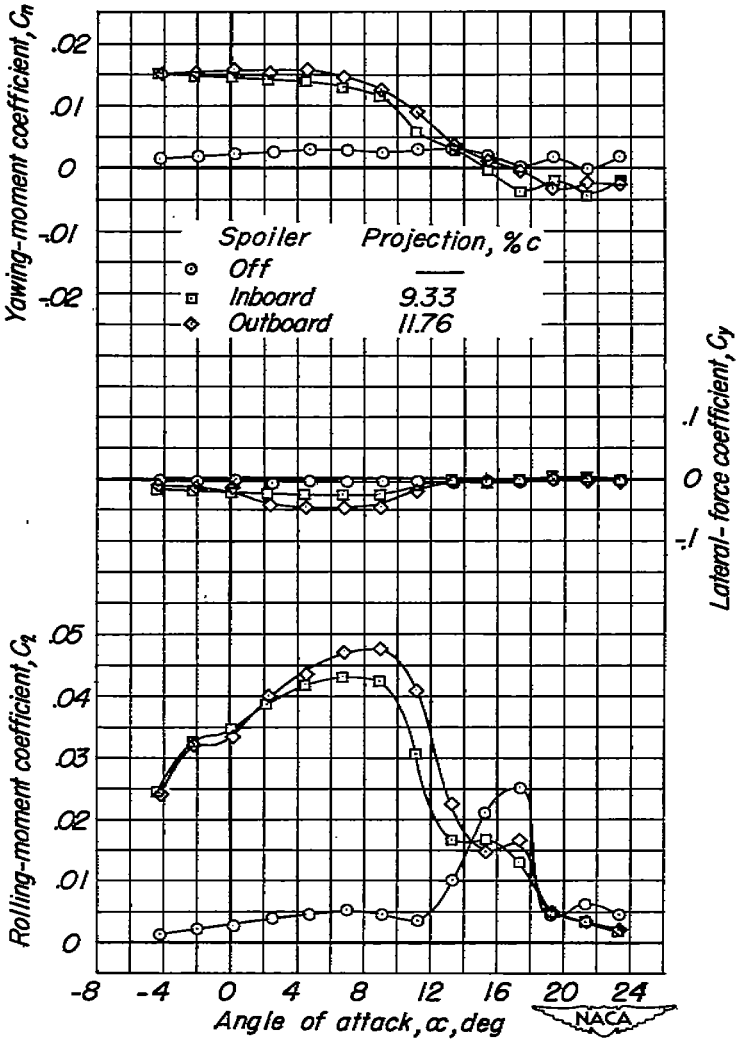

Figure 41.- The effect of a right-wing spoiler position on the aerodynamic characteristics in pitch of the test model. $\Lambda = 20^\circ$; slats retracted; $\delta_f = 0^\circ$; $i_t = -\frac{3^\circ}{4}$.

[redacted]

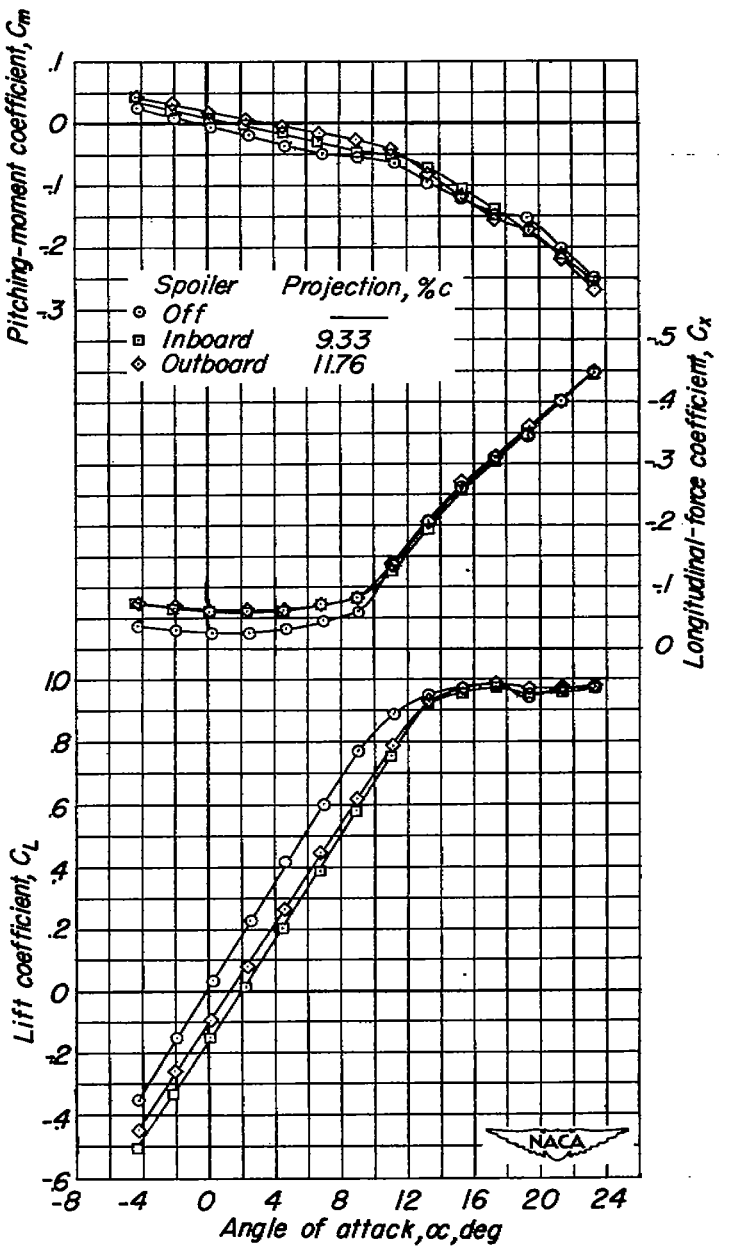

Figure 41.- Concluded.

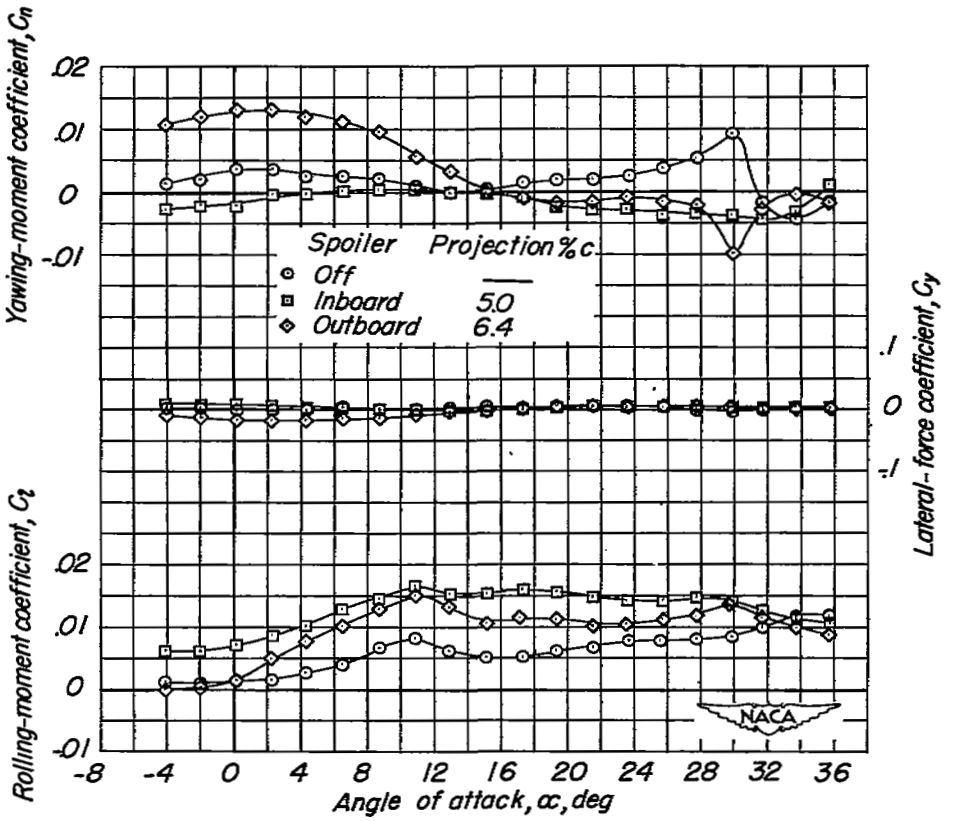

Figure 42.- The effect of a right-wing spoiler position on the aerodynamic characteristics in pitch of the test model. $\Lambda = 60^\circ$; slats retracted; $\delta_f = 0^\circ$; $i_t = -5^\circ$.

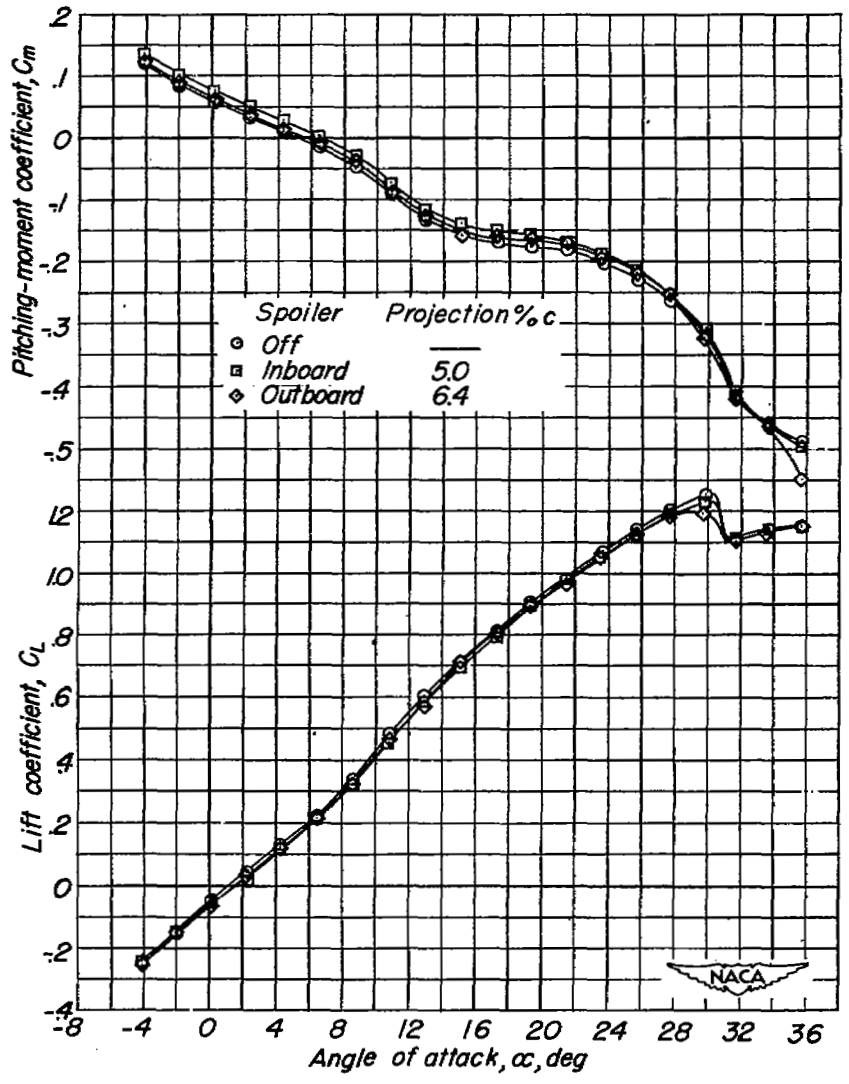

Figure 42.- Continued.

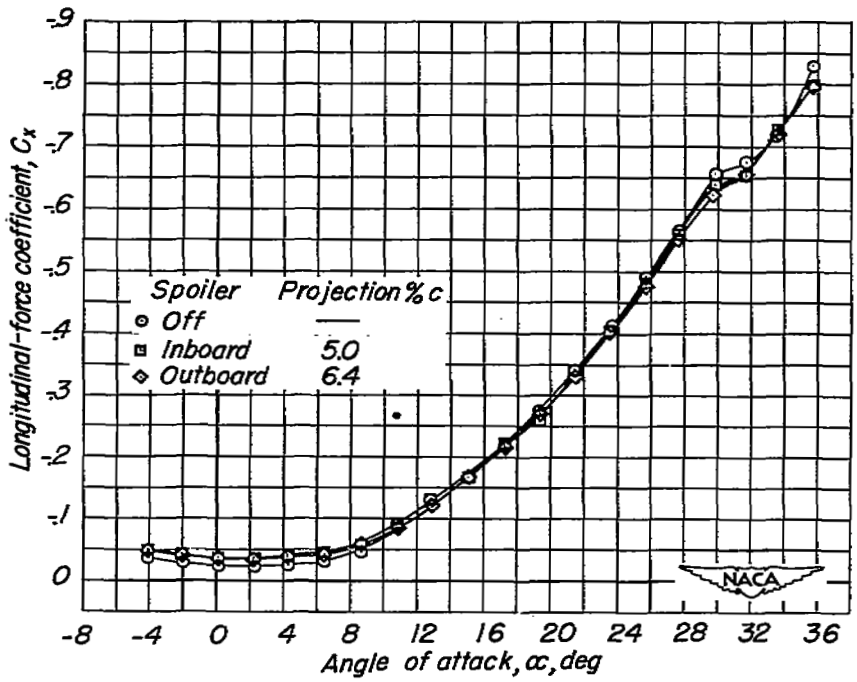

Figure 42.- Concluded.

[redacted]